Spring 1995

A Kinetic Investigation of the Mechanism of Muscle Contraction with a Series of Nucleotides

Wei Jiang
Old Dominion University

A KINETIC INVESTIGATION OF THE MECHANISM OF MUSCLE CONTRACTION WITH A SERIES OF NUCLEOTIDES

BY

Wei Jiang
B.S., July 1985, Jilin University
Changchun, The People's Republic of China
M.S., July 1988, Jilin University
Changchun, The People's Republic of China

A Dissertation Submitted to the Faculties of
Old Dominion University
and
Eastern Virginia Medical School
in Partial Fulfillment of the
Requirements for the Degree of

DOCTOR OF PHILOSOPHY

Biomedical Sciences

OLD DOMINION UNIVERSITY
and
EASTERN VIRGINIA MEDICAL SCHOOL
February, 1995

Approved by:

_____
Howard D. White, Ph.D, Director

_____
Frank A. Lattanzio, Ph.D

_____
Laura K. Moen, Ph.D

_____
Paul H. Ratz, Ph.D

ABSTRACT

A Kinetic Investigation of the Mechanism of Muscle Contraction with A Series of Nucleotides

Wei Jiang

Old Dominion University

and

Eastern Virginia Medical School

Director: Dr. Howard D. White

Muscle contraction is thought to be accomplished by sliding of myosin filaments along actin filaments. Although actomyosin naturally uses ATP as an energy source, it can also use other nucleoside triphosphates (NTP) as substrates. In this work, the dependence of rate and equilibrium constants of the various steps in the muscle contraction mechanism upon nucleotide structure was investigated to unravel the dependence of the mechanical properties of the muscle upon changes in different biochemical steps of the mechanism.

The experiments measuring the dissociation of actomyosin by NTP (or mant-NTP) shows that both the rate constant of actomyosin-S1 dissociation and second order rate constant of NTP binding to acto-S1 are dependent upon NTP structure. The magnitude of some of the rate constants may vary as much as

20 fold with different nucleoside triphosphates.

The step sizes calculated from muscle fiber shortening experiments or in-vitro motility assays and pre-steady state measurements in solution give a constant value (4 ~ 6 nm), which is independent of the NTP structure (for ATP, CTP, mant-ATP and mant-CTP) and protein species (for acto-RS.HMM and acto-BV.myosin). This indicates that the geometric constraints of the myolattice and/or high concentration of actin and myosin in the fibers does not significantly affect the rate of NTP binding. The step size, as a structural parameter, is a more fundamental property of the actomyosin interaction.

The rate constant of the dissociation of nucleoside diphosphate (NDP) from actomyosin, the equilibrium constant of NDP to actomyosin (K_i), and the binding rate constant of NDP to actomyosin are all dependent upon the structure of NDP.

A large fluorescence decrease observed in actin binding to rabbit skeletal myosin-S1-mant-NDP is thought to measure the conformation change preceding mant-NDP release, the slowest step in this reaction.

The release of mant-ADP from acto-bovine cardiac myosin-S1, the rate-limiting step in this reaction, is also accompanied by fluorescence decrease. The dissociation of acto-S1-mant-NDP limited by different steps is a significant difference between skeletal and cardiac muscle contraction mechanisms.

DEDICATION

This dissertation is dedicated

to the memory of my grandmother,

Liang-Jue Yu

whom I love most and pay special respect to.

ACKNOWLEDGEMENTS

I especially wish to thank Dr. Howard D. White, my advisor, who guided me into the realm of science, and gave me advice, support with which I am able to finish my Ph.D training.

I also wish to thank the rest of my committee members: Dr. Frank Lattanzio, Dr. Laura Moen, and Dr. Paul Ratz, for their advice and help on my research and invaluable suggestions and comments on my dissertation.

To the faculty, staff, and graduate students in Department of Biochemistry, I extend my sincere thanks for their kindness and friendship, especially, Betty Belknap, for her generous help on my research.

Thanks are also given to my parents, Yu Jiang and Qinlin Wei, my wife, Pei He, and my M.S. advisor Xue-zhong Zhang, for their emotional support and encouragement.

TABLE OF CONTENTS

LIST OF TABLES

LIST OF FIGURES

INTRODUCTION

I. BACKGROUND

General Description of Muscle Contraction

Muscle contraction is thought to be accomplished by the interaction of two proteins, actin and myosin. In striated muscle, actin monomer (MW. 42 kd) polymerizes with regulatory proteins, troponin and tropomyosin, to form a filament structure in physiological conditions. Myosin consists of six polypeptide chains: two identical heavy chains (each about 230 kd), and four light chains (each about 20 kd). The N terminus of each heavy chain forms a globular head, known as S1, which contains actin-activated ATPase activity. Each myosin head contains two light chains. The rest of the two heavy chain forms an alpha-helical coiled-coil tail. In skeletal muscle, myosin molecules assemble bi-directionally to form a filament structure.

Each functional unit of skeletal muscle, designated as a sarcomere, consists of actin "thin filaments," with each filament attached to one peripheral region, known as "Z line," and myosin "thick filaments" in the middle of the sarcomere. The myosin thick filaments partially overlap with actin thin filaments, sliding past each other during muscle

contraction in the presence of ATP as an energy source.

A crossbridge model has been proposed to describe the mechanism of muscle contraction (Huxley, 1969). The basic steps are shown in Model 1.

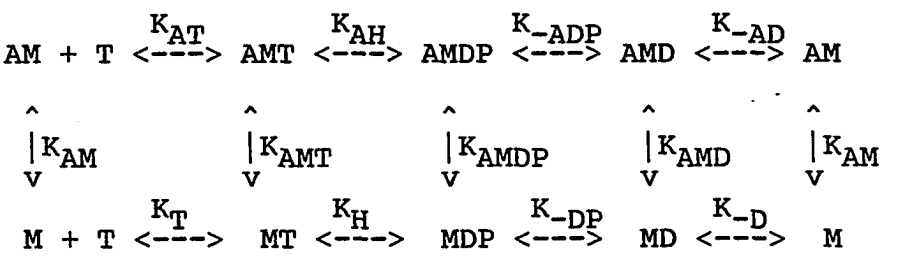

Model 1

Here A=actin, M=myosin-S1, T=ATP, D=ADP, P=phosphate, K's are equilibrium constants.

In resting striated muscle, the functional interaction of myosin heads with actin filaments is inhibited by regulatory proteins, troponin and tropomyosin. Myosin heads bind ATP and hydrolyze it into ADP and phosphate, which then dissociate slowly. When muscle is stimulated to contract, the S1 heads extend from the thick filaments and attach to actin units on thin filaments. Then, phosphate is released from the actomyosin-ADP-Pi complex, and myosin-S1 heads concomitantly change in structure. This change in orientation of S1 relative to actin is thought to cause the power stroke, during which the thin filament is pulled a distance called "step size." The dissociation of ADP at the end of the power stroke and the subsequent binding of ATP reverses the conformational change in myosin-S1 and leads to rapid release of myosin-S1 from actin. Finally, the bound

ATP is hydrolyzed by myosin-S1, which then resets itself for the next interaction with the actin filaments (Stryer, 1988). This model has been supported by considerable experimental evidence, while some aspects of this model still remain unproved.

The Structure of Myosin-S1

The primary structure of myosin

There is extensive information about the sequence similarity between different myosins (Nyitray et al., 1991). There is a relatively large degree of sequence similarity between myosins of all types and very high degree of similarity between related myosins. For example, there is 80 percent sequence similarity between the heads of two fairly distantly related vertebrate striated myosins, chicken skeletal (Maita et al., 1991) and rat cardiac myosin, and a 93 percent sequence similarity between the head portions of alpha and beta isozymes of rat cardiac myosin (McNally et al., 1989). The difference between the sequence of the alpha and beta isozymes of rat cardiac myosin heavy chain is shown in Figure 1(A). The vertical lines show the position of sequence differences. Most of the sequence differences come in five clusters from 2-38; 210-216; 304-350; 618-637; 793-814. The sequences between the cluster are highly conserved and contain several areas that are highly conserved among

Fig. 1. Structural information of myosin-S1. (A) The difference between the sequence of the alpha and beta isozymes of rat cardiac myosin heavy chain. (B) The difference between the sequence of chicken skeletal and rat cardiac alpha myosin heavy chain. The vertical lines show the position of sequence differences (White, H.D., personal communication). (C) The three dimensional structure of myosin-S1 obtained from X-ray diffraction studies (Rayment et al., 1993b).

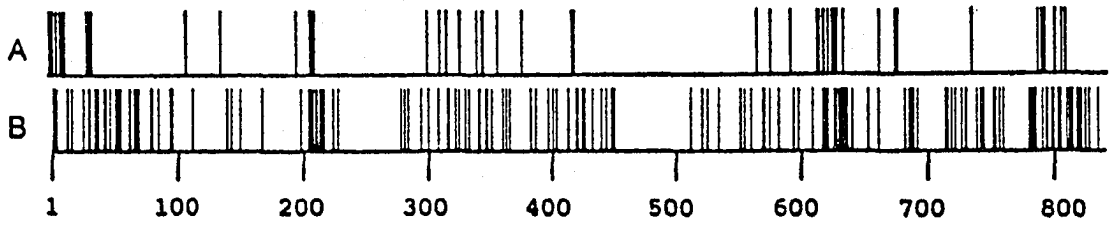

C

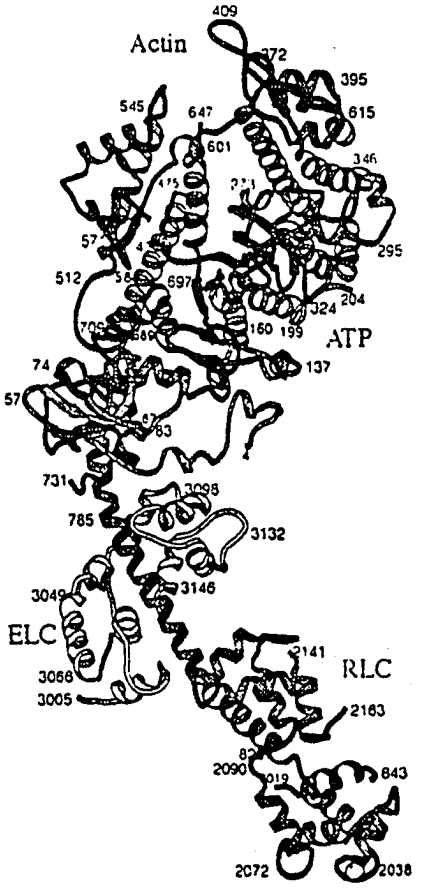

all myosins (Nyitray et al., 1991). A similar comparison between the sequence of chicken skeletal and rat cardiac alpha myosin is shown in Figure 1(B). The differences between these two myosins are more extensive with additional changes appearing in the regions from 60-100; 400-450; 745-800; 815-860 and 880-930.

The secondary and tertiary structure of myosin-S1

Myosin-S1 domain structure was approached using limited proteolysis, and three proteolytic fragments (25 kd, 50 kd and 20 kd, arranged from N to C terminus) were obtained. The 50 kd and 20 kd fragments and their junctions are involved in actin binding (Mornet et al., 1979, 1981; Sutoh, 1982), while ATP binds to 25 kd fragment (Szilagyi et al., 1979).

Recently, myosin-S1 crystal structure was demonstrated using X-ray diffraction at 2.8 Å resolution (Rayment et al., 1993b). Figure 1(C) shows the ribbon diagram of the myosin-S1 head with the actin and nucleotide binding sites indicated. Myosin-S1 (the mixture of A1 and A2 isozymes) was prepared from papain digested chicken pectoralis myosin and methylated at lysine residues. The current model contains 1072 of 1157 amino acids. The myosin head is a very asymmetrical molecule with a globular portion containing the actin and ATP binding sites and an alpha helical tail to which the essential (ELC) and regulatory (RLC) light chains are bound. An alpha helix from Asp 327 to Ile 340 forms the top of the nucleotide binding cleft; Gly 179 begins a phosphate binding loop that is followed by an alpha helix at

the base of the nucleotide cleft; a large loop from Thr 667 to Glu 687 forms the end of the nucleotide binding site. Two alpha helices, His 688 to Asn 698 and Val 700 to Arg 708, occupy a position underneath the nucleotide binding site. Several amino acids previously located by chemical labeling, Trp 131, Ser 243 and 324 (Yount et al., 1992; Grammer and Yount, 1991), are located in the vicinity of the active site. The loop between residue 204 and 216 is not visible in the electron density map. This sequence forms the junction between 25-50 kd and is located at the opening of the active site cleft.

Reductive methylation of myosin-S1 is required for crystallization (Rayment et al., 1993b). In this process, 97 percent of the lysine residues in native myosin-S1 were converted to dimethyllysine without detectable modification of other amino acid side chains. The enzyme is catalytically active, and the changes in the kinetic mechanism produced by reductive methylation of lysine are qualitatively and quantitatively similar to the changes induced by either SH1 modification or substrate analogs such as GTP (White and Rayment, 1993).

The muscle contraction mechanism based on structural information

Based on the demonstrations of the structures of actin (Kabsch et al., 1990) and of myosin-S1 at high resolution (Rayment et al., 1993b), a mechanism by which the interaction between actin and myosin produces motion and

force in muscle was proposed (Rayment et al., 1993a). Myosin-S1 crystal structure shows a cleft which divides the 50 kd fragment into upper and lower domains. The opening and closure of this cleft was thought to play an important role in the communication between actin binding site and nucleotide binding site. They proposed that the closure of this cleft causes strong binding of myosin-S1 to actin in the absence of ATP. ATP binding to myosin-S1 is a two-step reaction. First, the binding of phosphates and ribose moiety of ATP to myosin-S1 causes cleft opening, disrupting the strong binding between myosin-S1 and actin. Second, the closure of the nucleotide binding pocket around the base causes complete dissociation of actin from myosin-S1. After ATP hydrolysis, actin re-associates with myosin-S1 by stereospecific interaction of its lower domain with actin. Then, incorporation of the upper domain and closure of the cleft causes strong binding and product release.

The two-step model of ATP binding to acto-S1 was supported by Biosca et al. (1994). They claimed an observation of a fast rate of 300 s^{-1} and a slow rate of 49 s^{-1} at 100 μM ATP, 50 mM ionic strength (pH 8) and 40 percent ethylene glycol at 15°C using stopped-flow and rapid flow quench. The fast rate, which is caused by the binding of the phosphate moiety of ATP to acto-S1 and dissociation, varies linearly with ATP concentration; while the slow rate, caused by the closure of the nucleotide binding pocket on myosin-S1, is saturated with maximum rate 63 s^{-1} and $K_{0.5}$ 28 μM.

The Kinetic Research of Crossbridge Model

The studies on myosin-S1 ATPase hydrolytic pathway

The detailed mechanism of ATP hydrolysis by myosin-S1 is shown in Model 2.

$$M+T \overset{K'_1}{<-->} MT \overset{k'_2}{<-->} M^*T \overset{k'_{2a}}{<-->} MD^{**}P \overset{k'_3}{<-->} M^*DP \overset{k'_4}{<-->} M^*D+P \overset{k'_5}{<-->} MD \overset{k'_{5a}}{<-->} M+D$$

Model 2

Here, M=myosin, T=ATP, D=ADP, P=phosphate, k's and K are rate and equilibrium constants, respectively. * and ** represent different fluorescence levels.

ATP binding to myosin-S1 is thought to be a two-step process: an intermediate is formed (K'_1 = 4.5x10^3 $M^{-1}s^{-1}$ at 21^{o}C, 0.1 M KCl, 5 mM $MgCl_2$, 50 mM Tris, pH 8), followed by a conformation change (k'_2 = 400 s^{-1}) which causes its intrinsic fluorescence change (Bagshaw et al., 1974). ATP hydrolysis by myosin is a reversible step (k'_{2a} > 160 s^{-1}, K'_{2a} = 9 at 20^{o}C, pH 8) (Lymn and Taylor, 1971; Bagshaw and Trentham, 1973), and is also accompanied by an intrinsic fluorescence change, since a biphasic fluorescence increase was observed upon mixing ATP and S1 in high ATP concentration and lower than 10^{o}C (Johnson and Taylor, 1978).

The release of phosphate from myosin-S1 is a two-step reaction (k'_3 = 0.06 s^{-1}, k'_{-3} > 3x10^{-9}, K'_4 > 1.5 mM), so is the release of ADP (k'_5 = 1.4 s^{-1}, k'_{-5} = 400 s^{-1}, K'_{5a} = 2.7x10^{-4}M) (Bagshaw et al., 1974). The product release from myosin-S1 limits the steady state rate of ATP hydrolysis.

The intrinsic fluorescence change also occurs in the release of phosphate and ADP (Trentham et al., 1972; Bagshaw and Trentham, 1973; Bagshaw et al., 1974).

The studies on actomyosin-S1 ATPase hydrolytic pathway

The detailed mechanism of the interaction of actomyosin-S1 with ATP was shown in Model 3.

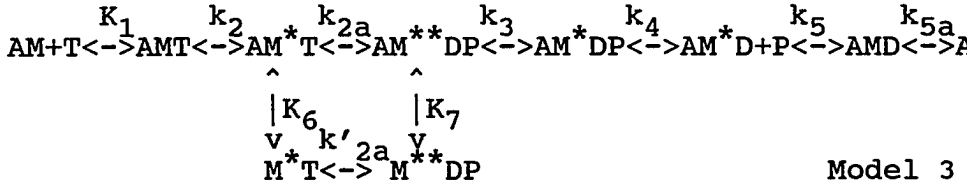

Model 3

Here, A=actin, M=myosin, T=ATP, D=ADP, P=phosphate, k's and K's are rate and equilibrium constants, respectively. * and ** represent different fluorescence levels.

ATP binding to actomyosin-S1 is rapid and produces a rapid dissociation (>1000 s^{-1}) of myosin-S1 from actin in dilute solution (White and Taylor, 1976). The myosin-S1 intrinsic fluorescence change preceding the dissociation caused by ATP binding to acto-S1 is too fast to be observed (Johnson and Taylor, 1978).

Although ATP is hydrolyzed through the dissociating pathway (M^*T <--> $M^{**}DP$, the lower row in Model 3) in dilute solution, the hydrolysis through the non-dissociating pathway (AM^*T<--> $AM^{**}DP$, the upper row in Model 3) does occur at high actin concentration, and the ATPase activity of myosin-S1 (A1 isozyme) is inhibited by high concentration of actin (Rosenfeld and Taylor, 1984; White et al., 1993). The hydrolysis step is rate limiting for skeletal acto-S1 ATP hydrolysis (Belknap et al., 1992).

After ATP hydrolysis, actin re-associates with S1-ADP-phosphate complex and increases the rate of product release by more than 100 fold (Lymn and Taylor, 1971). A simple system is used to study the model of actin binding to myosin-S1-ADP. This reaction is a multi-step process: a collision complex (AMD) is formed and followed by two isomerization forms, the attached state (A-MD) and the rigor-like state (A.MD) (Geeves and Gutfreund, 1982; Criddle et al.,1985; Coates et al., 1985)(Model 4):

$$A + MD \underset{}{\overset{}{\longrightarrow}} AMD \overset{a}{\longrightarrow} A\text{-}MD \overset{b}{\longrightarrow} A.MD$$

Model 4

here A, M and D are F-actin, myosin-S1 and ADP, respectively; Step b is fluorescence sensitive and is monitored when pyrene-actin is used in pressure-relaxation studies, while light scattering monitors step a.

Woodward et al.(1991) claimed that they observed the attached state and rigor-like state by dissociating rabbit skeletal acto-S1-2'(3')-o-(N-methylanthraniloyl)-ADP (acto-RS.S1-mant-ADP) (Fig. 2) with ATP. A fast light scattering decrease and a slow fluorescence decrease in this reaction were assigned to dissociation of rigor-like state (A.MD) and conversion of attached state (A-MD) to rigor-like state, respectively. The attached state dissociates much slower than rigor-like state does.

Phosphate release from actomyosin is thought to be a two-step reaction, in which force generation is involved (Kawai

Fig. 2. The structure of methylanthraniloyl derivatives of nucleoside triphosphate and nucleoside diphosphate (mant-NTP and mant-NDP).

mant-ATP: B = Adenine, n = 2;
mant-CTP: B = Cytosine, n = 2;
mant-GTP: B = Guanine, n = 2;

mant-NTP: n = 2;
mant-NDP: n = 1.

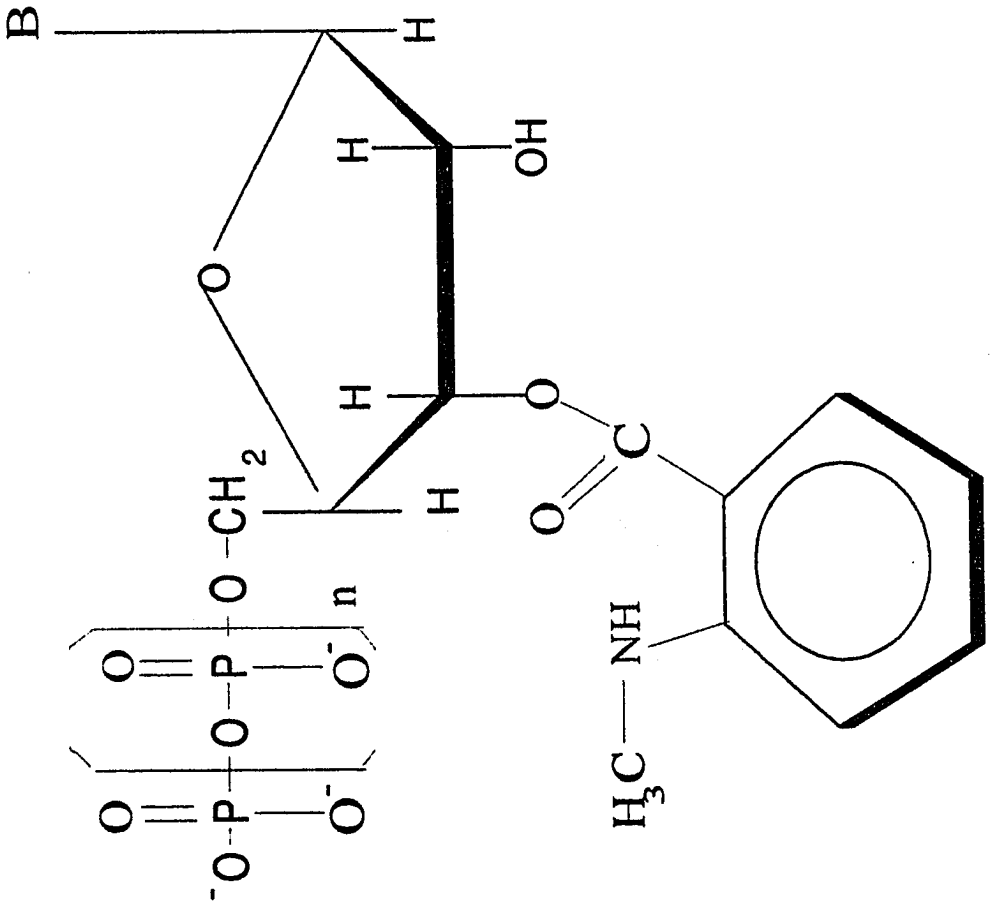

and Halvorson, 1991). An isometric force decrease was observed when orthophosphate was incorporated into actomyosin-ADP state in skinned muscle fiber (Hibberd et al., 1985; Millar and Homsher, 1990), although excess phosphate would not affect the rate of acto-S1-ADP dissociation by ATP in solution (White, H.D., unpublished data).

The initial evidence for more than one actomyosin-S1-ADP intermediate in the hydrolytic pathway was that the rate of catalysis of medium phosphate into ATP by rabbit skeletal actomyosin-S1 was found to be independent of ADP concentration (in the range of 2 - 5 mM ADP, Sleep and Hutton, 1980). This indicates that phosphate does not exchange into medium ATP by binding directly to the equilibrium acto-S1-ADP intermediate (AMD in Model 3), which is formed by adding ADP to actomyosin-S1. The exchange reaction must therefore, predominantly occur by phosphate binding to another acto-S1-ADP intermediate (AM^*D in Model 3) that is present during steady state hydrolysis.

In cardiac muscle, ADP release is thought to be the rate-limiting step for acto-S1-ADP complex dissociation by ATP, and presumably, also limits the rate of crossbridge detachment and the unloaded shortening velocity in contracting muscle (Siemankowski et al., 1985).

Relationship between shortening velocity and the rate of ATP hydrolysis

A criterion for a step to limit shortening velocity is that this step be on the non-dissociating kinetic pathway (the upper row in Model 1)(Siemankowski and White 1984), while ATP hydrolysis mainly occurs in the dissociating pathway in dilute solution (the lower row in Model 1). Although the rates of actomyosin ATP hydrolysis and shortening velocity both increase or decrease together, there is no evidence that the rate of ATP hydrolysis directly limits shortening velocity. Barany (1967) found that the temperature dependence of the shortening velocity had a Q_{10} (the ratio of activation energy at temperature of T + 10 and T) of 2-3, whereas the Q_{10} of actomyosin ATP hydrolysis was 4-5. The different temperature dependence of the rate of ATP hydrolysis and shortening velocity suggests that they are not limited by the same process. Subsequently, the evidence was found for good correlation between the rate of force development and the maximum rate of ATP hydrolysis, rather than between shortening velocity and rate of ATP hydrolysis (Brenner and Eisenberg, 1986; Burton and Sleep, 1987).

Relationship between rate constants measured for the mechanism of actomyosin ATP hydrolysis in solution and those in contractile apparatus of muscle

Some of the rate constants of the nucleotide hydrolysis mechanism in myofibrils were measured for comparison with

those obtained with actomyosin-S1 in solution. The relatively small enhancement of tryptophan fluorescence observed in myofibrils prevents a detailed kinetic analysis of the mechanism of ATP hydrolysis in myofibrils (White, 1985), so that a fluorescent ATP analog 1,N^6etheno-2-aza-ATP (aza-ATP) was chosen to study this reaction (Smith and White, 1985a&b). The time course of nucleotide fluorescence (emission at 420-450 nm) measured in a front-face stopped-flow cell upon mixing aza-ATP with bovine cardiac myofibrils, is essentially the same as that measured with bovine cardiac acto-S1. This work indicated that the measurement of molecular rate constants of the nucleotide binding steps in the mechanism are unperturbed by the three dimensional structure of the contractile lattice. Goldman et al. (1982) observed that the rate constants of binding of ATP released from caged ATP to crossbridges in muscle fibers is 10-20 fold slower than those obtained in solution, but more recent data indicate that the rate may have been inhibited by binding of ADP or caged ATP to the active site (Thirlwell et al., 1993).

The dependence of the rate and equilibrium constants in muscle contraction mechanism upon the structure of nucleotides Actomyosin is a relatively nonspecific enzyme and can use the energy from a series of nucleoside triphosphates (NTP) to produce tension and work (Weber,1969; Tonomura, 1973; Eccleston and Trentham, 1979). The dependence of the rate and equilibrium constants upon

different nucleotides in skinned muscle fiber was measured by Pate et al. (1993). The data show that the maximum unloaded shortening velocity (V_m) and the K_m do depend upon the structure of substrates. From our previous experiments in solution, the magnitude of some of the rate and equilibrium constants varies by as much as 20-fold with different nucleoside triphosphates (White et al., 1993).

The measurement of step size

The step size, the distance over which crossbridges remain attached to actin in a muscle contraction cycle, is one of the fundamental properties in the muscle contraction mechanism. The step size was either estimated from structural information (Hanson and Huxley, 1955; Huxley, H.E. 1964; Huxley, H.E. 1969; and Huxley, A.F. 1957), or calculated using experimental results (Ford et al., 1977; Toyoshima et al., 1990). Its value was generally thought to be no more than a few tens of nanometers, or even smaller (Huxley and Kress, 1985).

Although the values of the step size mentioned above seem to be consistent, some challenging data were obtained by observing the movement of fluorescently labeled actin filaments in shortening myofibrils (Yanagida et al.,1985), or in an in-vitro motility assay in which the myosin were immobilized on a silicone-treated surface (Harada et al.,1990). In these studies, sliding velocity and ATPase activity were measured. The sliding distance of actin filament induced by one ATP hydrolysis was calculated to be

in the range of 60 - 200 nm. However, a sliding distance of 5 - 28 nm per ATP hydrolyzed was obtained by Uyeda et al. (1990) using a similar assay system, which is more consistent with conventional crossbridge theory. This controversy has attracted considerable attention recently (Burton, 1992). The measurement of step size with various nucleotides is very important for the comparison of the properties of biochemical steps in solution with the force generation mechanism in muscle fiber.

II. THE SPECIFIC AIMS OF THIS RESEARCH

The long-term aim of this research is to use the dependence of rate and equilibrium constants of the various steps in the mechanism upon nucleotide structure as a probe to investigate the dependence of the mechanical properties of the muscle upon changes in different biochemical steps of the mechanism in solution. The research presented in this dissertation can be divided into following aspects:

I) the measurement of rate and equilibrium constants for each step in solution, in which i) the dissociation of actomyosin-S1 (or acto-HMM) by NTP and mant-NTP is to test the steps of NTP (or mant-NTP) binding to actomyosin, actin dissociation from myosin-NTP, and myosin-S1 conformation change preceding and/or after actomyosin dissociation; ii)

the dissociation of nucleoside diphosphate (NDP) or mant-NDP from actomyosin-S1 (or acto-HMM) by ATP is to measure the dissociation rate constant and equilibrium constant of NDP (or mant-NDP) to actomyosin; iii) actin binding to myosin-S1-mant-NDP is to test the conformation changes preceding the mant-NDP release step and possibly, the different forms of actomyosin-NDP states.

II) The measurement of the dependence of velocity upon structure and concentration of the NTP in in-vitro motility assays. In-vitro motility assays can be used to determine the dependence of velocity upon NTP concentration in a similar manner to skinned fibers. This method can also be used to test the influence of myolattice on the muscle contraction mechanism since there is no myolattice structure in the in-vitro motility assay. Besides, the in-vitro motility assay is an advantage in motility measurement of cardiac HMM, since cardiac muscle fibers are not parallel and can't be easily dissected into bundle suitable for mechanical experiments.

III) The preparation of bovine cardiac HMM is preferable for the kinetic investigation of acto-BV.myosin, since the structure of cardiac HMM is more similar to that of cardiac myosin than cardiac myosin-S1. Also, cardiac HMM (but not cardiac S1) can be used for in-vitro motility measurement. The kinetic investigation of cardiac actomyosin is important because it has different kinetic properties from skeletal actomyosin due to its different physiological functions.

Cardiac actomyosin also has slower rate constants of some steps at the hydrolysis mechanism which can't be easily measured for skeletal actomyosin.

The pre-steady state and steady state kinetics of bovine cardiac HMM were determined to evaluate and characterize the cardiac HMM preparation. This includes i) steady state ATPase activity and steady state binding of BV.HMM to actin in saturated ATP; and ii) the burst kinetics of ATP hydrolysis by acto-BV.HMM using quench-flow technique.

MATERIALS AND METHODS

I. Kinetic Methods

Pre-steady state measurements of changes in light scattering at 90 degrees, and in fluorescence were made with an Applied Photophysics stopped-flow fluorimeter (Leatherhead, United Kingdom) illuminated by a 100-watt mercury arc lamp. The excitation wavelength was selected with a 0.124-m monochrometer (Farrand Corp). Data points were collected with a Nicolet Explorer III digital oscilloscope and transferred to a Sharp 480-3 PC for permanent storage and analysis.

1. The dissociation of acto-S1 (or acto-HMM) by NTP (or mant-NTP) was measured by observing light scattering change and fluorescence change simultaneously upon mixing acto-S1 (or acto-HMM) with various concentrations of NTP (or mant-NTP) in the stopped-flow. The excitation and emission wavelengths used for light scattering and fluorescence measurement were listed in Table I. Improved signal/noise ratios were obtained by averaging several traces. Each time course was fit to single or double exponential equations as

Table I. The excitation and emission wavelengths used for light scattering and fluorescence measurement of the dissociation of acto-S1 (or acto-HMM) by NTP (or mant-NTP).

	excitation(nm)	emission(nm)
Light scattering	365 (for aza-ATP) 295 (the rest of the NTP or mant-NTP)	same as excitation
Intrinsic tryptophan fluorescence	295	320 - 380
aza-ATP fluorescence	365	> 400
mant-NTP fluorescence	295	> 400

follows:

single exponential $I(t) = Ie^{-kt} + C$ Eq. 1

double exponential $I(t) = I_a e^{-kat} + I_b e^{-kbt} + C$ Eq. 2

Here I's and k's are amplitude and rate constants, respectively. C is a constant.

Single exponential fitting represents a simple reaction as follows:

$$S \xrightarrow{k} P$$

Here, S=substrate, P=product, and k is a rate constant.

Double exponential fitting represents the sum of two events, which is a complicated situation and sometimes its physical meaning is difficult to interpret.

The hyperbolic dependence of observed rate constant, k(obs), upon NTP concentration was fit to equation 3 for the simplest models.

$$k(obs) = Vmax/ (1 + K_{0.5}/X) \quad \text{Eq. 3}$$

Here Vmax is maximum rate, $K_{0.5}$ is the apparent equilibrium constant (the concentration of the variable at which the rate reaches 0.5Vmax), X is the concentration of the variable.

The possible reaction models were analyzed using a computer program (Zhang et al., 1989). In the model fitting, a candidate model was chosen, and the known rate constants for each step were input into the computer. The dependence

of amplitude coefficient upon the variable concentration was calculated and compared with experimental data. The criterion for a desirable model is that the theoretical dependence of amplitude coefficient upon the variable concentration matches the experimental one.

2. The dissociation of actomyosin-NDP and actomyosin-mant-NDP by ATP was measured by observing the light scattering change and fluorescence change in stopped-flow. The excitation and emission wavelengths used for light scattering and fluorescence measurement were listed in Table II. Each time course was fit to single exponential equation (Eq. 1). The $k_{(obs)}$ was plotted against ATP concentration and fit to equation 3. The equilibrium constant (K_i) for NDP (or mant-NDP) binding to acto-S1 (or acto-HMM) was calculated using equation 4.

$$K_i = [NDP]/\{(V_{max}/K_{0.5})_o/(V_{max}/K_{0.5})-1\} \qquad \text{Eq. 4}$$

Here $(V_{max}/K_{0.5})_o$ and $(V_{max}/K_{0.5})$ are apparent second-order rate constants in the absence or presence of nucleoside diphosphate, respectively.

The second order rate constant of NDP binding to actomyosin, k_{AD}, was calculated using equation 5:

$$k_{AD} = k_{-AD}/K_i \qquad \text{Eq. 5}$$

3. Actin binding to myosin-mant-NDP was measured by observing the fluorescence change (excitation and emission wavelengths 295 nm and greater than 400 nm, respectively) at various actin concentrations in stopped-flow. Each time

Table II. The excitation and emission wavelengths used for light scattering and fluorescence measurement of the dissociation of actomyosin-NDP and actomyosin-mant-NDP by ATP.

	excitation(nm)	emission(nm)
Light scattering		
actomyosin-NDP	435	435
actomyosin-mant-NDP	295	295
Fluorescence		
actomyosin-mant-NDP	295	> 400

course was fit to single exponential or double exponential equations (Eq. 1 or Eq. 2). The $k_{(obs)}$ was plotted against actin concentration and fit to equation 3. The possible reaction models were analyzed using a computer program (Zhang et al., 1989).

4. The pre-steady state hydrolysis of ATP by myosin-S1 or acto-S1 was measured using quench-flow technique. Myosin-S1 or acto-S1 was mixed with equal volume of gamma-^{32}P-labeled ATP at various time intervals, then quenched with 2 N HCl and 0.35 M NaH_2PO_4.^{32}P-ATP was adsorbed with charcoal, and the radioactivity in supernatant and entire solution was counted. The ratio of counts hydrolyzed over total counts was plotted against time and fit to single or double exponential equations (Eq.1 or Eq. 2). This ratio is a measurement of the fraction of ATP hydrolyzed.

5. Steady state nucleoside triphosphate hydrolysis was measured using a colorimetric procedure (White, 1982) from at least four time points/actin concentration by the method of initial rates. The data were then fit to equation 3 to calculate $K_{0.5}$ and Vmax.

II. In-vitro Motility Measurement and Step Size Calculation

The in-vitro motility assay was measured following the method of Kron et al.(1991). RS.HMM and BV.myosin were immobilized on a glass surface coated with nitrocellulose (for RS.HMM), or dimethyldichlorosilane (diluted 1:50 v/v in

chloroform)(for BV.myosin). Actin filaments were labeled with the fluorescently active reagent tetramethylrodamine-phalloidin. In the presence of NTP (or mant-NTP), the movement of actin filaments was observed and video-taped under an image intensified fluorescence microscope (X400, Nikon), and analyzed using the computer program "Motion Submenu" of "Image"(Revised for specific use, by Larry Phillips of Universal Imaging Co.). The $k_{(obs)}$ was plotted against NTP concentration and fit to equation 3.

In muscle fiber shortening experiments, the minimum rate constant for the dissociation of strongly attached crossbridge states, k_{min}, can be calculated from the half-sarcomere length SL (1100 nm), the maximum shortening velocity, V_m (SL/sec.), and the step size, D, over which crossbridges can remain attached to actin, using equation 6 (Siemankowski et al., 1985).

$$k_{min} = V_m.SL/D \qquad \text{Eq. 6}$$

In in-vitro motility assay, the term $V_m.SL$ (μm/sec.) is directly obtained from image analysis. The apparent second order rate constant of nucleoside triphosphate binding to crossbridge in myofibrils is equal to that of nucleoside triphosphate binding to acto-S1 in solution (Smith and White, 1985a). It is therefore reasonable to equate the second order rate constant of nucleoside triphosphate

binding to acto-S1 in solution, k_a/K_o, with the second order rate constant of nucleoside triphosphate binding to crossbridge in in-vitro motility assay or muscle fiber shortening experiment, k_{min}/K_m (equation 7a and 7b). Equation 7b is obtained by substitution of k_{min} from equation 6 to equation 7a.

$$k_a/K_o = k_{min}/K_m \qquad \text{Eq. 7a}$$

$$k_a/K_o = V_m.SL/D.K_m \qquad \text{Eq. 7b}$$

Re-arrangement of equation 7b to equation 8 provides a simple method to determine the step size D (White et al., 1993).

$$D = SL.(V_m/K_m)/(k_a/K_o) \qquad \text{Eq. 8}$$

III. Protein Preparation, Purification and Characteristics

1. Rabbit skeletal actin and myosin were prepared as previously described (White and Taylor, 1976). The RS.S1 and RS.HMM were prepared from RS.myosin with chymotrypsin digestion by the method of Weeds and Taylor (1975) except that in myosin-S1 preparation, 2 mg of lima bean trypsin inhibitor/mg of chymotrypsin was used to inhibit chymotrypsin. In RS.HMM preparation, 5 mM $MgCl_2$ rather than 1 mM EDTA was used in digestion system. Then, RS.S1 or RS.HMM was purified on DEAE-cellulose column (50 mM

imidazole-HCl, pH 7.0, 1 mM DTT, gradient KCl 0 - 0.1 M for RS.S1, 50 mM - 0.25 M for RS.HMM). RS.HMM was eluted in a single peak, while RS.S1 was shown in two partially overlapped peaks, from which two isoforms of RS.S1, A1 and A2, and a mixture of approximately equal amount of A1 and A2 were obtained.

2. Bovine cardiac HMM preparation followed Margossian's method (1985) with the following changes:

a). In BV.myosin preparation, after Triton X-100 treatment and buffer wash, the extraction supernatant was dialyzed against 10x volume of 10 mM potassium phosphate (pH 6.2) overnight to precipitate myosin.

b). After the first DEAE column, purified myosin solution was dialyzed against 30 mM KCl, 10 mM potassium phosphate (pH 6.3) with one change. Precipitated myosin was spun and re-suspended in 0.6 M KCl, 2 mM MgCl2, 1 mM DTT, and 10 mM Tris-HCl(pH 7.6). The myosin concentration was 4 - 5 mg/ml.

3. The binding constant of BV.HMM to actin during steady state ATP hydrolysis was measured as follows: BV.HMM (0.025 mg/ml) was spun with various concentrations of actin (0 - 25 μM) in the presence of 1 mM ATP, 15^{o}C, 45000 rpm for 20 min. The aliquots of supernatant were taken out to test ATPase activity at 25^{o}C. The ATPase activity (Y) was plotted against actin concentration (X) to calculate the binding constant (C_{bind}) using equation 9.

$$Y = C1(1-1/(1 + C_{bind}/X)) \qquad \text{Eq. 9}$$

IV. The Nucleoside Di- and Triphosphates

ATP (disodium salt, from equine muscle), CTP (sodium salt, type VII), GTP (sodium salt, type III), 2′-dATP (disodium salt), UTP (type III), AMP-PNP (tetralithium salt), ADP (from equine muscle, grade IX), CDP (type I), GDP (sodium salt, type I), 2′-dADP (sodium salt), and $A_{p5}A$ were all purchased from Sigma Chemical Co. Aza-ATP as a gift from Betty Belknap, was synthesized and purified as previously described (Smith and White, 1985b). Mant-nucleotides were prepared and purified following Hiratsuka's method (1983). Since mant-GTP could not be separated from GTP by chromatography over a Sephadex LH-20 column, an additional DEAE-cellulose column (2.2 X 20 cm, for 0.7 mmol GTP substrate) was used. Mant-GTP was eluted with 10 mM to 0.8 M triethylammonium bicarbonate (Neal et al, 1990; Woodward et al, 1991), collected and lyophilized. The salt was removed by three additions and evaporations of methanol in a nitrogen atmosphere at room temperature.

The extinction coefficient of mant-CDP was measured as described by Hiratsuka and Uchida (1973). Basically, acid-labile phosphate in CDP or mant-CDP was released in 1 M HCl at 100°C for 8 min, and determined by a colorimetric procedure as described earlier (White, 1982). CDP was chosen as a standard, with extinction coefficient 9144 $M^{-1}cm^{-1}$ at pH 7.0. The absolute concentration of mant-CDP was determined by measuring acid labile phosphate released from

mant-CDP, assuming that the percentage of acid-labile phosphate released from mant-CDP was equal to that from CDP.

V. Miscellaneous Chemical and Biochemical Reagents

Tetramethylrodamine-phalloidin and N-methylisatoic anhydride were purchased from Molecular Probes. Nitrocellulose solution was from Ernest F. Fullam Inc. Dimethyldichlorosilane, glucose oxidase, catalase were purchased from Sigma. Other chemical reagents were purchased from Sigma with various grades: dithiothreitol (DTT), 99 percent, molecular biology; 3-[N-morpholino]propane sulfonic acid (MOPS), 99.5 percent; magnesium chloride hexahydrate, cell culture tested; imidazole, 99 percent, recrystallized; potassium acetate, ACS reagent; the rest of the chemicals were not lower than chemical reagent grades. Distilled water was prepared by deionization and distillation.

RESULTS

The Light Scattering Measurement of Actomyosin Dissociation by Nucleoside Triphosphates and Nucleoside Triphosphate Analogs

The kinetics of dissociation of actomyosin-S1 (or acto-HMM) by nucleoside triphosphates (NTP or mant-NTP) was measured by observing light scattering and fluorescence changes simultaneously at different conditions for accompanying muscle fiber contraction or in-vitro motility assay experiments. The light scattering measurement of this reaction is to investigate the binding of NTP (or mant-NTP) to acto-S1, and acto-S1 dissociation. The biochemical steps expected to be involved in this measurement were indicated in bold in the following simplified model (Model 1a).

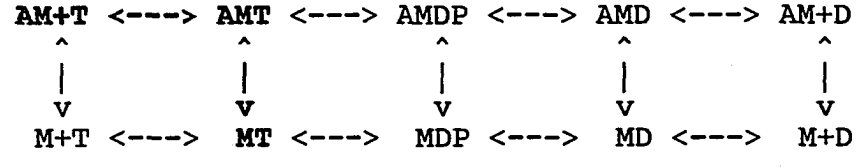

Model 1a

Here, A=actin, M=myosin, T=ATP, D=ADP, P=phosphate.

The time courses in light scattering measurement were fit to single exponential equation for simplified analysis, and the observed rate constant, $k_{(obs)}$, was plotted against NTP

concentration. Actually, the light scattering time courses measured in high ionic strength conditions were fit well to single exponential equation, while the double exponential time courses were observed at very low ionic strength condition (5 mM MOPS buffer, pH 7, unpublished data of mine). The double exponential time courses in light scattering and fluorescence measurement were also observed previously by Smith and White (1985b). It was thought that ionic strength, the species of myosin-S1 and the types of NTP are the factors which may affect the shape of the time course. A possible mechanism for double exponential light scattering time course is that myosin-S1-ATP is only partially dissociated from actin in the rapid phase, and that the slower phase follows hydrolysis to myosin-S1-product. The evidence to support this mechanism is that the rate of slow component of light scattering is similar to that of NTP hydrolysis. This tends to occur especially for acto-BV.S1 at low ionic strength since the binding of actin to BV.myosin-S1-ATP is strong in low ionic strength condition (Walker et al., 1994).

The time courses of the decrease in light scattering upon mixing rabbit skeletal actomyosin-S1 (acto-RS.S1) with 100 μM of ATP, CTP, aza-ATP or GTP is shown in Fig. 3. The experimental conditions are the same as used in skinned fiber contraction experiments (Pate et al., 1993). Since the isolated A1 and A2 isozymes of myosin-S1 gave identical results (White et al., 1993), a mixture of two isozymes was

Fig. 3. The time courses in light scattering measurement of the dissociation of acto-RS.S1 by ATP, CTP, GTP, and aza-ATP. Final concentrations in stopped-flow cell were 1.5 μM F-actin, 1 μM myosin-S1 (mixed A1 and A2 isozymes), 0.18 M potassium acetate, 20 mM MOPS (pH 7.0), 20 mM phosphocreatine, 5 mM $MgCl_2$, 1 mM EGTA, and 100 μM of the indicated nucleoside triphosphate, 10°C. Light scattering was measured at 365 nm for aza-ATP, and 295 nm for ATP, CTP, and GTP. The data were fit to single exponential equation (Eq. 1). The rates are 219 (ATP), 15 (CTP), 26 (GTP), and 53 (aza-ATP) s^{-1}.

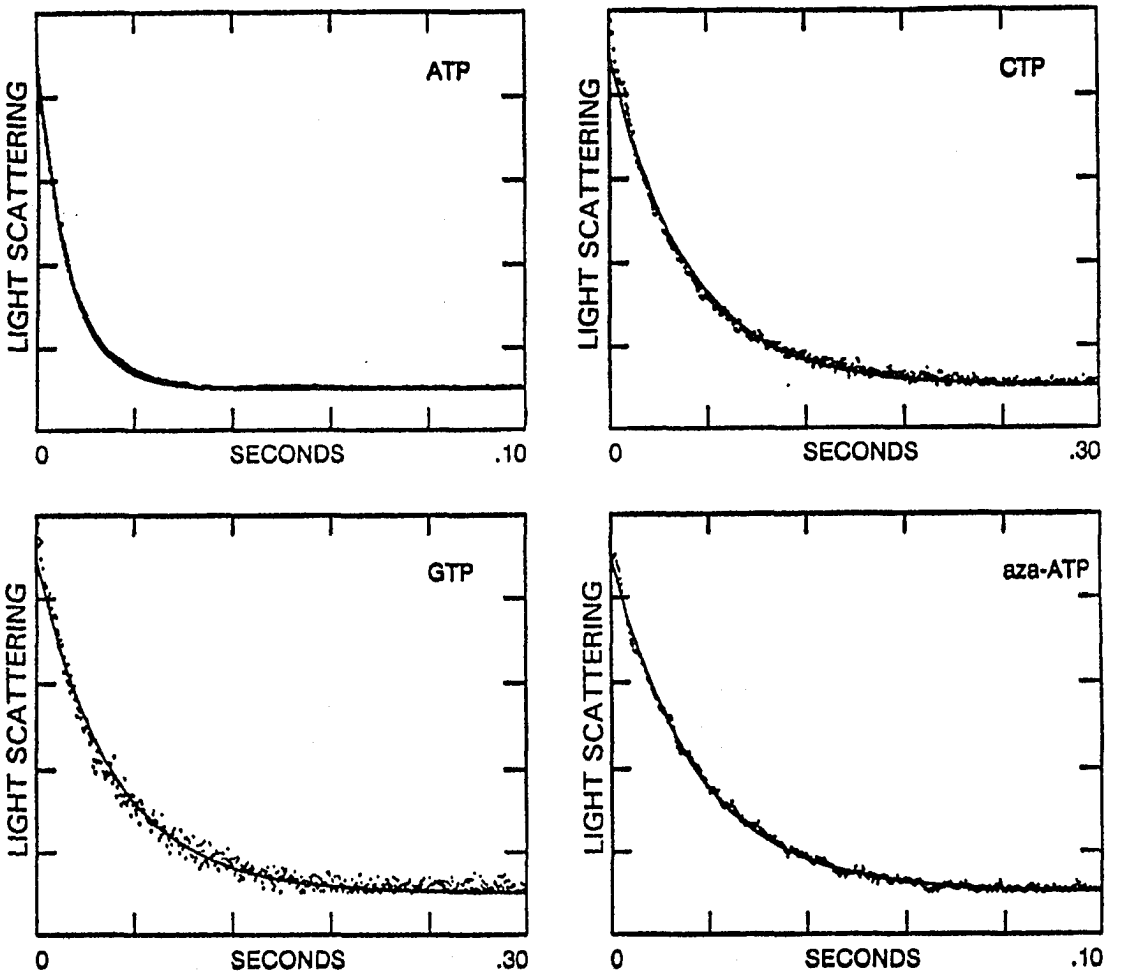

used in this experiment. The $k_{(obs)}$ increases with NTP concentration, and reaches a maximum value when NTP is saturated (Fig. 4). The rate constants (k_a) and equilibrium constants (K_o) measured in various experiment conditions were listed in Table III. In these conditions, actomyosin-S1 (or acto-HMM) can be completely dissociated by ATP, CTP, aza-ATP or GTP, respectively.

The time courses for light scattering measurement of the dissociation of acto-RS.S1 (A2 isozyme) and acto-bovine cardiac myosin-S1 (acto-BV.S1) by mant-ATP, mant-CTP and mant-GTP were measured using the same conditions as Kron et al. (1991) for in-vitro motility assay (Fig. 5). The dependence of $k_{(obs)}$ upon mant-NTP concentration was fit to a hyperbolic equation (Eq.3) (Fig. 6). The data were listed in Table III.

The dissociation of acto-BV.S1 by mant-NTP were complete, except for mant-GTP which only partially dissociates acto-BV.S1. The dissociation fraction varied from 18 percent to 44 percent at 10 μM and 50 μM mant-GTP, respectively. The amplitude of the time courses in the light scattering measurements increased with mant-GTP concentration at low mant-GTP concentrations. The amplitude of dissociation by 10 μM ATP in the same condition and voltage was taken as a standard of complete dissociation. The dependence of $k_{(obs)}$ in light scattering measurements upon mant-GTP concentration was bell-shaped.

The apparent second order rate constant determined by

Fig. 4. The dependence of $k_{(obs)}$ in light scattering measurement of the dissociation of acto-RS.S1 by ATP, CTP, GTP, aza-ATP upon NTP concentration. The experimental conditions were the same as in the legend to Fig. 3 except for the NTP concentrations. The data were fit to equation 3. Values for k_a and K_o are listed in Table III.

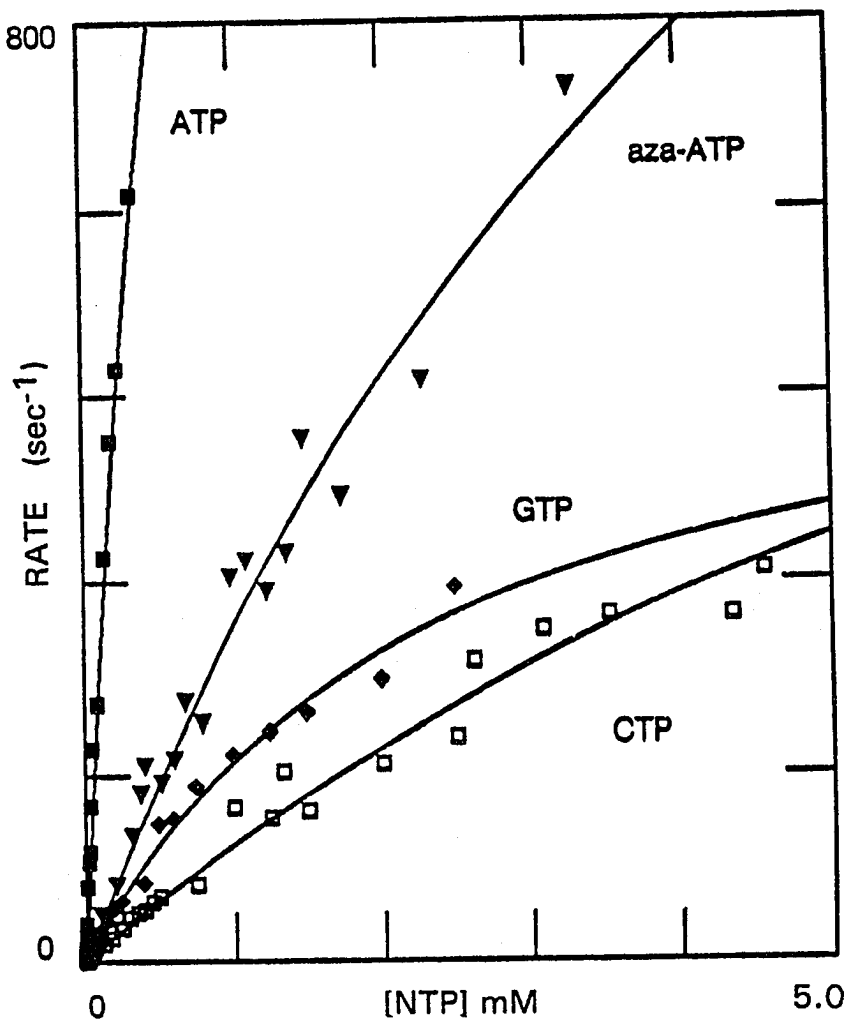

Fig. 5. The time courses in light scattering measurement of the dissociation of acto-RS.S1 (A2 isozyme) (A, C and E) and acto-BV.S1 (B, D and F) by mant-ATP, mant-CTP and mant-GTP. The final concentrations in stopped-flow cell were 2.5 μM F-actin, 2 μM RS.S1 (A2), 25 mM imidazole-HCl (pH 7.4), 25 mM KCl, 4 mM $MgCl_2$, 1mM EGTA, 1mM DTT, and 20 μM indicated mant-NTP, at 20°C. Light scattering was observed at 295 nm. The time courses were fit to single exponential equation. The rates are (A) 121, (B) 60, (C) 9.6, (D) 2.9, (E) 13.8, and (F) 3.8 s^{-1}.

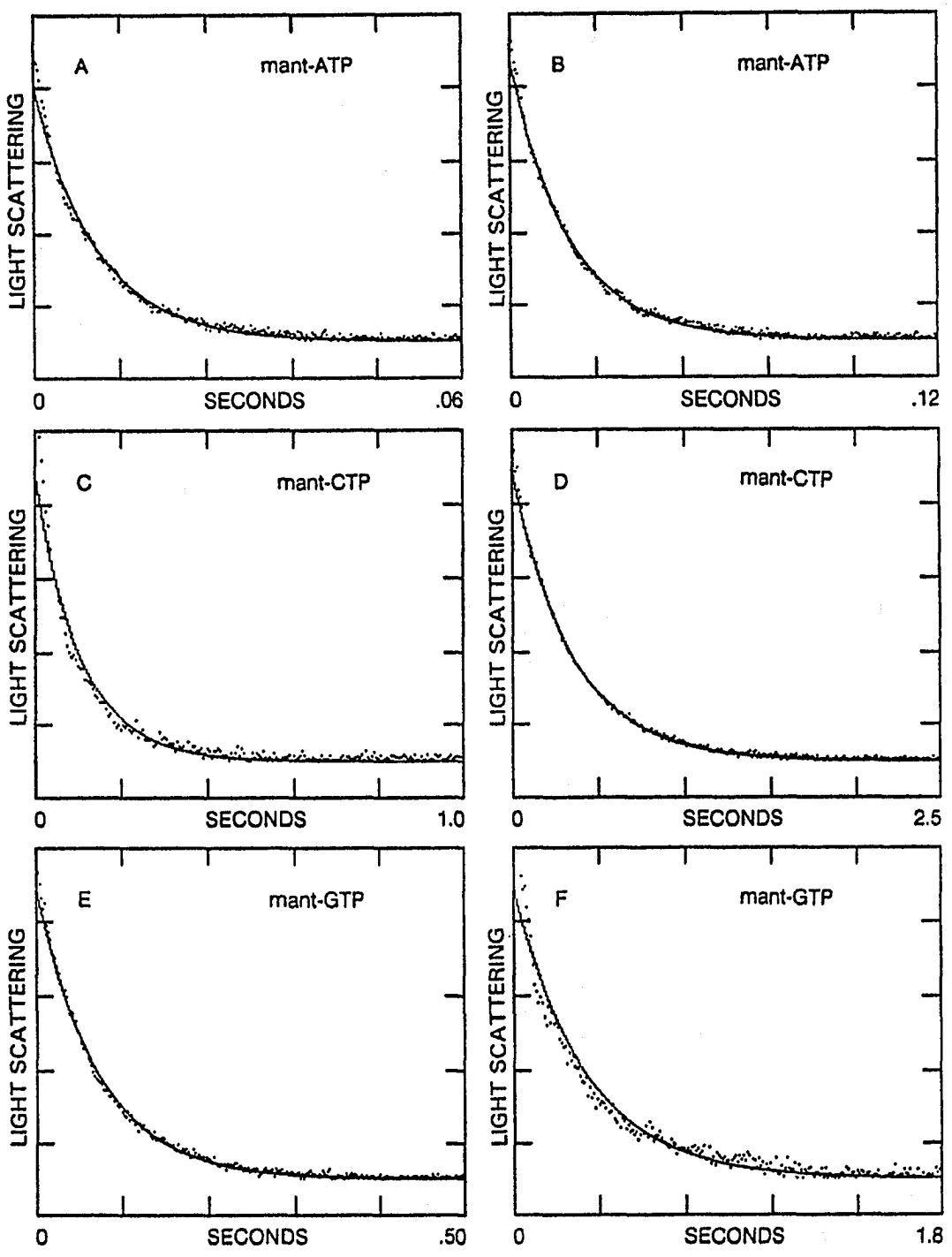

Fig. 6. The dependence of $k_{(obs)}$ in light scattering measurement of the dissociation of acto-RS.S1(A2)(A, C and E) and acto-BV.S1 (B and D) by mant-ATP, mant-CTP and mant-GTP upon mant-NTP concentration. The experimental conditions were the same as in the legend to Fig. 5 except for the mant-NTP concentrations which were varied as indicated. The time courses were fit to equation 3. The k_a and K_o values were listed in Table III. The incomplete dissociation of acto-BV.S1 by mant-GTP was not shown.

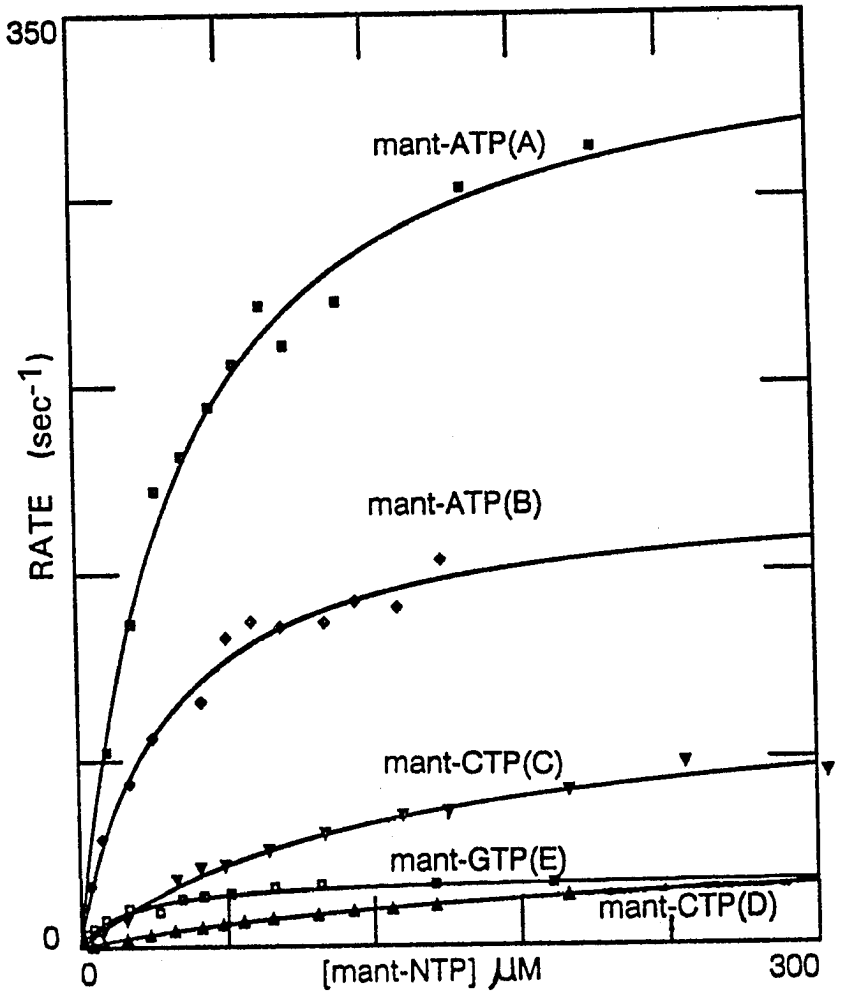

Table III. Comparison of K_o and k_a by the light scattering measurement of the dissociation of acto-RS.S1 and acto-BV.S1 by ATP, CTP, GTP, aza-ATP, mant-ATP, mant-CTP and mant-GTP in stopped-flow.

	NTP	Temp. (^oC)	K_o (μM)	k_a (s^{-1})	k_a/K_o ($M^{-1}s^{-1}$)
acto-RS.S1(A1A2)*a*	ATP	10	806	2154	2.7x10E6
acto-RS.S1(A1A2)*a*	CTP	10	5569	717	1.3x10E5
acto-RS.S1(A1A2)*a*	aza-ATP	10	7435	2210	3.4x10E5
acto-RS.S1(A1A2)*a*	GTP	10	2256	558	2.5x10E5
acto-RS.S1(A1A2)*a'*	ATP	4	ND	ND	1.1x10E6
acto-RS.S1(A1A2)*a'*	UTP	4	3445	446	1.3x10E5
acto-RS.HMM*a''*	ATP	10	ND	ND	2.2x10E6
acto-RS.S1(A1A2)*b*	ATP	24	501	2830	5.6x10E6
acto-RS.S1(A1)*c*	mant-ATP	20	66	327	4.9x10E6
acto-RS.S1(A1A2)*a*	mant-ATP	10	60	170	2.8x10E6
acto-RS.S1(A1A2)*a*	mant-CTP	10	175	48	2.8x10E5
acto-RS.S1(A1)*b'*	mant-ATP	10	50	204	4.1x10E6
		20	41	343	8.3x10E6
		25	57	535	9.4x10E6
acto-RS.S1(A2)*b'*	mant-ATP	20	42	352	8.4x10E6
		25	33	425	1.3x10E7
acto-RS.S1(A2)*b'*	mant-CTP	20	132	96	7.3x10E5
		25	76	104	1.4x10E6
acto-RS.S1(A2)*b'*	mant-GTP	20	20	25	1.3x10E6
		25	12	39	3.2x10E6
acto-RS.S1(A2)*b'*	mant-AMP-PNP	20	68	34	5.0x10E5
acto-BV.S1 *b'*	ATP	20	138	589	4.3x10E6
acto-BV.S1 *b'*	CTP	20	1900	220	1.2x10E5
acto-BV.S1 *b'*	mant-ATP	20	36	170	4.8x10E6
acto-BV.S1 *b'*	mant-CTP	20	220	39	1.7x10E5

Table III. continued

a, Experimental conditions: 0.18 M potassium acetate, 20 mM MOPS (pH 7.0), 20 mM phosphocreatine, 5 mM $MgCl_2$, 1 mM EGTA, at 295 nm (ATP, CTP and GTP) or 365nm (aza-ATP). Final protein concentrations: 1.5 µM F-actin, 1 µM myosin-S1.

a', Experimental conditions: 0.18 M potassium acetate, 20 mM imidazole-HCl (pH 7.0), 20 mM phosphocreatine, 5 mM $MgCl_2$, 1 mM EGTA, at 295 nm.

a'', Experimental conditions were the same as in *a*), measured at 435 nm.

b, Experimental conditions: 25 mM KCl, 25 mM imidazole-HCl (pH 7.4), 4 mM $MgCl_2$, 1 mM EGTA, and 1 mM DTT, at 365 nm. Final protein concentrations: 2.5 µM F-actin, 2 µM myosin-S1.

b', Experimental conditions were the same as *b*) except the wavelength was 295 nm. Final protein concentrations: 2.5 µM F-actin, 2 µM myosin-S1.

c, Experimental conditions: 0.1 M KCl, 50 mM sodium cacodylate (pH 7.0), 5 mM $MgCl_2$, at 365 nm. Final protein concentrations: 1.5 µM F-actin, 1 µM myosin-S1.

The data for incomplete dissociation of acto-BV.S1 by mant-GTP were not shown.
ND: not determined.

light scattering measurements of the dissociation of acto-BV.S1 by ATP, CTP and mant-CTP at 25°C were similar to those at 20°C (data not shown).

The light scattering data in Table III show that both the rate constant of acto-S1 dissociation, k_a, and the apparent second order rate constant of NTP binding to acto-S1, k_a/K_o, are dependent on the structure of nucleoside triphosphates. The dependence of k_a upon NTP structure is ATP ~ aza-ATP > CTP ~ GTP, and ATP > mant-ATP > mant-CTP > mant-GTP. The dependence the of second order rate constant (k_a/K_o) of NTP binding to acto-RS.S1 upon NTP structure is ATP > aza-ATP ~ GTP > CTP, and mant-ATP > ATP > mant-GTP > mant-CTP.

The maximum rates of acto-RS.S1 dissociation are 2200 s^{-1} for ATP and 2000 s^{-1} for aza-ATP (Table III), which are approximately three times that of the highest measured rates. Generally, for a maximum rate greater than 1000 s^{-1}, its reliability should be interpreted with caution. However, the apparent second order rate constant of dissociation (the slope, k_a/K_o, Table III) can be measured accurately (better than ten percent).

The Fluorescence Measurement of Actomyosin Dissociation by Nucleoside Triphosphates and Nucleoside Triphosphate Analogs

The fluorescence measurement of dissociation of acto-S1 is to investigate the microenvironmental change around the fluorophore or myosin-S1 conformation change preceding and/or after acto-S1 dissociation, and possibly, the step of

NTP hydrolysis. The steps indicated in bold in Model 1b are expected to be involved in this measurement.

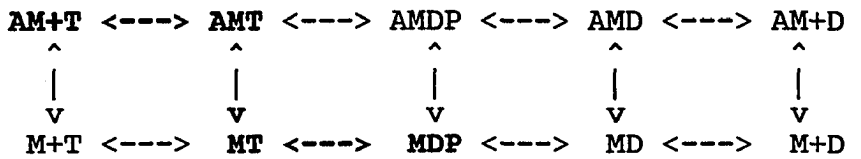

Model 1b

Here, A=actin, M=myosin, T=ATP, D=ADP, P=phosphate.

The increase in myosin-S1 intrinsic tryptophan fluorescence by ATP and CTP, and in aza-ATP fluorescence by aza-ATP observed upon mixing acto-RS.S1 with 100 μM ATP, CTP or aza-ATP, respectively, was shown in Fig. 7. The time courses were fit well to a single exponential equation. The dependence of $k_{(obs)}$ upon NTP concentration was fit to equation 3 (Fig. 8). The attempt to measure the fluorescence change at high aza-ATP concentration was unsuccessful because of the light absorption by aza-ATP. No fluorescence change could be observed when GTP was used as substrate. The rate constants (k_b) and equilibrium constants (K_b) were listed in Table IV. The order for the maximum rate is aza-ATP > CTP > ATP. The order for apparent second order rate constant follows ATP > aza-ATP > CTP.

The fluorescence change induced by ATP probably measure ATP hydrolysis. The aza-ATP fluorescence change may reflect acto-S1 dissociation or aza-ATP binding to acto-S1 (AMT <-> AM^*T in Model 3). It is difficult to interpret CTP induced fluorescence change because of the limited data.

Fig. 7. The time courses in fluorescence measurement of the dissociation of acto-RS.S1 (mixture of A1 and A2) by ATP, CTP, and aza-ATP. Experimental conditions and NTP concentrations were the same as in the legend to Fig. 3. Excitation and emission wavelengths were 295 nm and 320 - 380 nm, respectively, for ATP and CTP, 365 nm and greater than 400 nm, respectively, for aza-ATP (Table I). Each time courses was fit to single exponential equation (Eq. 1). The $k_{(obs)}$ are 24 (ATP), 7.4 (CTP), and 28 (aza-ATP) s^{-1}.

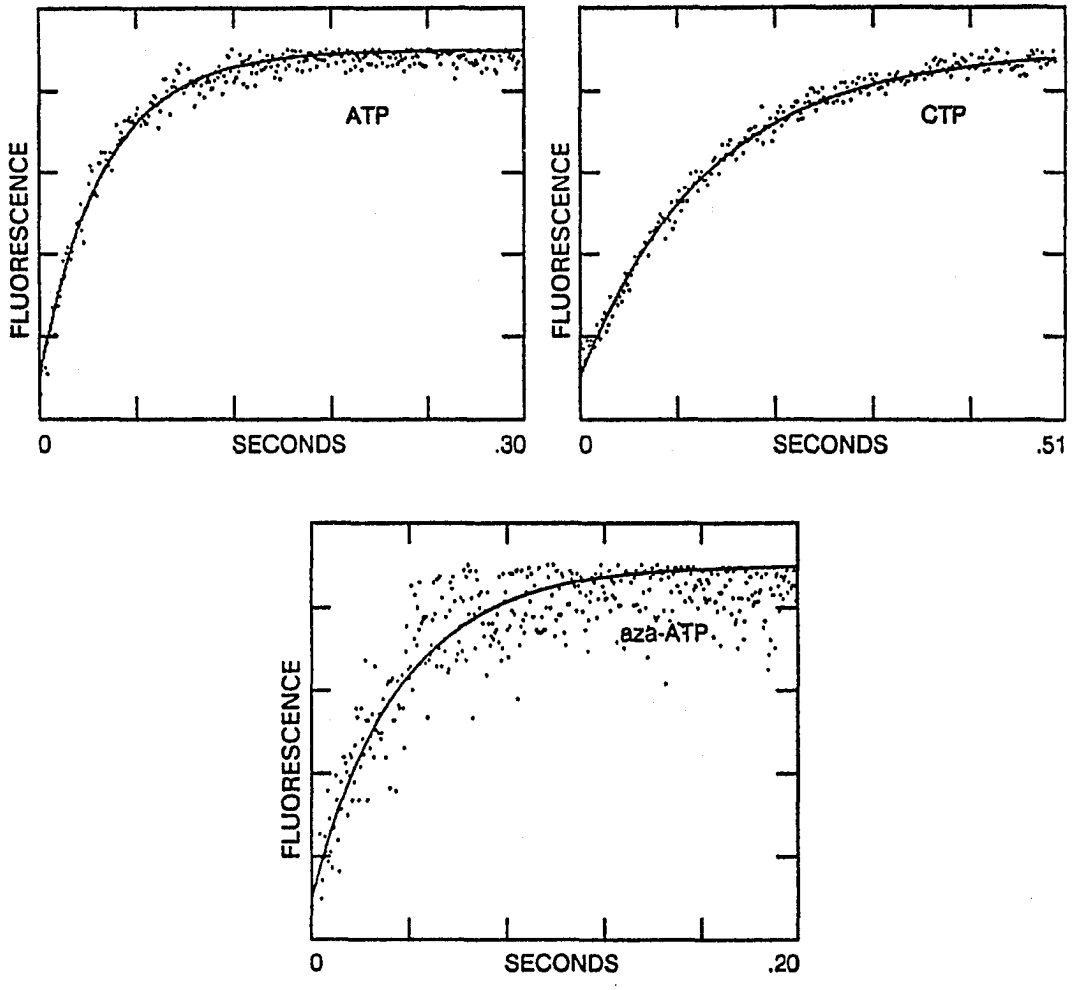

Fig. 8. The dependence of $k_{(obs)}$ in fluorescence measurement of the dissociation of acto-RS.S1 by ATP, CTP, aza-ATP upon NTP concentration. The experimental conditions were the same as in the legend to Fig. 3 except for the NTP concentrations. The data were fit to equation 3. The values of k_b and K_b were shown in Table IV.

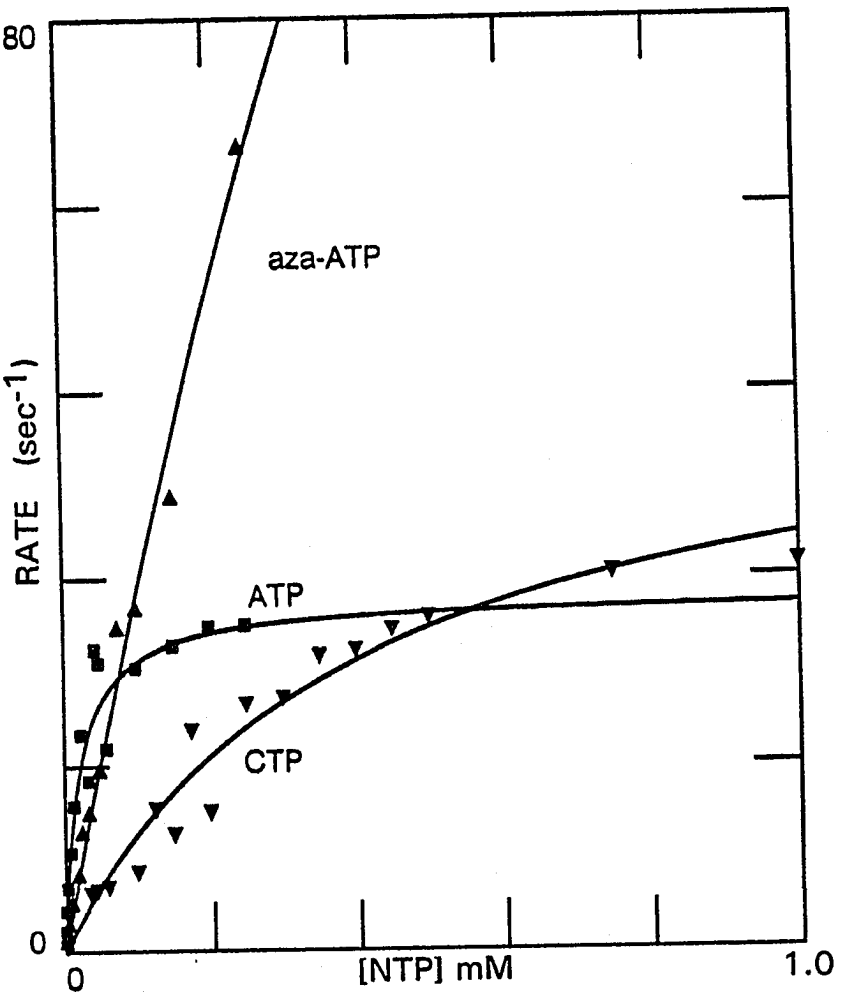

The fluorescence change caused by mant-NTP in this reaction is complicated and must be described individually. In the dissociation of acto-RS.S1(A2) by mant-ATP, the dependence of $k_{(obs)}$ in fluorescence measurement upon mant-ATP concentration was bell-shaped if the time courses were fit to single exponential equation (data not shown). A fast phase could be isolated from slow phase if the time courses were fit to a double exponential equation (Fig. 9A). The dependence of $k_{(obs)}$ for the fast and slow phases, and the amplitude coefficient (faster component divided by total amplitude, I_f/I_{tot}) upon mant-ATP concentration are shown in Fig. 10A. The steps AM + T <--> AMT <--> AM^*T <--> A + M^*T <--> $M^{**}(T)$ (Model 3) are thought to be involved in this reaction, in which (T) means mant-ATP may or may not be hydrolyzed. The fast and slow fluorescence changes are thought to measure AMT<-->AM^*T and M^*T<-->$M^{**}(T)$, respectively.

In the dissociation of acto-RS.S1(A2) by mant-CTP, the time course of fluorescence increase was fit to a single exponential equation (Fig. 9B); the dependence of $k_{(obs)}$ upon mant-CTP concentration was fit to equation 3 (Fig. 10B). The rate of fluorescence change induced by mant-CTP was about half as much as that of light scattering, so that the fluorescence change is thought to measure the step after acto-S1 dissociation MT <--> $M^*(T)$, while the fluorescence change preceding the dissociation was not observed.

The time course of fluorescence increase observed for the

Fig. 9. The time courses in fluorescence measurement of the dissociation of acto-RS.S1(A2) by mant-ATP(A), mant-CTP(B), and mant-GTP(C, D, E and F, see the text for details) in stopped-flow. The experimental conditions were the same as in the legend to Fig. 5, the final mant-NTP concentrations were (A) 20 μM, (B) 20 μM, (C) 10 μM, (D) 30 μM, (E) & (F) 80 μM. Excitation wavelength 295 nm, emission wavelength greater than 400 nm. The time courses were fit to single exponential equation (B, D, E and F) or double exponential equation (A, C). The $k_{(obs)}$ are (A) fast phase 128, slow phase 65, (B) 7.7, (C) fast phase 233, slow phase 8.1, (D) 405, (E) 652, (F) 20 s^{-1}. The fluorescence changes in dissociation of acto-BV.S1 by mant-NTP were in the same pattern.

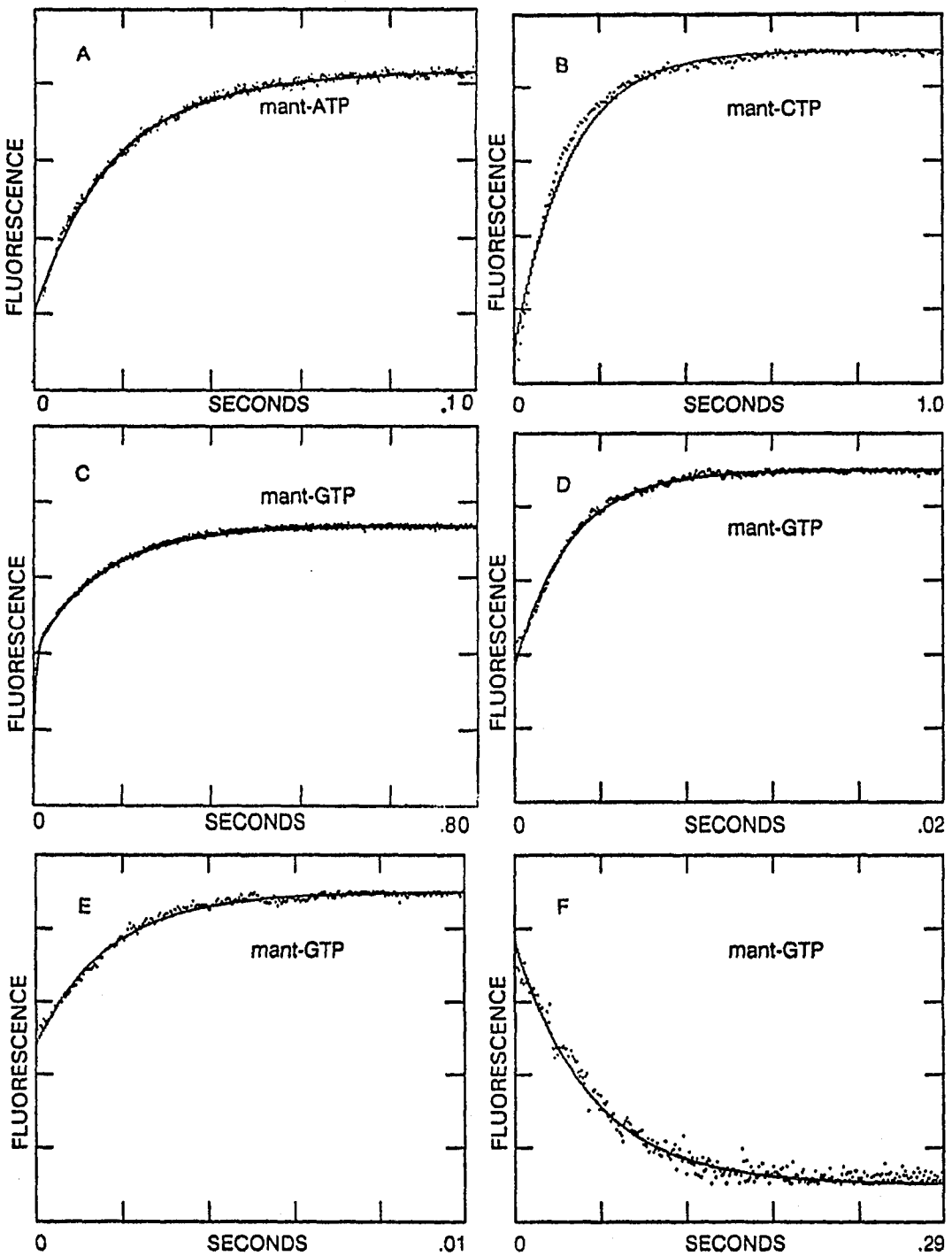

Fig. 10. The dependence of $k_{(obs)}$ in fluorescence measurement of the dissociation of acto-RS.S1(A2) by mant-ATP(A), mant-CTP(B) and mant-GTP(C and D) upon mant-NTP concentration. (A): the time courses were fit to double exponential equation, and the $k_{(obs)}$ of slow phase were fit to hyperbolic equation (Eq. 3). The dependence of amplitude coefficient (faster component divided by total amplitude, I_f/I_{tot}) upon mant-ATP concentration was shown in upper panel. (B): the time courses were fit to single exponential equation, the $k_{(obs)}$ were fit to equation 3. (C): the dependence of $k_{(obs)}$ of fast increasing phase upon mant-GTP concentration. The time courses were fit to double exponential equation, the $k_{(obs)}$ of fast phase were fit to equation 3. The dependence of amplitude coefficient (faster component divided by total increasing amplitude, I_f/I_{tot}) upon mant-GTP concentration was shown in lower panel. (D): the dependence of $k_{(obs)}$ of slow increasing phase (triangle down) and decreasing phase (triangle up) upon mant-GTP concentration. The time courses were fit to single exponential equation, and the $k_{(obs)}$ were fit to equation 3. The experimental conditions were the same as in the legend to Fig. 5 except for the mant-NTP concentrations. The fit rate constants are summarized in Table IV.

The dependence of $k_{(obs)}$ of fluorescence changes in dissociation of acto-BV.S1 by mant-ATP, mant-CTP and mant-GTP upon mant-NTP concentration shared the same pattern.

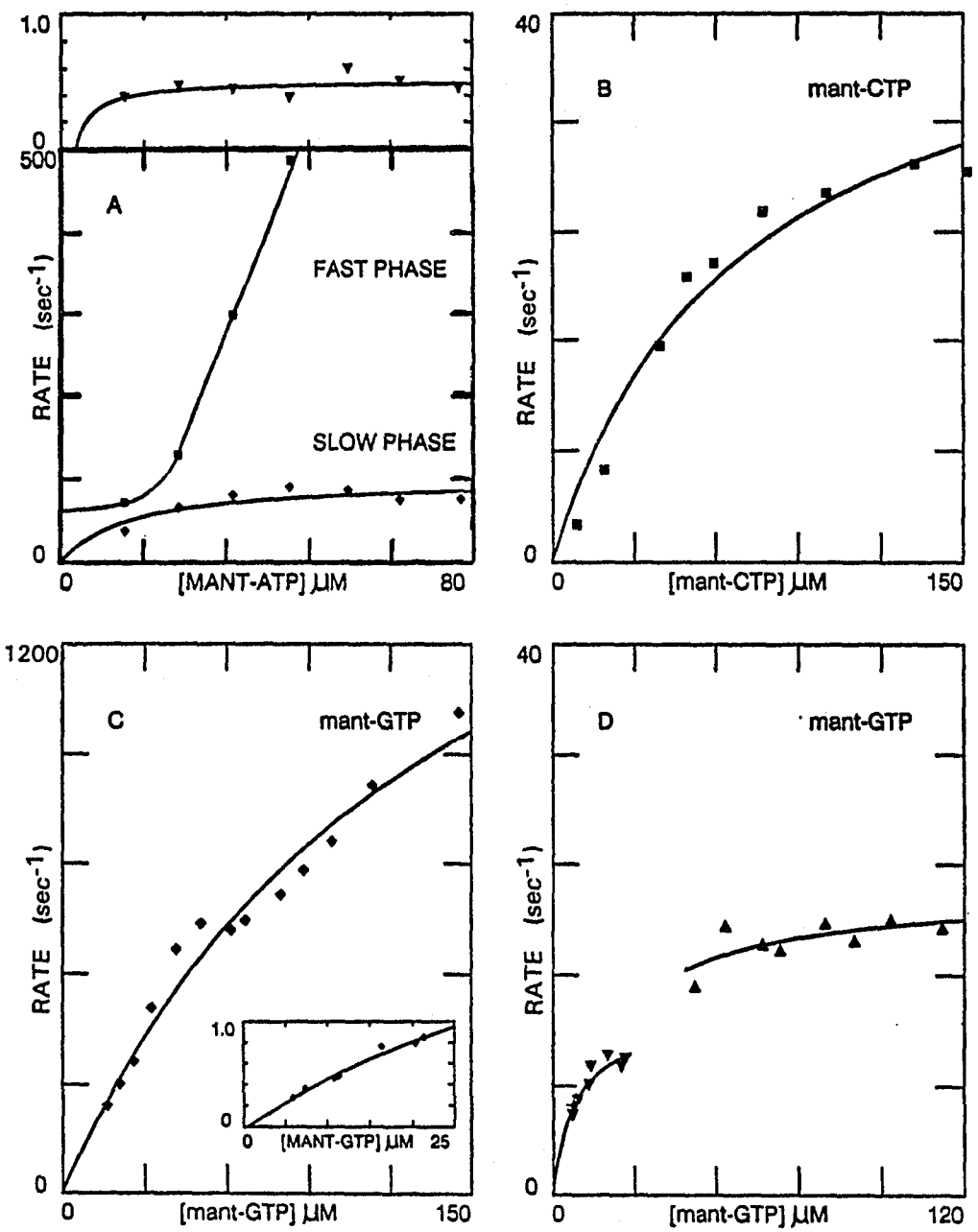

dissociation of acto-RS.S1 by mant-GTP was fit to a double exponential equation at mant-GTP concentrations lower than 25 μM (Fig. 9C). The amplitude coefficient (faster component divided by total increasing amplitude, I_f/I_{tot}) increased with mant-GTP concentration (Fig. 10C). The slow phase disappears for mant-GTP concentrations between 25 μM and 80 μM (Fig. 9D). When mant-GTP concentrations were higher than 80 μM, a fast increasing phase (Fig. 9E) followed by a decreasing phase (Fig. 9F) was observed. The dependence of $k_{(obs)}$ upon mant-GTP concentration was shown in Fig. 10C (fast increasing phase) and 10D (slow increasing phase and decreasing phase). The proper model for mant-GTP induced fluorescence change is not formulated yet. The fluorescence changes in dissociation of acto-BV.S1 by mant-NTP completely share the same pattern. The values of K_b and k_b are listed in Table IV.

The dissociation of acto-RS.S1 (A2 isozyme) by mant-5′--adenylylimidodiphosphate (mant-AMP-PNP) was also observed (see Table III for experimental conditions). Mant-AMP-PNP dissociates acto-RS.S1 incompletely (about 50 percent dissociation at 25 μM mant-AMP-PNP). The kinetic data for light scattering and fluorescence changes were shown in Table III and IV, respectively. This experiment was repeated in two percent polyethylene glycol (PEG, MW. 20 Kd). Both the amplitudes of light scattering and fluorescence were decreased, while neither of the rates were affected.

Table IV. Comparison of K_b and k_b in the fluorescence measurement of the dissociation of acto-RS.S1 and acto-BV.S1 by ATP, CTP, aza-ATP, mant-ATP, mant-CTP and mant-GTP in stopped-flow.

	NTP	Temp. (^oC)	K_b (μM)	k_b (s^{-1})	k_b/K_b ($M^{-1}s^{-1}$)
acto-RS.S1(A1A2)*a*	ATP	10	21	30	1.45x10E6
acto-RS.S1(A1A2)*a*	CTP	10	385	49	1.28x10E5
acto-RS.S1(A1A2)*a*	aza-ATP	10	1038	348	3.35x10E5
acto-RS.S1(A2)*b*	mant-ATP	20			
fast phase			ND	ND	1.61x10E7
slow phase			13	100	7.59x10E6
acto-RS.S1(A2)*b*	mant-CTP	20	71	45	6.31x10E5
		25	68	57	8.43x10E5
acto-RS.S1(A2)*b*	mant-GTP	20			
fast increasing phase			144	1982	1.37x10E7
slow increasing phase			7	13	2.00x10E6
decreasing phase			---	20	---
acto-RS.S1(A2)*b*	mant-AMP-PNP	20	61	31	5.08x10E5
acto-BV.S1 *b*	mant-CTP	20	305	44	1.45x10E5
acto-BV.S1 *b*	mant-GTP	20			
fast increasing phase			59	594	9.99x10E6

a, Experimental conditions: 0.18 M potassium acetate, 20 mM MOPS (pH 7.0), 20 mM phosphocreatine, 5 mM $MgCl_2$, 1 mM EGTA, excitation wavelength 295 nm (ATP and CTP) or 365 nm (aza-ATP), emission wavelength 320 - 380 nm (ATP and CTP) or greater than 400 nm (aza-ATP). Final protein concentrations: 1.5 µM F-actin, 1 µM myosin-S1.

b, Experimental conditions: 25 mM KCl, 25 mM imidazole-HCl (pH 7.4), 4 mM $MgCl_2$, 1 mM EGTA, and 1 mM DTT, excitation and emission wavelengths 295 nm and greater than 400 nm, respectively. Final protein concentrations: 2.5 µM F-actin, 2 µM myosin-S1.

Kinetics of Actomyosin-Nucleoside Diphosphate Dissociation By ATP

These experiments were designed to measure the rate of the dissociation of NDP or (mant-NDP) from acto-S1, and equilibrium constant of NDP binding to acto-S1. The steps to be measured are indicated in bold in Model 1c. The dissociation of NDP (or mant-NDP) from actomyosin is rate limiting step when ATP is saturated (White, 1977).

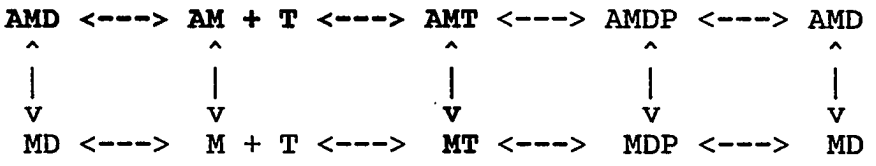

Model 1c

ATP induced dissociation of acto-RS.HMM-NDP, acto-RS.S1-NDP (or mant-NDP), and acto-BV.S1-mant-NDP was measured by observing light scattering at various conditions. In each experiment, ATP dissociated actomyosin-NDP (or actomyosin-mant-NDP) completely, and the $k_{(obs)}$ reached maximum value (k_{-AD}) at saturated ATP, with a decreased apparent second order rate constant ($k_{-AD}/K_{0.5}$) compared to the control experiment in the absence of NDP (or mant-NDP). Fig.11 shows the dependence of $k_{(obs)}$ of light scattering measurement for the dissociation of acto-RS.HMM-ADP(A), acto-RS.HMM-CDP(B), acto-RS.HMM-GDP(C), and acto-RS.HMM-aza-ADP(D) upon ATP concentration. The dependence of $k_{(obs)}$ in light scattering measurement of acto-RS.HMM-ADP dissociation upon ATP

Fig.11. The dependence of $k_{(obs)}$ in light scattering measurement of the dissociation of acto-RS.HMM-ADP(A), acto-RS.HMM-CDP(B), acto-HMM-GDP(C), and acto-RS.HMM-aza-ADP(D) by ATP upon ATP concentration. The final concentrations were: 1.5 μM F-actin, 0.5 μM RS.HMM, 0.29 mM ADP, or 5 mM CDP, or 2.5 mM GDP, or 2.5 mM aza-ADP, varied ATP concentrations, 0.18 M potassium acetate, 20 mM MOPS (pH 7.0), 20 mM phosphocreatine, 5 mM $MgCl_2$, 1 mM EGTA, 1 μM $A_{P5}A$, at 10°C, 435 nm. The time courses were fit to single exponential equation, and the $k_{(obs)}$ were fit to equation 3. The values of $K_{0.5}$, k_{-AD}, K_i and k_{AD} were listed in Table V.

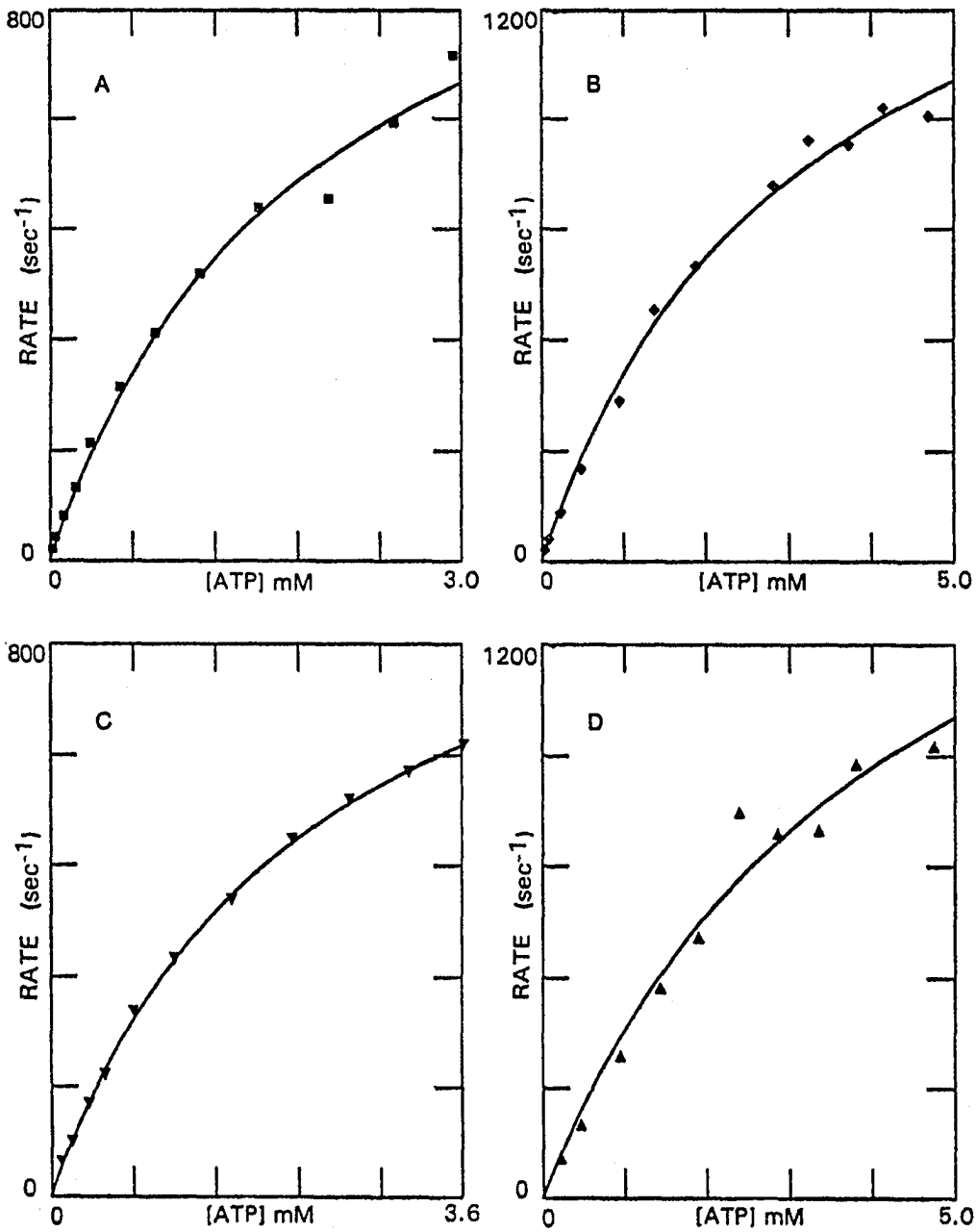

concentration at various ADP concentrations was shown in Fig.12. The values of k_{-AD} (the rate constant of NDP dissociation), $K_{0.5}$ (ATP concentration at which the rate reaches 0.5Vmax), K_i (the equilibrium constant of NDP or mant-NDP to actomyosin), and k_{AD} (the rate constant of NDP binding to actomyosin) in each experiment are listed in Table V. Both the k_{-AD} and K_i are independent of ADP concentration. The dependence of k_{-AD} upon NDP structure is CDP ~ aza-ADP > ADP ~ GDP, and mant-CDP > mant-ADP ~ mant-GDP. The second order rate constant of NDP binding to actomyosin (k_{AD}) can be calculated from k_{-AD}/K_i. Its dependence upon NDP structure is mant-ADP > ADP > aza-ADP > CDP ~ GDP, and mant-ADP > mant-CDP ~ mant-GDP. The dependence of equilibrium constant (K_i) of NDP to actomyosin upon NDP structure is CDP > GDP ~ aza-ADP > ADP > mant-ADP, and mant-CDP > mant-GDP > mant-ADP.

The rate of dissociation observed after mixing acto-RS.HMM-ADP (1 mM ADP) with ATP is equal to that observed after mixing acto-RS.HMM-ADP (0.5 mM ADP) with 0.5 mM ADP and ATP in stopped-flow. Therefore, ADP must bind more rapidly to acto-S1 than ATP.

A fluorescence decrease was also observed when acto-BV.S1-mant-ADP was dissociated by ATP. The time courses were fit to single exponential equation (Eq.1)(Fig.13A), and the $k_{(obs)}$ was fit to equation 3 (Fig.13B). In the case of dissociation of acto-BV.S1-mant-CDP and acto-BV.S1-mant-GDP, the fluorescence change was too small to be measured due to

Fig.12. The dependence of $k_{(obs)}$ in light scattering measurement of the dissociation of acto-RS.HMM-ADP by ATP upon ATP concentration with various ADP concentrations. Experimental condition and acto-RS.HMM concentration were the same as in the legend to Fig.11. ADP final concentrations were 0, 0.2, 0.4, 0.8 mM, respectively. The kinetic data were listed in Table V.

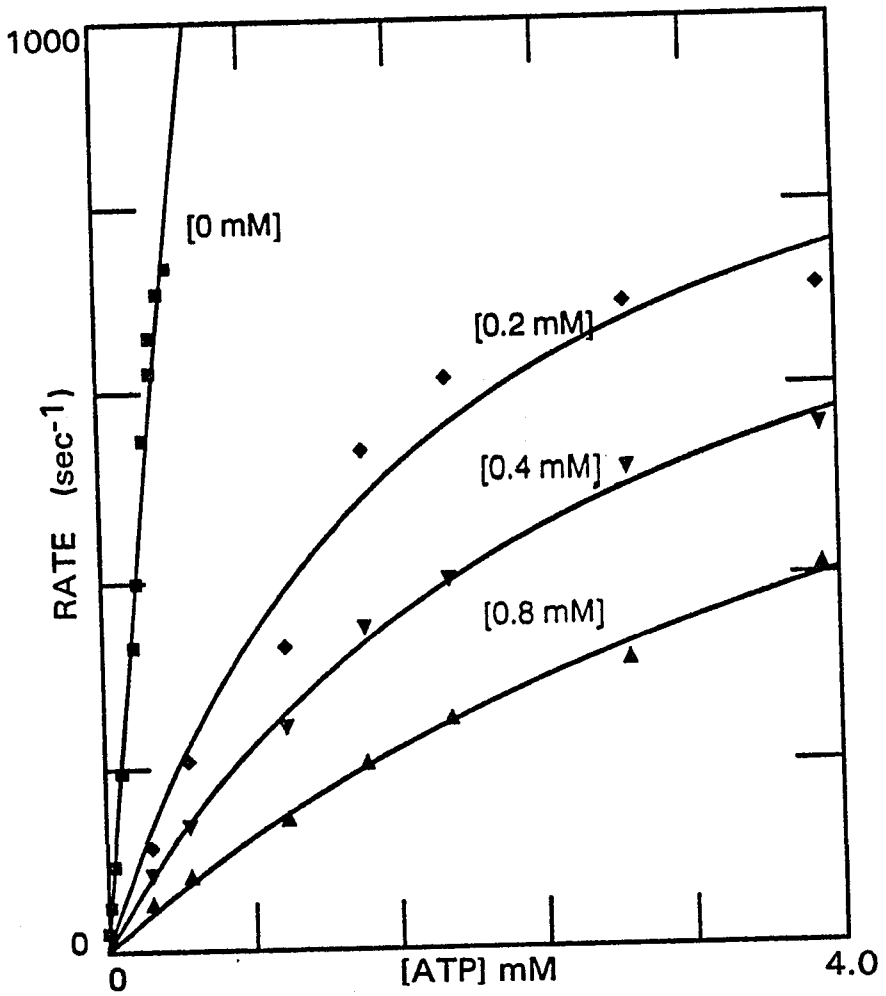

Fig.13. The time course and $k_{(obs)}$ dependence upon ATP concentration in fluorescence measurement of the dissociation of acto-BV.S1-mant-ADP by ATP.

(A) The fluorescence decrease upon mixing 1.5 μM F-actin, 1 μM BV.S1, and 50 μM mant-ADP with 100 μM ATP in 5 mM MOPS (pH 7.0), 2 mM $MgCl_2$, 0.5 mM DTT, at 20°C, excitation and emission wavelengths 295 nm and greater than 400 nm, respectively. The time course was fit to single exponential equation. The $k_{(obs)}$ was 9.9 s^{-1}.

(B) The dependence of $k_{(obs)}$ in fluorescence measurement of acto-BV.S1-mant-ADP dissociation by ATP upon ATP concentration. The experiment condition and concentrations were the same as in (A) except for the ATP concentration. The $k_{(obs)}$ were fit to equation 3. The data were listed in Table V.

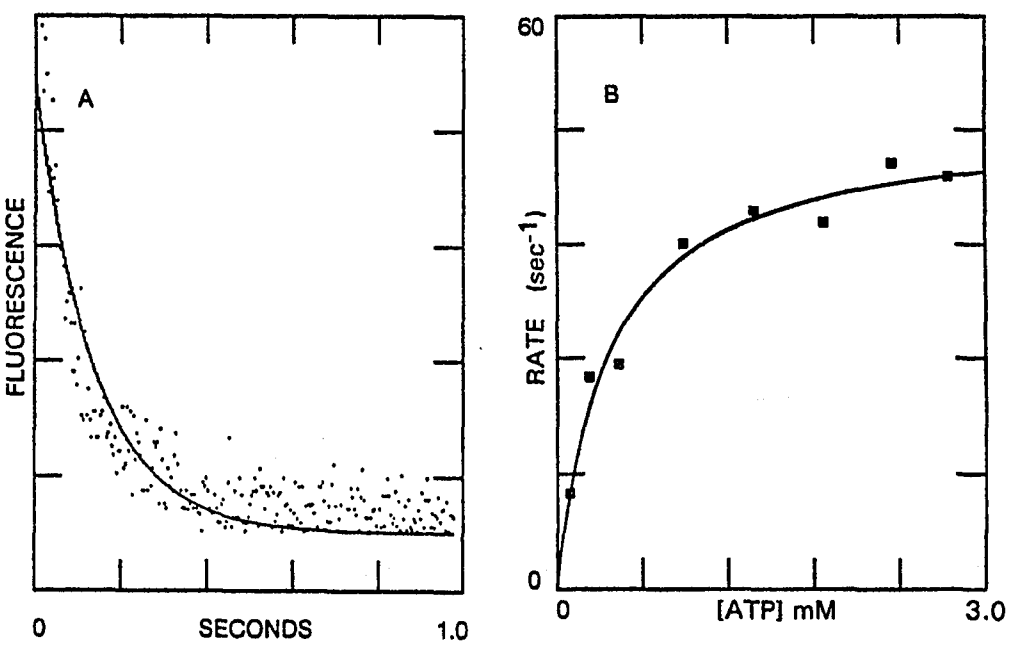

Table V. The values of $K_{0.5}$, k_{-AD}, K_i and k_{AD} in the light scattering and fluorescence measurement of the dissociation of actomyosin-NDP (or actomyosin-mant-NDP) by ATP.

ACTO-S1-NDP*	Temp. (^oC)	$K_{0.5}$ (mM)	k_{-AD} (s^{-1})	$k_{-AD}/K_{0.5}$ ($M^{-1}s^{-1}$)	K_i (mM)	k_{AD}[c] ($M^{-1}s^{-1}$)
actoRS.HMM-ADP(0.1mM)*a*	10	0.85	940	1.1x10E6	0.100	9.4x10E6
actoRS.HMM-ADP(0.2mM)*a*	10	1.78	1090	6.1x10E5	0.076	1.4x10E7
actoRS.HMM-ADP(0.29mM)*a*	10	1.91	1131	5.9x10E5	0.074	1.5x10E7
actoRS.HMM-ADP(0.4mM)*a*	10	2.65	954	3.6x10E5	0.078	1.2x10E7
actoRS.HMM-ADP(0.8mM)*a*	10	5.27	938	1.8x10E5	0.070	1.3x10E7
actoRS.HMM-CDP(5.0mM)*a*	10	3.24	1715	5.3x10E5	1.570	1.1x10E6
actoRS.HMM-GDP(2.5mM)*a*	10	2.31	1072	4.6x10E5	0.666	1.6x10E6
actoRS.HMM-aza-ADP(2.5mM)*a*	10	4.43	1970	4.4x10E5	0.570	3.5x10E6
actoRS.S1(A1A2)-ADP(0.5mM)*a*	10	2.34	793	3.4x10E5	0.072	1.1x10E7
actoRS.S1(A1)-CDP(5mM)*a*	10	2.67	1320	4.9x10E5	1.136	1.2x10E6
actoRS.S1(A1A2)-ADP(0.5mM)*a*	4	5.59	870	1.6x10E5	0.093	9.4x10E6
actoRS.S1(A1A2)-ADP(0.25mM)*a*	4	ND	ND	4.1x10E5	0.178	---
actoRS.S1(A1)-ADP(0.125mM)*b*	10	ND	ND	2.1x10E6	0.165	---
actoRS.S1(A1)-CDP(5mM)*b*	10	ND	ND	1.0x10E6	1.952	---
actoRS.S1(A1)-GDP(2.5mM)*b*	10	0.79	707	8.9x10E5	0.807	8.8x10E5
actoRS.S1(A1)-mantADP(0.25mM)*b*	10	2.33	913	3.9x10E5	0.030	3.0x10E7
actoRS.S1(A1)-mantCDP(2.5mM)*b*	10	3.49	1310	3.8x10E5	0.288	4.6x10E6
actoRS.S1(A1)-mantGDP(0.5mM)*b*	4	2.26	995	4.4x10E5	ND	ND
actoRS.HMM-mantADP(0.25mM)*b*	10	4.40	849	1.9x10E5	ND	ND

Table V. continued

	Temp. (°C)	$K_{0.5}$ (mM)	k_{-AD} (s^{-1})	$k_{-AD}/K_{0.5}$ ($M^{-1}s^{-1}$)	K_i (mM)	k_{AD} [c] ($M^{-1}s^{-1}$)
actoBV.S1-mantADP(0.05mM)*b*						
	20	0.55	77	1.4x10E5	0.002	3.9x10E7
actoBV.S1-mantCDP(1.0mM)*b*						
	20	3.22	657	2.0x10E5	0.071	9.3x10E6
actoBV.S1-mantGDP(0.25mM)*b*						
	20	0.64	129	2.0x10E5	0.018	7.2x10E6
actoBV.S1-mantADP(0.05mM)*b* (Fluorescence)**						
	20	0.37	49	1.3x10E5		

Control experiments (absence of NDP)

	Temp. (°C)	K_o (mM)	k_a (s^{-1})	k_a/K_o ($M^{-1}s^{-1}$)
actoRS.HMM*a*	10	ND	ND	2.2x10E6
actoRS.S1(A1A2)*a*	10	0.81	2154	2.7x10E6
actoRS.S1(A1A2)*a*	4	2.03	2010	9.9x10E5
actoRS.S1(A1)*b*	10	0.29	1047	3.6x10E6
actoBV.S1 *b*	20	0.05	161	3.0x10E6

a, in 0.18 M KAc, 20 mM MOPS (pH 7.0), 20 mM phosphocreatine, 5 mM $MgCl_2$, and 1 mM EGTA, at 435 nm (for actomyosin-NDP) or 295 nm (for actomyosin-mant-NDP).

b, in 5 mM MOPS (pH 7.0), 2 mM $MgCl_2$, and 0.5 mM DTT. Wavelengths were the same as in (*a*).

c, k_{AD} was calculated using equation $k_{AD} = k_{-AD}/K_i$.

*: NDP final concentration.

**: Data from fluorescence measurement, the rest of them from light scattering measurement.

ND: not determined.

the high absorption by the high concentrations of mant-NDP.

Kinetics of Actin Binding To Myosin-S1- (or HMM-) Mant-Nucleoside Diphosphate

These experiments were designed to investigate the step(s) preceding the dissociation of NDP from acto-S1, and possibly the step of NDP release from acto-S1. These steps are indicated in bold in Model 1d.

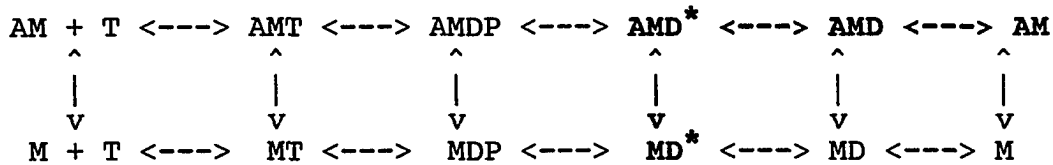

Model 1d

Actin binding to RS.S1(A1)-mant-NDP, RS.S1(A2)-mant-NDP, RS.HMM-mant-NDP and BV.S1-mant-NDP was measured by observing fluorescence decrease under various conditions. In the case of actin binding to RS.S1 (or RS.HMM)-mant-NDP, the time courses could be fit to single exponential equation, but were usually better fit to double exponential equation (Fig.14). The dependence of $k_{(obs)}$ upon actin concentration was fit to a hyperbolic equation (Fig.15 & Fig.16, For the time courses fit to single and double exponential equations, respectively), the amplitude coefficient (I_f/I_{tot}) was independent of actin concentration. The kinetic data were listed in Table VI(A) and VI(B), respectively. Both the second order rate constants of actin binding to myosin-S1-

Fig.14. The time courses in fluorescence measurement of actin binding to RS.S1(A1)-mant-ADP(A), RS.S1(A1)-mant-CDP(B), RS.S1(A1)-mant-GDP(C), and RS.S1(A1)-mant-dADP(D) measured in stopped-flow at $4^{o}C$, excitation and emission wavelengths 295 nm and greater than 400 nm, respectively. Final concentrations were 12 µM F-actin, 1 µM RS.S1(A1), and 2.5 µM mant-NDP, 5 mM MOPS (pH 7.0), 2 mM $MgCl_2$, 0.5 mM DTT. The time courses were fit to double exponential equation. The rates of fast and slow phases were (A) 30, 6.3; (B) 35, 12; (C)186, 47; and (D)59, 14 s^{-1}.

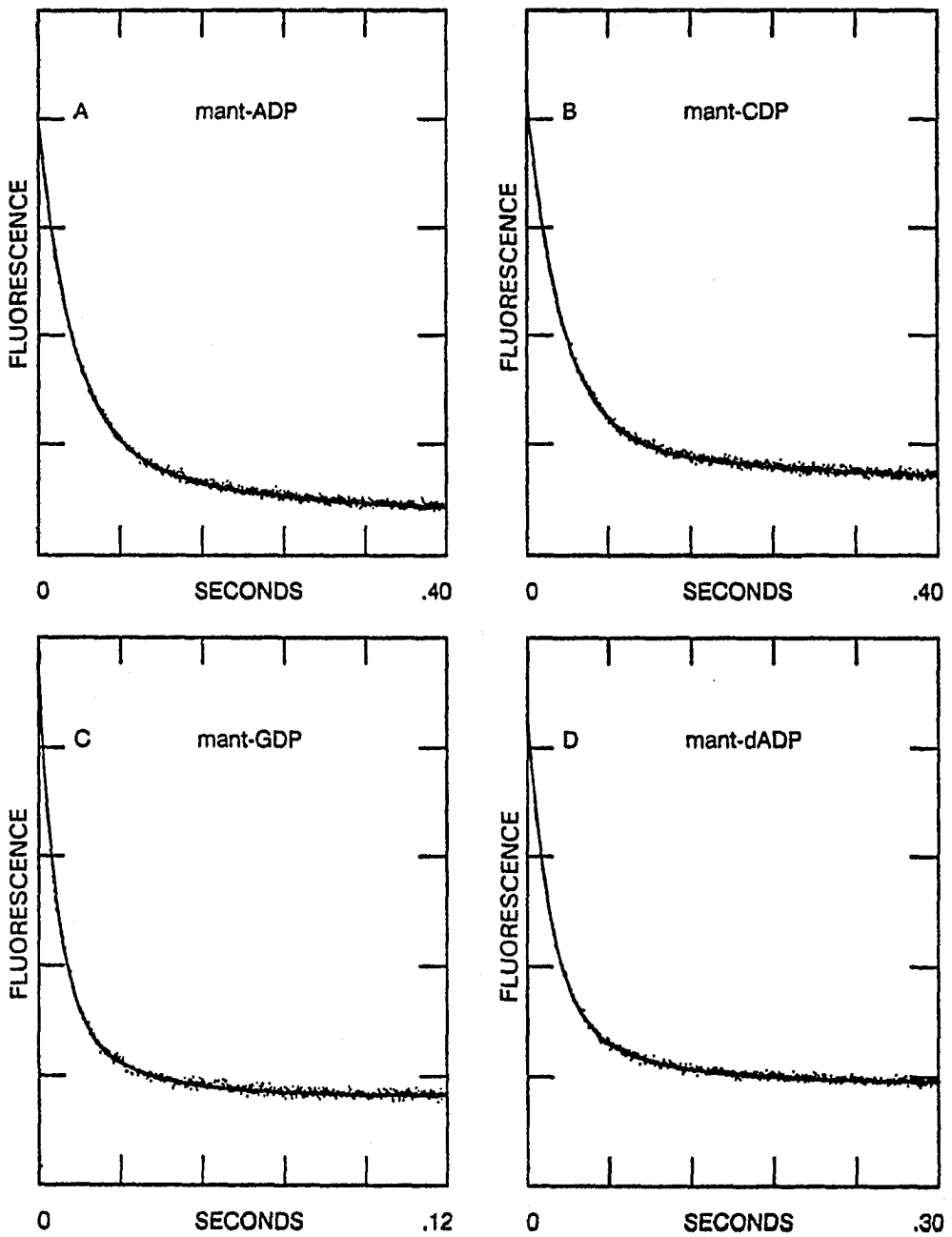

Fig.15. The dependence of $k_{(obs)}$ in fluorescence measurement of actin binding to RS.S1(A1)-mant-NDP upon actin concentration at various temperatures. The experimental conditions were the same as in the legend to Fig.14 except for the actin concentration. The time courses were fit to single exponential equation and the $k_{(obs)}$ were fit to equation 3. The kinetic data were listed in Table VI(A).

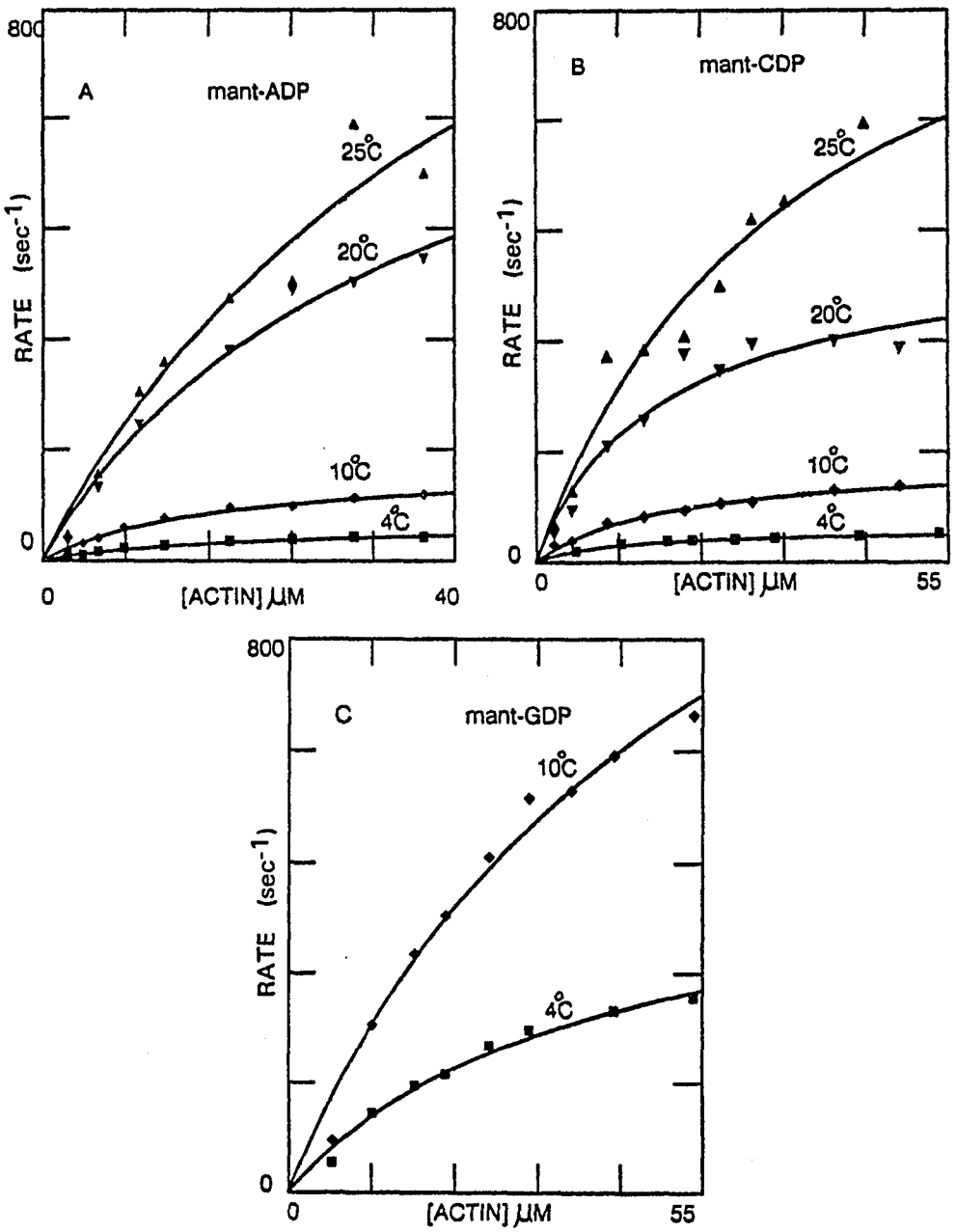

Fig.16. The dependence of $k_{(obs)}$ of the fast and slow components in fluorescence measurement of actin binding to RS.S1(A1)-mant-NDP upon actin concentration at 4°C. The experiment conditions were the same as in the legend to Fig.14 except for the actin concentration. The time courses were fit to double exponential equation and the $k_{(obs)}$ of fast and slow phases were fit to equation 3, respectively. The kinetic data were listed in Table VI(B).

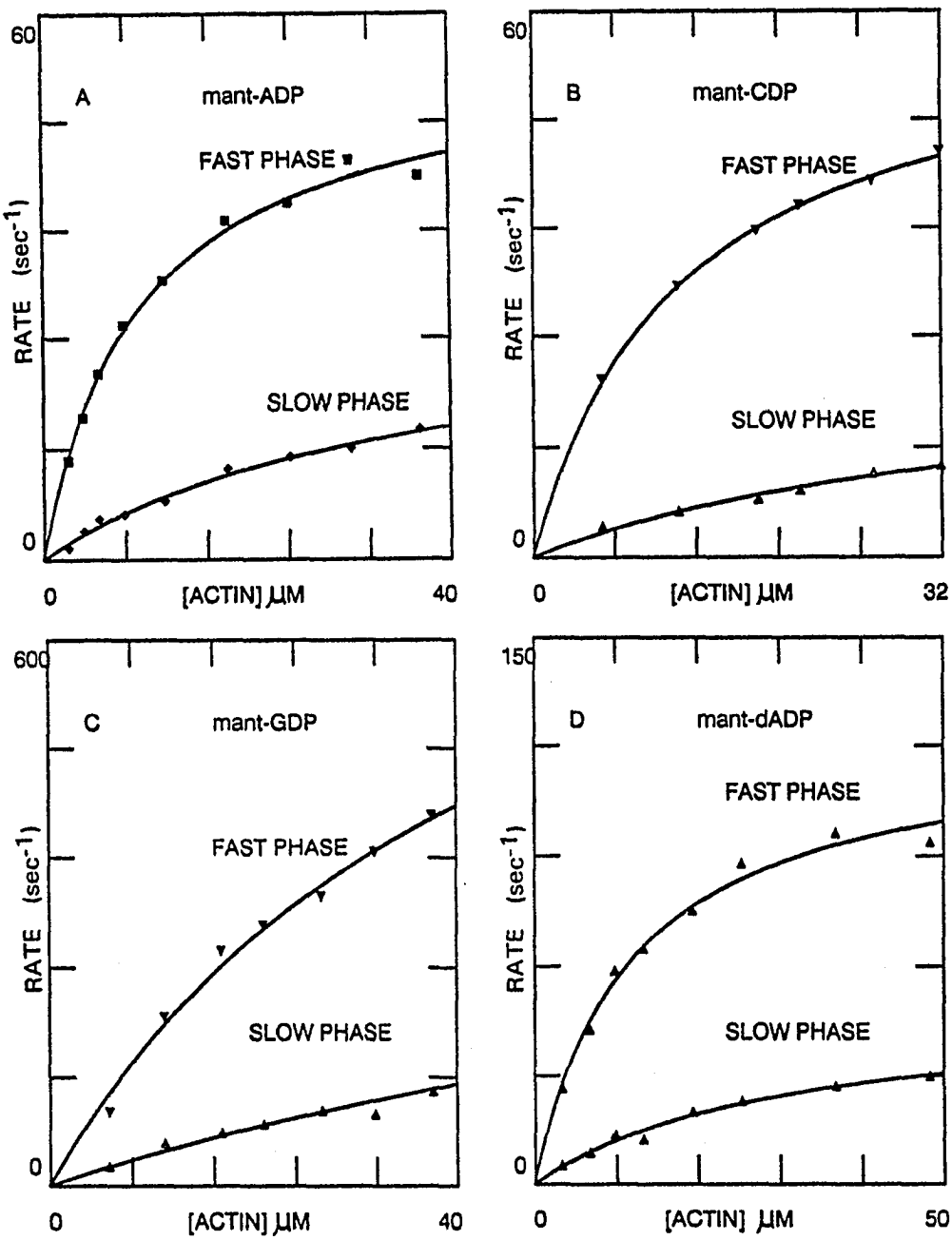

Table VI. The K_{FL} and k_{FL} values in the fluorescence measurement of the dependence of $k_{(obs)}$ of actin binding to myosin-S1-(or HMM-)mant-NDP upon actin concentration.

(A)	Temp. (^oC)	K_{FL} (μM)	k_{FL} (s^{-1})	k_{FL}/K_{FL} ($M^{-1}s^{-1}$)
RS.S1(A1)[1μM]-	4	22	56	2.60x10E6
mant-ADP[2.5μM]a	10	16	182	1.12x10E7
	20	19	729	3.81x10E7
	25	21	945	4.39x10E7
RS.S1(A2)[1μM]-	4	58	21	3.46x10E5
mant-ADP[2.5μM]a	10	108	73	6.78x10E5
	20	141	414	2.93x10E6
	25	359	1378	3.84x10E6
RS.HMM[0.5μM]-	4	6.7	39	5.83x10E6
mant-ADP[2.5μM]a	10	6.8	62	9.15x10E6
	20	15	366	2.37x10E7
	25	25	731	2.96x10E7
RS.S1(A1)[1μM]-	4	11	46	4.37x10E6
mant-CDP[2.5μM]a	10	18	147	8.08x10E6
	20	16	457	2.77x10E7
	25	35	1059	2.99x10E7
RS.S1(A2)[1μM]-	4	70	25	3.58x10E5
mant-CDP[2.5μM]a	10	81	96	1.18x10E6
	20	44	302	6.93x10E6
	25	36	441	1.22x10E7
RS.HMM[0.5μM]-	4	5.7	39	6.84x10E6
mant-CDP[2.5μM]a	10	9.7	125	1.29x10E7
	20	21	505	2.42x10E7
	25	21	623	2.95x10E7
RS.S1(A1)[1μM]-	4	40	509	1.28x10E7
mant-GDP[2.5μM]a	10	53	1405	2.67x10E7
RS.S1(A2)[1μM]-	4	69	147	2.14x10E6
mant-GDP[2.5μM]a	10	ND	ND	5.09x10E6
	20	ND	ND	2.03x10E7
RS.HMM[0.5μM]-	4	16	153	9.75x10E6
mant-GDP[2.5μM]a	10	40	699	1.73x10E7

Table VI. continued

(A)	Temp. (°C)	K_{FL} (μM)	k_{FL} (s^{-1})	k_{FL}/K_{FL} ($M^{-1}s^{-1}$)
RS.S1(A1)[1μM]-mant-ADP[2.5μM]*b*	4	2.5	49	1.95x10E7
RS.S1(A2)[1μM]-mant-ADP[2.5μM]*b*	4	29	15	5.04x10E5
RS.HMM[0.5μM]-mant-ADP[2.5μM]*b*	4	5.0	22	4.48x10E6
	10	23	59	2.64x10E6
	20	56	209	3.74x10E6
	25	30	226	7.66x10E6
RS.S1(A1)[1μM]-mant-CDP[2.5μM]*b*	4	4.1	51	1.24x10E7
RS.S1(A2)[1μM]-mant-CDP[2.5μM]*b*	4	94	59	6.28x10E5
RS.HMM[0.5μM]-mant-CDP[2.5μM]*b*	4	14	35	2.52x10E6
	10	125	274	2.20x10E6
	20	ND	ND	3.37x10E6
	25	ND	ND	4.16x10E6
RS.S1(A1)[1μM]-mant-GDP[2.5μM]*b*	4	25	408	1.62x10E7
RS.S1(A2)[1μM]-mant-GDP[2.5μM]*b*	4	94	59	6.28x10E5
RS.HMM[0.5μM]-mant-GDP[2.5μM]*b*	4	33	52	1.61x10E6
	10	49	156	3.16x10E6
RS.S1(A1)[1μM]-mant-dADP[2.5μM]*b*	4 (first peak)	11	81	7.33x10E6

Table VI. continued

(B)	Temp. (°C)	K_{FL} (μM)	k_{FL} (s^{-1})	I_f/I_{tot}
RS.S1(A1)[1μM]-mant-ADP[2.5μM]*a*				
fast phase	4	9.1	53	0.80
slow phase		22	19	
fast phase	10	24	337	0.71
slow phase		30	104	
RS.S1(A1)[1μM]-mant-CDP[2.5μM]*a*				
fast phase	4	12	61	0.87
slow phase		40	22	
fast phase	10	39	496	0.60
slow phase		89	242	
RS.S1(A1)[1μM]-mant-GDP[2.5μM]*a*				
fast phase	4	63	1132	0.81
slow phase		60	268	
RS.S1(A1)[1μM]-mant-dADP[2.5μM]*a*			(first peak)	
fast phase	4	12	123	0.85
slow phase		32	50	
RS.S1(A1)[1μM]-mant-GDP[2.5μM]*b*				
fast phase	4	25	895	0.66
slow phase		19	193	
BV.S1[1.5μM]-mant-ADP[4μM]*a*				
fast phase	10	8.4	270	
slow phase		1.3	34	
BV.S1[2.5μM]-mant-ADP[7.5μM]*a*				
fast phase	20	10	566	
slow phase		0.9	49	
fast phase	25	5.9	590	
slow phase		3.4	105	
BV.S1[2.5μM]-mant-ADP[75μM]*a*				
fast phase	20	13	845	
slow phase		ND	48	
BV.S1[2.5μM]-mant-CDP[10μM]*a*				
fast phase	20	4.3	390	
slow phase		ND	2 - 96, scattered	
BV.S1[2.5μM]-mant-GDP[10μM]*a*				
fast phase	20	0.8	80	
slow phase		ND	0.5 - 2, scattered	

(A): each time course was fit to single exponential equation.

(B): each time course was fit to double exponential equation.

Experimental conditions: *a*, in 5 mM MOPS (pH 7.0), 2 mM $MgCl_2$, and 0.5 mM DTT; *b*, in 1 mM MOPS (pH 7.0), 0.4 mM $MgCl_2$, and 0.1 mM DTT. Excitation and emission wavelengths were 295 nm and greater than 400 nm, respectively. All concentrations were final.

ND: not determined.

mant-NDP (k_{FL}/K_{FL}) and the rate constants of fluorescence change (k_{FL}) are dependent upon the isozymes of myosin-S1 (RS.S1-A1-mant-NDP > RS.HMM-mant-NDP > RS.S1-A2-mant-NDP), and the structure of mant-NDP (mant-GDP > mant-ADP ~ mant-CDP).

The time courses in fluorescence measurement of actin binding to BV.S1-mant-NDP could be fit to single exponential equation, but better fit to double exponential equation (Fig.17). The dependence of $k_{(obs)}$ upon actin concentration was shown in Fig.18. The K_{FL} and k_{FL} values were listed in Table VI(B). The maximum rates are dependent upon mant-NDP structure (mant-ADP > mant-CDP > mant-GDP). The different dependence of the rate constants upon mant-NDP structure between skeletal and cardiac myosin-S1 suggests a difference in these two myosin structures.

In these experiments, light bleaching was not observed in control experiment in which the myosin-S1-mant-NDP was mixed with buffer. Therefore, the slow components in double exponential fitting of the time courses were not caused by light bleaching.

The amplitude of actin binding to BV.S1-mant-NDP was two to four times lower than that of actin binding to RS.S1-mant-NDP. The dependence of amplitude coefficient upon actin concentration was shown in the upper panel of Fig.18A.

The binding of actin to RS.S1(A2)-mant-ADP in 6.5 percent polyethylene glycol (PEG, MW. 20 kd) was also measured in 5 mM MOPS (pH 7), 2 mM $MgCl_2$ and 0.5 mM DTT, at 20°C. Both the

Fig.17. The time courses in fluorescence measurement of actin binding to BV.S1-mant-ADP(A), BV.S1-mant-CDP(B), and BV.S1-mant-GDP(C) measured in stopped-flow at 20°C. Excitation and emission wavelengths were 295 nm and greater than 400 nm, respectively. Final concentrations were 12 μM F-actin, 2.5 μM BV.S1, 7.5 μM mant-ADP, or 10 μM mant-CDP, or 10 μM mant-GDP, 5 mM MOPS (pH 7.0), 2 mM $MgCl_2$, 0.5 mM DTT. The time courses were fit to double exponential equation. The $k_{(obs)}$ of fast and slow phases were (A) 285, 36; (B) 285, 2.2; and (C) 74, 0.42 s^{-1}.

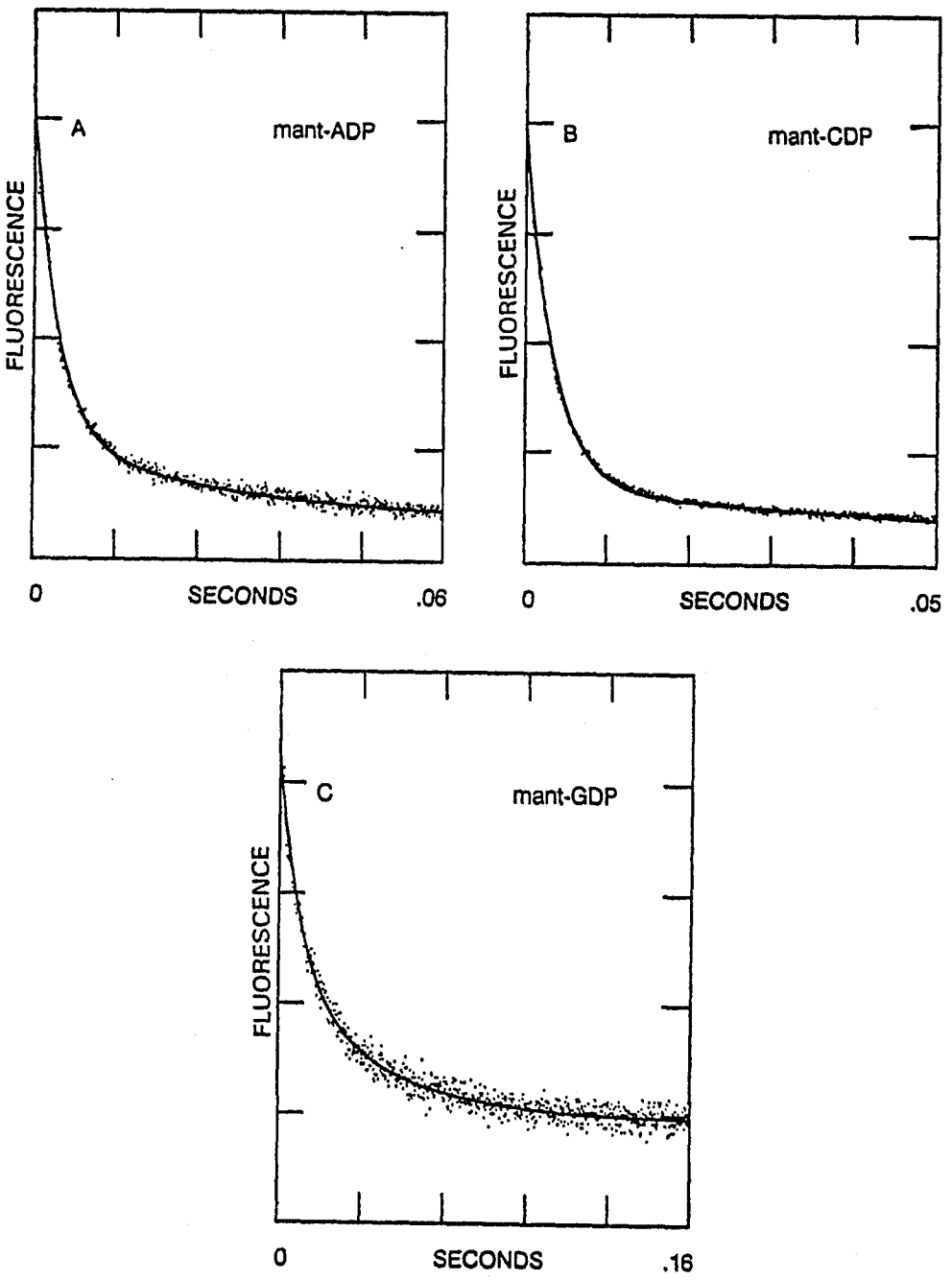

Fig.18. The dependence of $k_{(obs)}$ of the fast and slow components in fluorescence measurement of actin binding to BV.S1-mant-NDP upon actin concentration at 20°C. The experimental conditions were the same as in the legend to Fig.17 except for the actin concentration. The time courses were fit to double exponential equation and the $k_{(obs)}$ of fast and slow phases were fit to equation 3. The data were listed in Table VI(B). (A) upper panel: the amplitude coefficient (I_f/I_{tot}) in actin binding to BV.S1-mant-ADP when final mant-ADP concentration was 7.5 μM (triangle) and 75 μM (square).

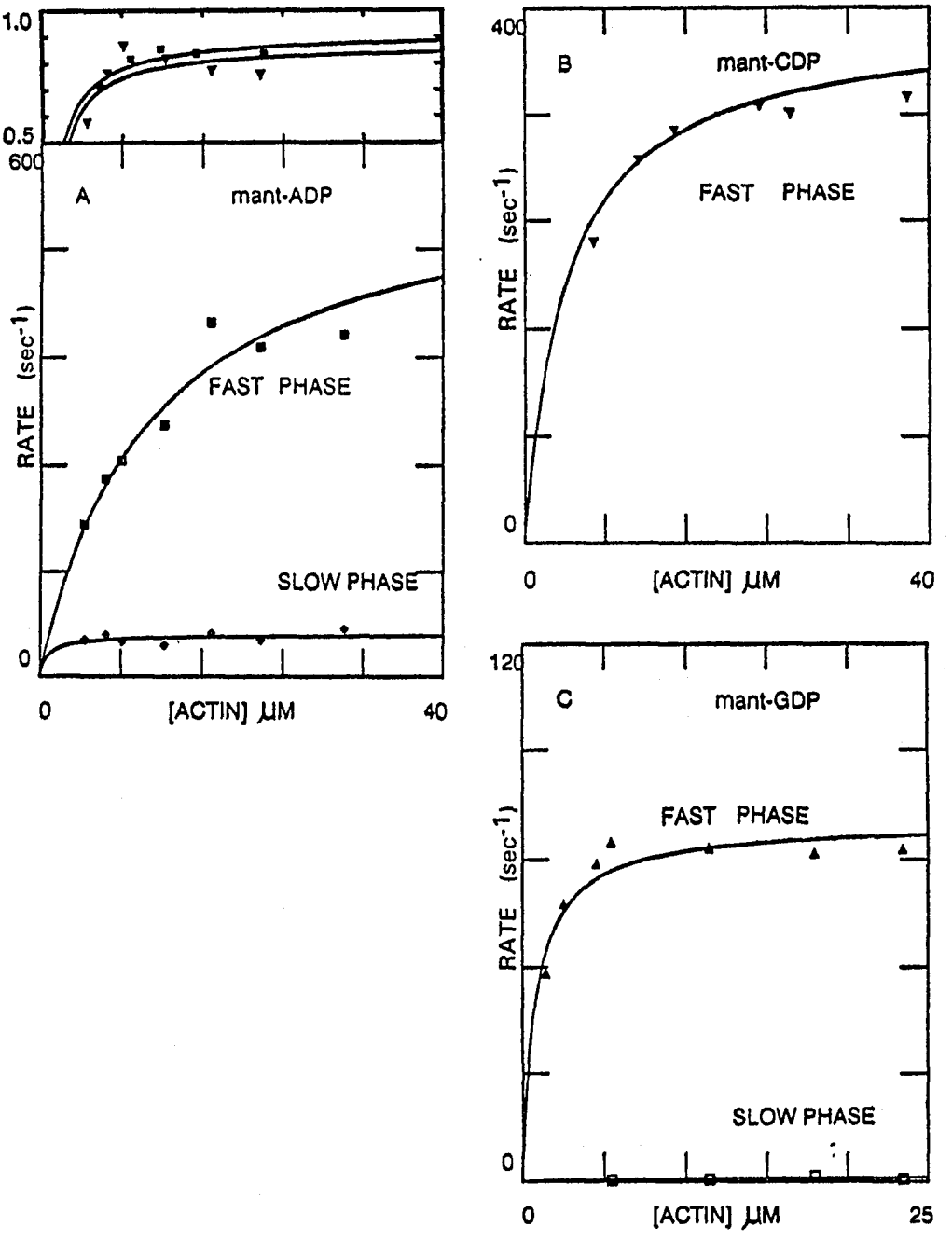

maximum rate and the affinity of actin binding to RS.S1-mant-ADP are increased (K_{FL} 25.45 μM, k_{FL} 447.1 s^{-1}, compared to K_{FL} 50.88 μM, k_{FL} 285.3 s^{-1} in the absence of PEG in the same condition). The amplitude of fluorescence change in the presence of PEG was only half as much as that in the absence of PEG.

In-vitro Motility Measurement and Step Size Calculation

The in-vitro motility assay was used to measure the dependence of steady state velocity of actin movement upon the structure and concentration of NTP (or mant-NTP). The measurements were used to obtain the dependence of velocity upon NTP concentration (in analogous to that of skinned fibers), and used for step size calculation (see "Method"). Compared with the data from fiber shortening experiments, in-vitro motility assays can test the restriction of myolattice upon the muscle contraction mechanism. It can also be used to measure the motility for cardiac muscle from which fibers suitable for mechanical experiments can't be prepared.

Fig. 19 shows the dependence of actin sliding velocity promoted by immobilized RS.HMM upon the concentration of mant-ATP and mant-CTP at 20°C and 25°C. The dependence of actin sliding velocity upon the concentration of ATP, CTP and mant-ATP was also measured using immobilized BV.myosin (Fig. 20). The kinetic data for in-vitro motility assay and step size calculations are listed in Table VII.

Fig.19. The dependence of actin sliding velocity promoted by RS.HMM upon the concentration of mant-ATP and mant-CTP. Actin filaments were fluorescently labeled with tetramethylrodamine-phalloidin. RS.HMM was immobilized on a nitrocellulose coated glass surface. The experimental conditions were 25 mM KCl, 25 mM imidazole-HCl (pH 7.4), 4 mM $MgCl_2$, 1 mM DTT, at 20°C and 25°C. The image was videotaped and analyzed using program "Motion Submenu" of "Image". In each rate analysis, eight *.tif files were established, each being obtained by averaging 16 images. The dependence of $k_{(obs)}$ upon mant-NTP concentration were fit to equation 3. The values of K_m and V_m were listed in Table VII.

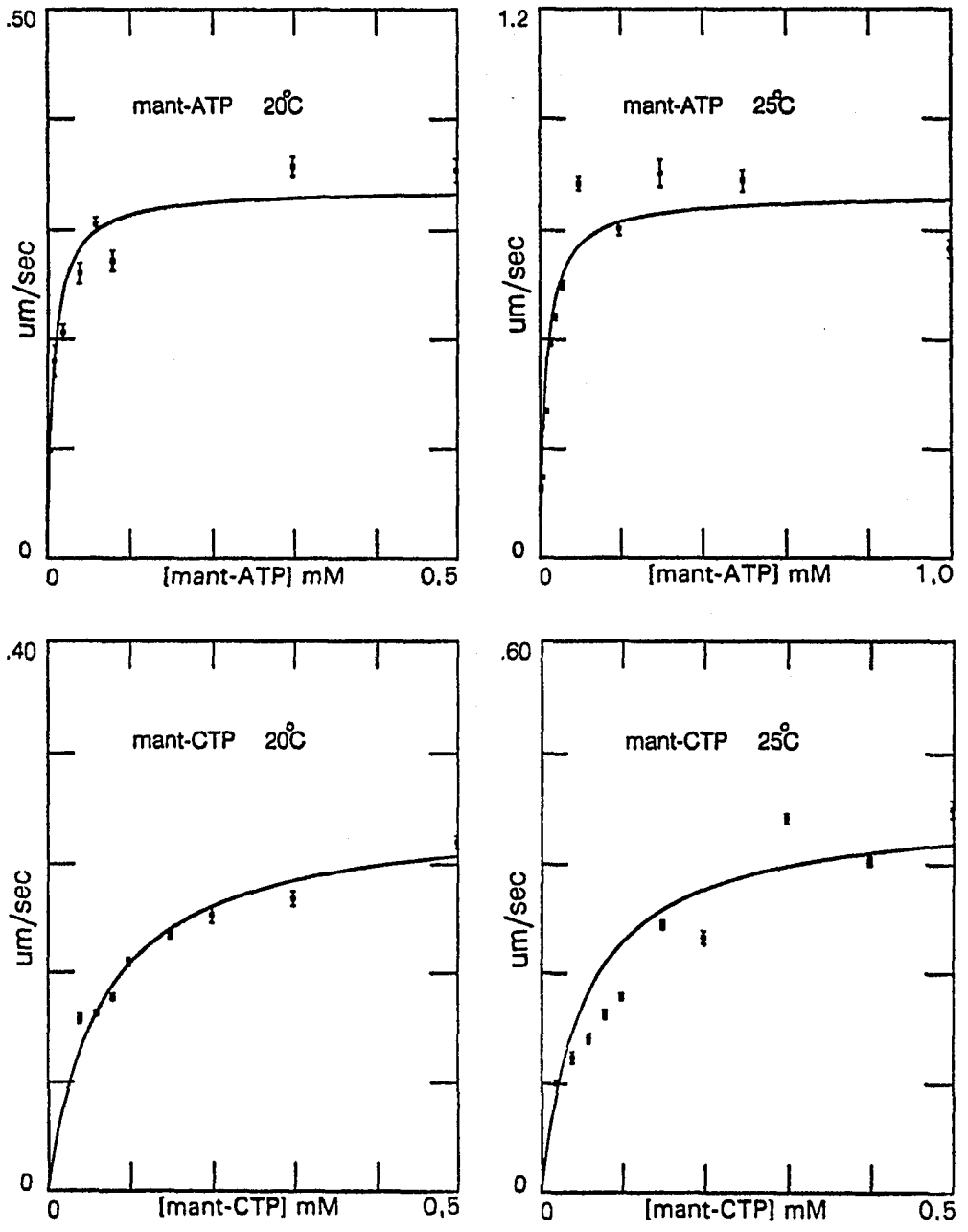

Fig.20. The dependence of actin sliding velocity promoted by BV.myosin upon the concentration of ATP, CTP, and mant-ATP. Actin filaments were fluorescently labeled with tetramethylrodamine-phalloidin. BV.myosin was immobilized on a glass surface coated with dimethyldichlorosilane (diluted 1:50 v/v in chloroform). The experimental conditions were 25 mM KCl, 25 mM imidazole-HCl (pH 7.4), 4 mM $MgCl_2$, 1 mM DTT, at 20°C. The image was videotaped and analyzed using program "Motion Submenu" of "Image". In each analysis, eight *.tif files were established, each being obtained by averaging 16 images. The dependence of $k_{(obs)}$ upon the concentration of ATP, CTP and mant-ATP were fit to equation 3. The values of K_m and V_m were listed in Table VII.

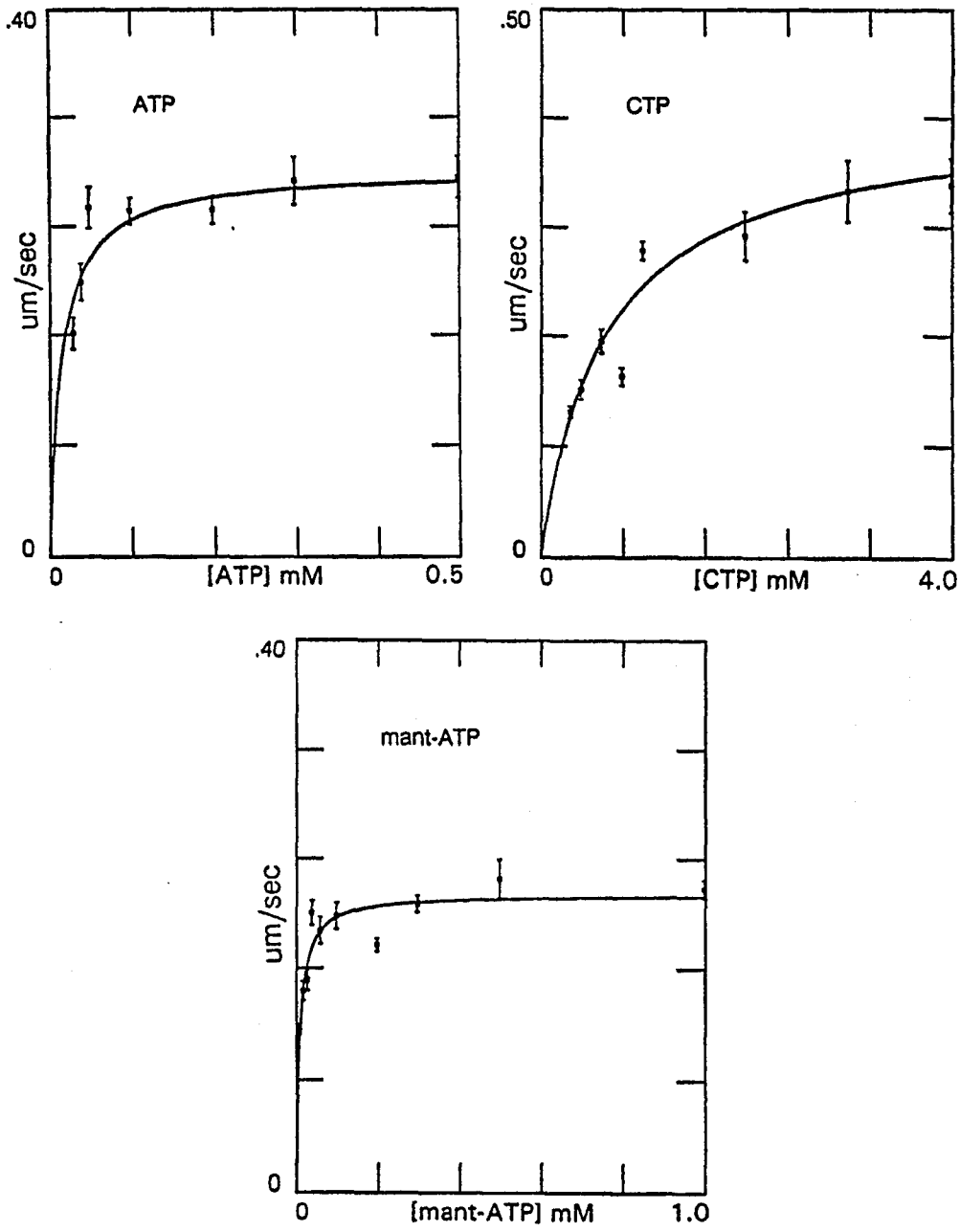

Table VII. The calculation of step size (D).

	Temp. (^oC)	K_m (μM)	V_m ($\mu m/s$)	V_m/K_m ($nm\ M^{-1}s^{-1}$)	k_a/K_o ($M^{-1}s^{-1}$)[d]	D (nm)[a]
RS.HMM						
ATP[b]	10	150[c]	1.8[c]	1.2x10E7[c]	2.7x10E6	4.6
CTP[b]	10	1900[c]	1.2[c]	6.2x10E5[c]	1.4x10E5	4.4
azaATP[b]	10	380[c]	0.4[c]	1.2x10E6[c]	3.4x10E5	3.9
GTP[b]	10	1600[c]	0.1[c]	5.9x10E4[c]	2.5x10E5	0.2
ATP[e]	24			3.0x10E7[f]	5.7x10E6	5.1
mantATP[e]	20	7.7[g]	0.34[g]	4.4x10E7[g]	8.4x10E6	5.2
mantATP[e]	25	17[g]	0.80[g]	4.8x10E7[g]	1.1x10E7	4.3
mantCTP[e]	20	68[g]	0.28[g]	4.1x10E6[g]	7.3x10E5	5.7
mantCTP[e]	25	55[g]	0.42[g]	7.7x10E6[g]	1.4x10E6	5.5
BV.myosin						
ATP[e]	20	15[g]	0.28[g]	1.9x10E7[g]	4.3x10E6	4.4
CTP[e]	20	642[g]	0.40[g]	6.3x10E5[g]	1.2x10E5	5.2
mantATP[e]	20	8.8[g]	0.21[g]	2.4x10E7[g]	4.8x10E6	5.1

a, Calculated using equation 8.
b, Experimental conditions: 0.18 M potassium acetate, 20 mM phosphocreatine, 20 mM MOPS (pH 7.0), 5 mM $MgCl_2$, 1 mM EGTA.
c, Determined from muscle fiber shortening experiments. Data from Pate et al.(1993).
d, Determined from stopped-flow experiments. Data from Table III.
e, Experimental conditions: 25 mM potassium chloride, 25 mM imidazole-HCl (pH 7.4), 4 mM $MgCl_2$, 1 mM EGTA, and 1 mM DTT.
f, Determined from in-vitro motility measurements. Data from Kron and Spudich (1986).
g, Determined from in-vitro motility measurements.

To improve the quality of image, the background was subtracted from each image, and region setting was used to eliminate the artifacts at the edge of image caused by background subtracting.

In the in-vitro motility assay, the maximum rates were repeatable, accurate, and followed the order of RS.HMM > BV.myosin, CTP > ATP > mant-ATP > mant-CTP. The apparent second order rate constants (the slopes) were less accurate, since the motility rates didn't reasonably decrease at low NTP concentrations. The minimum rates could be measured were at the range of 0.09 - 0.16 μm/s. Even in the absence of NTP, a value of 0.134 μm/s was obtained for acto-BV.myosin at 25°C. This could cause error especially when the maximum rate was slow. To avoid this, some unreasonable high values at low NTP concentrations were omitted.

BV.myosin showed very similar motility behavior to BV.HMM. BV.myosin gave K_m 14.89 μM, V_m 0.281 μm/s at 20°C, when ATP as substrate, which was comparable to BV.HMM, K_m 14.62 μM, V_m 0.303 μm/s in the same condition (data from Amy Robinson). This suggests that the motility of BV.HMM is intact and can be used to represent BV.myosin in in-vitro motility assay.

The dimethyldichlorosilane (DMDCL) coating (for BV.myosin in-vitro motility measurement) was less satisfactory than nitrocellulose, as a large fraction of the fluorescence-labeled actin filaments on DMDCL coating were washed out by high concentrations of NTP solution. The remaining actin

filaments were difficult to focus in the same plane, and moved in and out of focus.

The image of mant-NTP lasted at least two to three times longer than that of NTP, possibly because the mant-group absorbed most of the light, and therefore, improved the life span of fluorescence labels on actin filaments.

Preparation and Characteristics of Bovine Cardiac HMM

The detailed procedure of bovine cardiac HMM preparation was shown in the "Method." Consistent BV.HMM preparations could be made according to this procedure. The ATPase assay in 5 mM MOPS (pH 7.0), 2 mM $MgCl_2$, 0.5 mM DTT, at 15°C, gave $K_{0.5}$ 5.6 - 22.2 μM and V_{max} 0.5 - 0.7 s^{-1} (Fig. 21A). The binding constant of actin to BV.HMM during steady state ATP hydrolysis under the same conditions was 13.54 μM (Fig.21B).

The best conditions for BV.myosin digestion were 10 min. at 20°C, using 0.05 mg/ml chymotrypsin and 4 - 5 mg/ml myosin, as described by Margossian (1985). During the digestion process, BV.myosin heavy chain was cleaved, and one of the two light chains was also partially degraded. The experiment of actin binding to acto-BV.HMM-mant-ADP gave an abnormal fluorescence change. The shape of the time course varied with each trace, and its amplitudes were not repeatable. This suggests the damage to the protein by proteolysis. Digestion of BV.myosin preceding the first DEAE column resulted in an extensive degradation by proteases (Amy Robinson, personal communication). An actin

Fig.21. The measurement of steady state ATPase activity and actin binding constant of BV.HMM during steady state ATP hydrolysis.

(A) The measurement of steady state ATPase activity for bovine cardiac HMM in 5 mM MOPS (pH 7.0), 2 mM $MgCl_2$, 0.5 mM DTT, at 15°C. The final concentrations in reaction system were 0.25 µM HMM, 0 - 25 µM F-actin, 1 mM ATP. $K_{0.5}$ = 11 µM, V_{max} = 0.73 s^{-1}.

(B) The measurement of binding constant of BV.HMM to actin during steady state ATP hydrolysis in 5 mM MOPS(pH 7.0), 2 mM $MgCl_2$, 0.5 mM DTT. The mixture of 0.025 mg/ml HMM, 0 - 25 µM F-actin, and 1 mM ATP was spun at 15°C, 50,000 RPM for 20 min. ATPase activity was measured at 25°C. The binding constant was 13.5 µM.

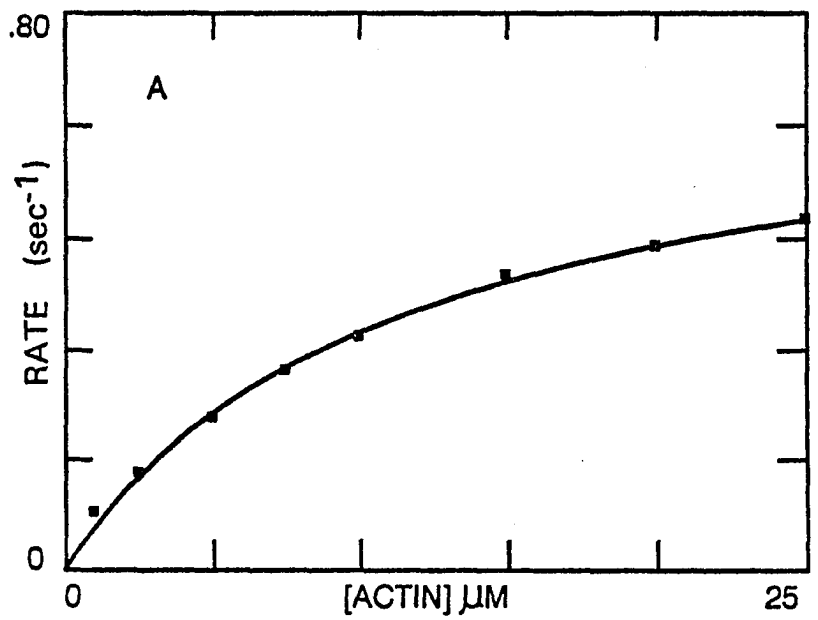

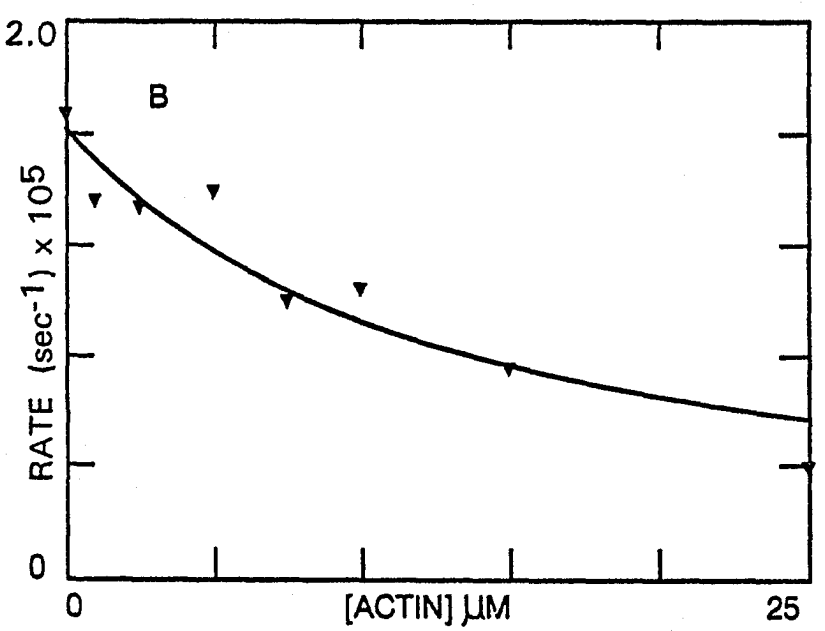

or ATP present during digestion considerably decreased the HMM's ATPase activity, which indicates the severe damage of BV.myosin.

Quench-flow experiments were done on acto-BV.HMM and acto-BV.myosin in 25 mM imidazole-HCl (pH 7.4), 4 mM $MgCl_2$, 1 mM EGTA, 1 mM DTT, and either 25 mM KCl (for HMM) or 0.5 M KCl (for myosin), at 20°C (Fig.22). All of them gave burst kinetics. The experiments using BV.HMM gave low and scattered data. This may be caused by bound ADP on BV.HMM heads. The bound ADP seems to be released after actin binding to BV.HMM since the larger burst sizes were observed with pre-steady state hydrolysis of ATP by acto-BV.HMM than BV.HMM. The rate and amplitude were summarized in Table VIII.

Preparation and Characteristics of Mant-Nucleotides

A series of fluorescently labeled mant-nucleoside triphosphates (mant-ATP, mant-CTP, mant-GTP, mant-dATP and mant-AMP-PNP) and mant-nucleoside diphosphates (mant-ADP, mant-CDP, mant-GDP, and mant-dADP) were prepared. Fig.23 showed the elution pattern of mant-ATP and mant-AMP-PNP on Sephadex LH-20 column. With the exceptions of mant-dADP, mant-GTP and mant-AMP-PNP, the mant-nucleotides followed the same elution pattern as mant-ATP: a parent nucleotide peak, followed by a fluorescent mant-nucleotide peak, then a small fluorescent peak, finally, the parent mant-reagent peak. In the case of mant-dADP, the second fluorescent peak was

Fig.22. The time courses for pre-steady state hydrolysis of gamma-^{32}P-ATP by RS.S1(A2), acto-BV.HMM, and acto-BV.myosin measured in quench-flow. The experimental conditions were 25 mM imidazole-HCl (pH 7.4), 4 mM $MgCl_2$, 1 mM EGTA, 1 mM DTT, and either 25 mM KCl (for HMM) or 0.5 M KCl (for myosin), at 20°C. The concentrations in the reaction cell were (A) 1 µM RS.S1(A2), 0.5 µM ^{32}P-ATP, (B) 1.5 µM F-actin, 0.5 µM BV.HMM (1 µM S1 heads), and 0.5 µM ^{32}P-ATP, (C) 1.5 µM F-actin, 0.5 µM BV.HMM (1 µM S1 heads), and 2 µM ^{32}P-ATP, (D) 2.5 µM F-actin, 1 µM BV.myosin (2 µM S1 heads), and 4 µM ^{32}P-ATP. The time courses were fit to double exponential equation. The values of amplitudes and rates were listed in Table VIII.

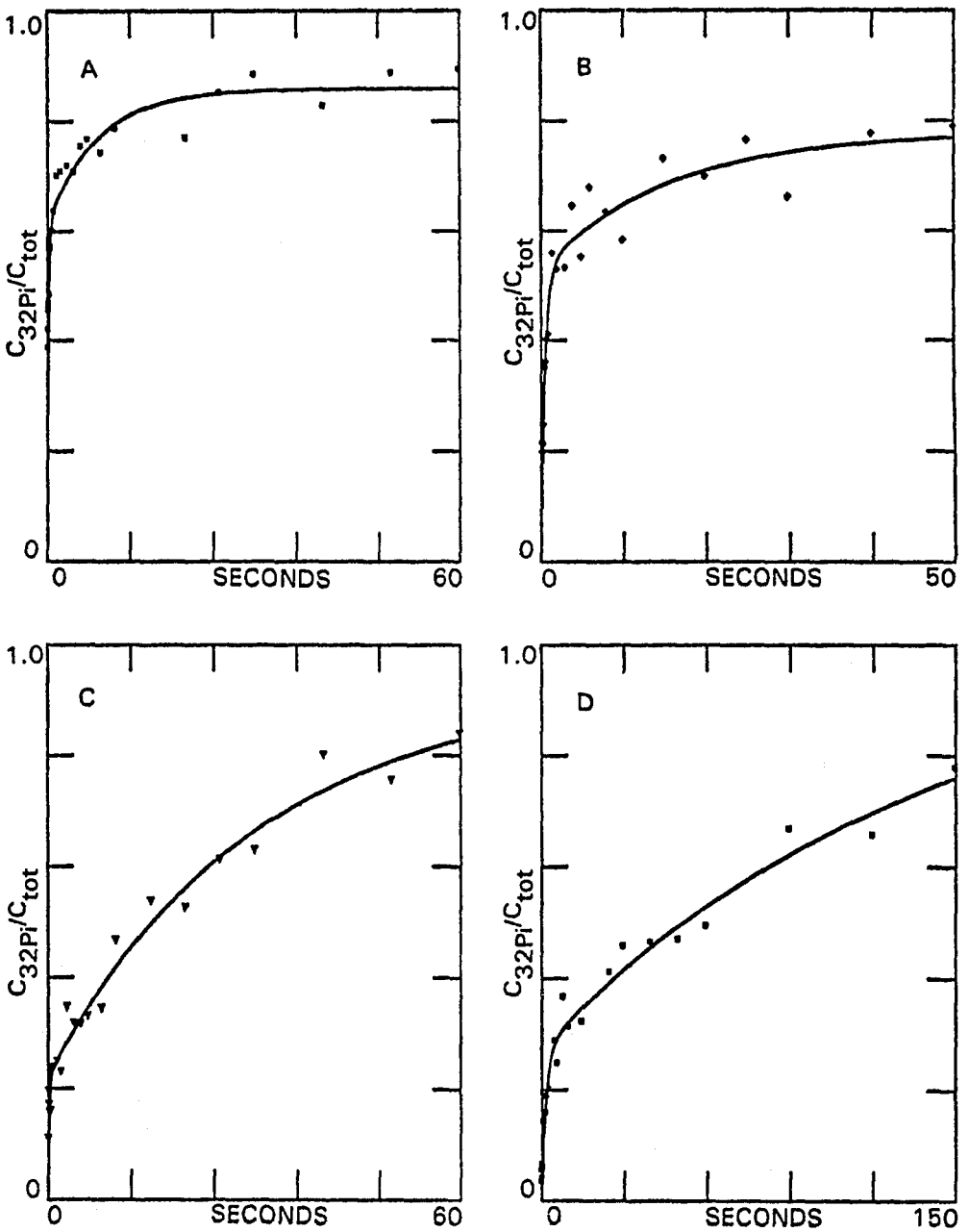

Table VIII. The amplitude and rate in quench-flow measurement of ATP hydrolysis by RS.S1, acto-BV.HMM, and acto-BV.myosin.

	fast phase		slow phase	
	amplitude	rate	amplitude	rate
RS.S1(A2)[2μM]-				
ATP[1μM]	0.61	4.9	0.25	0.14
acto[3μM]BV.HMM[1μM]-				
ATP[1μM]	0.47	1.2	0.25	0.041
acto[3μM]BV.HMM[1μM]-				
ATP[4μM]	0.22[a]	5.0	0.70	0.033
acto[5μM]BV.myosin[2μM]-				
ATP[8μM]	0.28[b]	0.53	0.87	0.005

The experimental conditions are shown in the legend to Fig.22.

The actual burst amplitudes are 0.44 (for *a*) and 0.56 (for *b*), since ATP concentrations are twice as much as that of acto-S1.

Fig.23. The elution pattern of (A) mant-ATP and (B) mant-AMP-PNP on Sephadex LH-20 column. The column was 2.5 cm x 95 cm in size. The absorption was measured at 255 nm and 356 nm, respectively, in 50 mM Tris-HCl (pH 8.0).

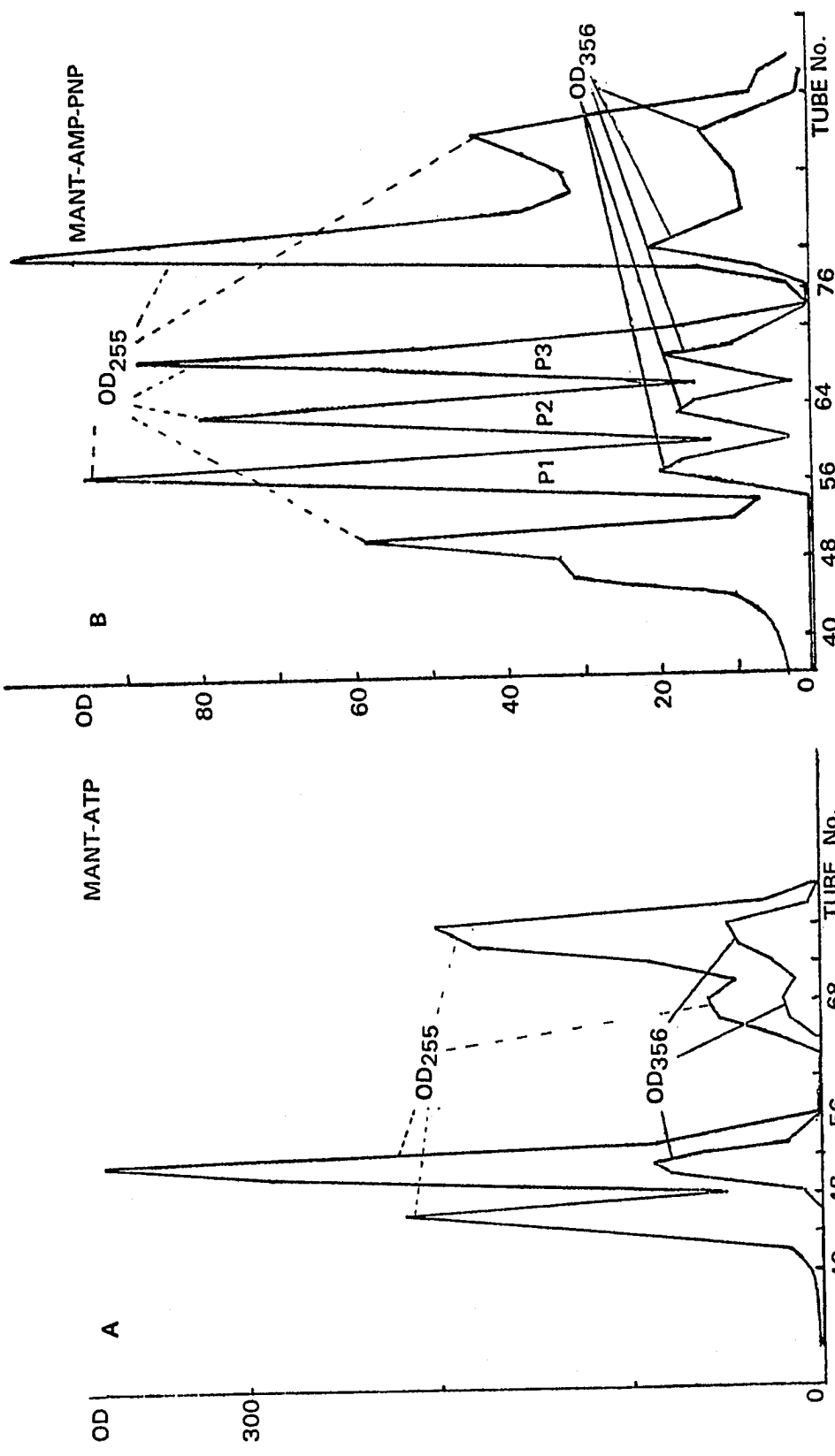

bigger than the first one. Both of the peaks have the same kinetic behavior in the reaction of actin binding to RS.S1(A1)-mant-dADP. Mant-GTP couldn't be separated from GTP, therefore, an additional DEAE-52 cellulose column was used. GTP eluted first, followed by mant-GTP peak. Mant-AMP-PNP was eluted in three mant-AMP-PNP peaks (P1, P2 and P3), and all of them have the same kinetic behavior in the reaction of acto-RS.S1 dissociation by mant-AMP-PNP.

The mant-NTP and mant-NDP prepared here probably contain a mixture of 2'- and 3'- isomers. The HPLC analysis on mant-ADP showed a small peak closely followed by a large peak, with a ratio of 0.15 : 0.85 (data from Belknap, B.).

The mant-nucleotide preparations were consistent, as was their kinetic behavior. For example, different preparations of mant-ADP show the same kinetic behavior in the reaction of actin binding to RS.S1-mant-ADP.

The absorption profile and extinction coefficient of mant-CDP were measured to determine the absorption peak for concentration measurement (see "Method"). Fig.24 shows the absorption profile of mant-CDP. It gave maximum absorption at 254 nm and 356 nm, at pH 6.5 - 7.0, in water. In the measurement of extinction coefficient of mant-CDP, CDP was chosen as a standard (extinction coefficient 9144 $M^{-1}cm^{-1}$ at pH 7.0), and 89.5 percent of the theoretical acid labile phosphate (beta phosphate) was released from CDP (in 1 M HCl, 8 min. in boiling water). The absolute concentration of mant-CDP was determined by measuring acid labile phosphate

Fig.24. The absorption profile of mant-CDP at pH 6.5 - 7.0, in water, measured in UV-visible spectrophotometer (Gilford 250). The two absorption peaks are at 254 nm and 356 nm, respectively.

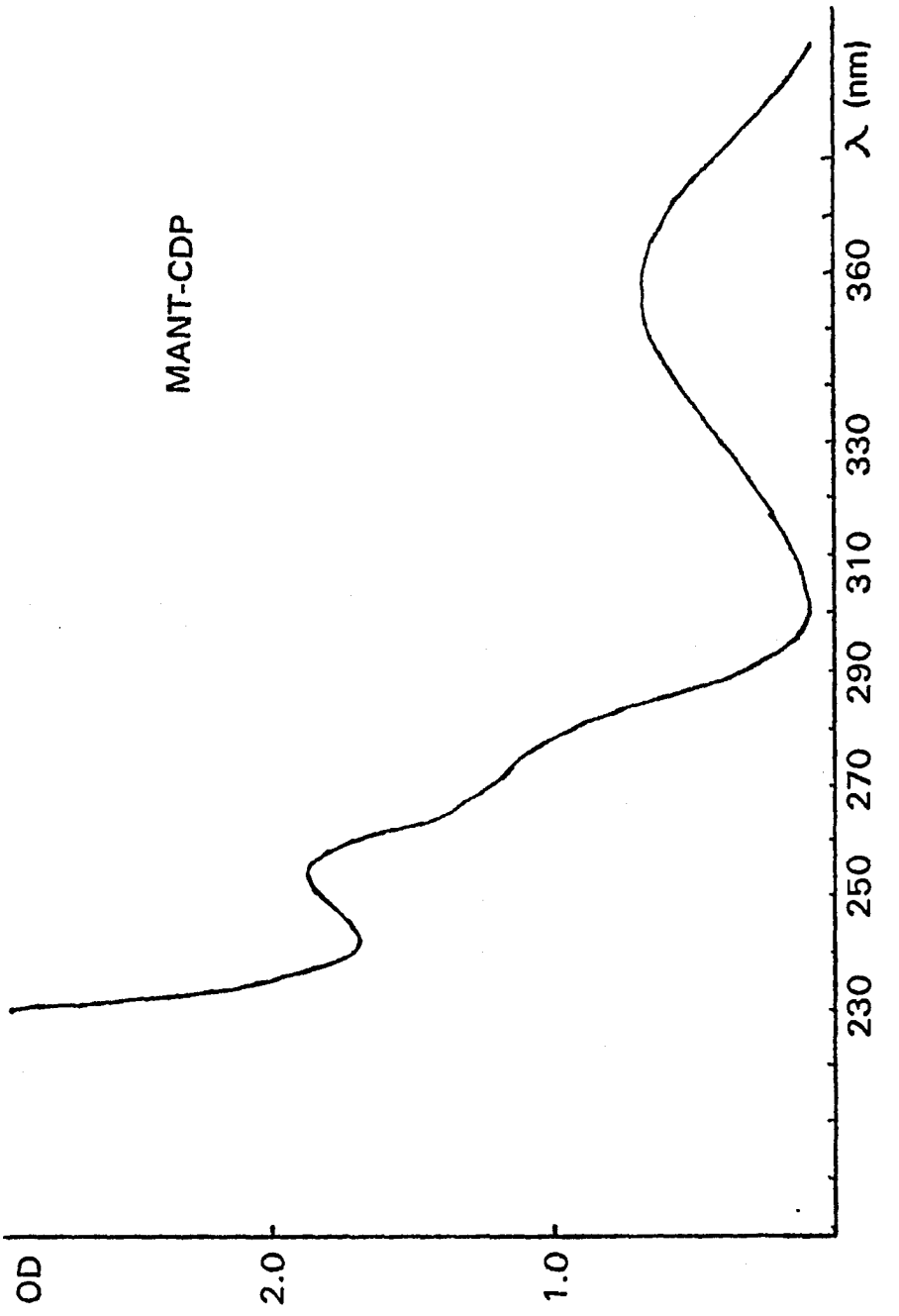

released from mant-CDP. It was assumed that the yield of acid labile phosphate released from mant-CDP was equal to that from CDP. The extinction coefficients at 254 nm and 356 nm were measured to be 16.37×10^3 ($M^{-1}cm^{-1}$) and 5.96×10^3 ($M^{-1}cm^{-1}$), respectively.

DISCUSSION

Muscle contraction is thought to be accomplished by cyclic interaction of actin and myosin using ATP as an energy source. During this process, force and tension are produced. A general subject in muscle contraction research is to establish the correlation between the biochemical steps of the mechanism and the mechanical properties in the muscle fiber. A successful approach has been made during past decades (Huxley and Simmons, 1971; Ferenczi et al., 1984; Goldman, 1987; Kawai and Halvorson, 1989).

The long term aim of this research is to investigate the dependence of the mechanical properties of the muscle upon the changes in different biochemical steps of the mechanism in solution. Since actomyosin is a relatively nonspecific enzyme, it can use a series of NTP and NTP analogs as energy sources. It has been found that the rate and equilibrium constants of the steps in the mechanism vary considerably with the structure of NTP (Pate, et al., 1993; White et al., 1993). The strategy in this dissertation is to use the dependence of the rate and equilibrium constants of the steps in the mechanism upon the structures of NTP and NTP analogs as a probe to investigate the dependence of mechanical properties upon the biochemical steps in the

mechanism.

Rabbit psoas muscle is an ideal material for fiber shortening studies. So, rabbit skeletal actomyosin was chosen to compare the fiber shortening data with biochemical kinetics. Moreover, rabbit skeletal actomyosin is relatively stable and is an established preparation. Bovine cardiac myosin was also used in this research because it has lower rate constants of steps which are too rapid to measure for skeletal myosin, and because it has unique kinetic properties which are different from those of skeletal myosin.

Rabbit skeletal actin was also used rather than bovine cardiac actin in studies of acto-BV.myosin mechanism since actin is evolutionally conservative, and actin molecules from skeletal and cardiac muscles are identical in function.

The Dissociation of Actomyosin-S1 By NTP and NTP Analogs

The dissociation of actomyosin-S1 by NTP (or mant-NTP) was monitored by stopped-flow light scattering upon mixing acto-S1 with various concentrations of NTP or mant-NTP. The light scattering measurement of this reaction was used to investigate the binding of NTP to acto-S1, and acto-S1 dissociation. The experimental data obtained at high ionic strength can be explained by the following simple model (Model 5):

$$AM + T \overset{1/K_o}{\longleftrightarrow} AM.T \xrightarrow{k_a} A + MT \qquad \text{Model 5}$$

Here A is actin, M is myosin-S1, T is NTP or mant-NTP. K_o and k_a are equilibrium and rate constants, respectively.

Table III shows that the maximum rate and apparent second order rate constant are dependent upon NTP structure. As a typical example, the k_a/K_o of acto-RS.S1 for ATP is about 20 times higher than that of CTP. The kinetic data are also slightly dependent upon the type of myosin-S1. Acto-BV.S1 has two fold lower k_a and k_a/K_o than that of acto-RS.S1.

The NTP and NTP analogs used here can be divided into several groups based on the difference in structures from the natural substrate, ATP: a) the modifications on the base moiety, such as CTP, aza-ATP and GTP, were found to decrease the apparent second order rate constant of NTP binding to acto-RS.S1 (k_a/K_o) by 8 - 20 times, while the maximum rate of acto-RS.S1 dissociation (k_a) is less affected (decreased 1 - 4 times). This result indicates the base moiety of NTP is important for the affinity of NTP to acto-RS.S1; b) the modifications on the ribose moiety, such as mant-ATP, were found to decrease k_a by 12 times, while k_a/K_o is essentially unchanged. This observation suggests that ribose moiety plays an important role on affecting the rate of acto-RS.S1 dissociation; c) the modifications on both the base and ribose moiety, such as mant-CTP and mant-GTP, which show additive effect on the decrease of both k_a and k_a/K_o; and d) the modification on ribose and triphosphate moieties, such

as mant-AMP-PNP, which also considerably decreases k_a and k_a/K_o and causes incomplete dissociation. The k_a and k_a/K_o for dissociation of acto-RS.S1 by AMP-PNP are considerably slower than that for ATP (> 50 s^{-1} and $1.1x10^4$ $M^{-1}s^{-1}$, respectively, in 0.1 M KCl at 20°C, Trybus and Taylor, 1982). This slower dissociation indicates the important role of the triphosphate moiety on the affinity of NTP to acto-RS.S1 and on the maximum rate of acto-RS.S1 dissociation.

In spite of the considerable difference discussed above, there is no correlation between the rate of NTP binding to acto-S1 and the steady state rate of hydrolysis and fiber contraction parameters such as active tension and unloaded shortening velocity (Table IX). For instance, CTP has lowest second order rate constant for binding to acto-S1; but it supports the highest steady state rate of hydrolysis and has higher active tension and unloaded shortening velocity than aza-ATP.

The dependence of the steady state rate of NTP hydrolysis upon NTP structure in skeletal muscle fibers is in good correlation with that in solution for CTP and aza-ATP (Table IX).

The Step Size Measurement

Step size is measured by determining the apparent second order rate constant of shortening velocity by the dependence of acto-S1 dissociation upon NTP concentration (Eq. 8).

The step sizes of RS.HMM give the values of 4 - 6 nm,

Table IX. Comparison of parameters for nucleoside triphosphate binding to, and hydrolysis by acto-RS.S1 in solution with those describing muscle fiber contraction produced by GTP, CTP, aza-ATP and ATP.

Values in this Table are all normalized relative to 1.0 for those measured for ATP.

	GTP	CTP	aza-ATP	ATP
Hydrolysis[a] (isometric fiber)	0.083	1.7	0.25	1.0
Hydrolysis[b]	0.02	1.4	0.13	1.0
(V_m/K_m)[a] (unloaded fiber)	0.005	0.05	0.10	1.0
(k_a/K_o)[c]	0.09	0.05	0.12	1.0
step size[d]	0.05	0.96	0.85	1.0
Active tension[a]	0.1	0.8	0.25	1.0
Active stiffness[a]	0.85	0.93	1.0	1.0
Unloaded shortening velocity[a]	0.05	0.66	0.23	1.0

a, Data from Pate et al. (1993).

b, Steady state rate of NTP hydrolysis by acto-RS.S1, data from White et al. (1993).

c, Second order rate constant of NTP binding to acto-RS.S1, data from Table III.

d, Data from Table VII.

calculated from either the data of muscle fiber shortening experiments at 10°C or in-vitro motility measurements at 20 - 25°C using various NTP or NTP analogs as substrate. Although the second order rate constant for the dissociation of acto-RS.S1 by ATP is about 20 times faster than that of CTP, the step size for ATP and CTP, 4.6 and 4.4 nm, respectively, are the same within experimental error.

The step size for ATP calculated using V_m/K_m from in-vitro motility assays, 5.1 nm, is in good agreement with that from fiber unloaded shortening experiments, 4.6 nm. This indicates that the geometric constraints of the myolattice and/or high concentration of actin and myosin in the fibers does not significantly affect the shortening mechanism.

The step sizes of BV.myosin, 4.4 - 5.2 nm, are the same within experimental error as those of RS.HMM. The step sizes are also independent of experimental conditions (ion strength, temperature, etc.), and nucleoside triphosphate structures (as long as it can be hydrolyzed and efficiently produce tension and work)(Table IX). This result suggests that step size, as a structural parameter, is a more fundamental property of the actomyosin interaction.

The apparent small value of step size measured with GTP (almost 20 times lower than that with ATP, CTP and aza-ATP), and the relatively high value of the second order rate constant (about twice as much as that of CTP) can be explained by its unusual kinetics: 1) the very slow rate of steady state hydrolysis in fiber and in solution (Table IX)

may not provide enough force generating intermediate and thus, causes low active tension (Table IX); 2) the absence of phosphate burst in the pre-steady state hydrolysis with cardiac myosin-S1 (Belknap et al., 1990) indicates that the predominant intermediate in GTP hydrolysis pathway is myosin-S1.GTP rather than myosin-S1.NDP.P, which is the predominant intermediate of the ATP hydrolysis pathway. Therefore, the large perturbation of the mechanism of GTP hydrolysis makes it likely that the calculation of the step size using equation 8 is not valid for GTP (White et al., 1993).

The Dissociation of Acto-RS.HMM By ATP

The second order rate constant of the binding of ATP to acto-RS.HMM (Table V) is quite similar to that of acto-RS.S1. The model of acto-RS.HMM dissociation by ATP is more complicated than that of acto-RS.S1 because there are two heads in each HMM molecule. The following model (Model 6) is proposed to describe the reaction of acto-RS.HMM dissociation.

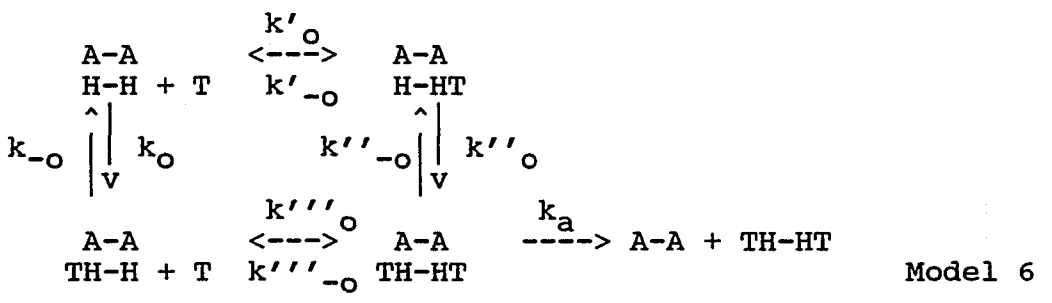

Model 6

Here, A-A, H-H and T are actin filaments, HMM, and ATP, respectively. Each "H" represents one HMM head. k's are rate constants.

This model can be simplified as the following linear model (Model 7), if $k_o = k'_o = k''_o = k'''_o$, and $k_{-o} = k'_{-o} = k''_{-o} = k'''_{-o}$.

$$AH + T \underset{k_{-o}}{\overset{2k_o}{<----->}} AHT + T \underset{2k_{-o}}{\overset{k_o}{<----->}} AHTT \xrightarrow{k_a} A + HTT$$

Model 7

Here, A, H and T are actin, HMM and ATP, while HT and HTT represent one and two ATP bound to each HMM, respectively.

Computer solutions of Model 7 (Zhang et al., 1989) give a sigmoidal dependence of $k_{(obs)}$ upon ATP concentration for mechanisms in which acto-RS.HMM and ATP are in fast equilibrium ($k_{-o} > k_a$), not tracing acto-S1 dissociation which is hyperbolic under the same conditions. The dependence of $k_{(obs)}$ upon ATP concentration observed in this experiment is essentially linear (Fig.12), which rules out the fast equilibrium mechanism. A sigmoidal dependence of $k_{(obs)}$ upon ATP concentration is also expected from model fitting when k_o is equal to the measured second order rate constant of ATP binding to acto-RS.HMM, 2.2×10^6 $M^{-1}s^{-1}$, and k_{-o} is greater than 10 s^{-1}. A linear dependence can only be obtained by decreasing k_{-o} to less than 5 s^{-1}. This gives an estimation of k_{-o} (< 5 s^{-1}), which is consistent with the observation of Sleep and Hutton (1978). This indicates that ATP release from acto-RS.HMM is quite slow.

Models for which $k_{-o} > 10s^{-1}$ also show a fast negative amplitude component in the time courses which causes a lag

at low ATP concentrations. However, this lag in time courses is difficult to be observed experimentally, and hence, is less reliable as a criterion.

The Fluorescence Changes Preceding and After Acto-S1 Dissociation

The fluorescence change observed during the dissociation of acto-S1 by NTP (or mant-NTP) may reflect the changes in the microenvironment of the fluorophore or in the conformation of myosin-S1 preceding and/or after the dissociation of acto-S1, and/or the step of NTP hydrolysis. The results support Model 8 proposed by Johnson and Taylor (1978), in which there is an initial fluorescence enhancement prior to acto-S1 dissociation.

$$AM + T \overset{1/K_{AT}}{<\!\!-\!\!>} AMT \overset{k_{TA}}{<\!\!-\!\!>} AMT^{*} \overset{k_{-A}}{<\!\!-\!\!>} A + MT^{*} \underset{k_{-H}}{\overset{k_{H}}{<\!\!-\!\!>}} M^{**}(T)$$

Model 8

Here A = actin; M = S1; T = NTP; K and k's are equilibrium and rate constants, respectively. (T) means NTP may or may not be hydrolyzed. * and ** represent different fluorescence states.

The rates of light scattering, fluorescence and NTP hydrolysis are listed in Table X. In the fluorescence measurement of acto-RS.S1 dissociation by ATP, the maximum rate of fluorescence change is almost the same as that measured in quench-flow experiment, and both of them are

Table X. Comparison of the rates of pre-steady state hydrolysis of gamma-^{32}P-NTP by acto-RS.S1 (v_H) with the rates in light scattering measurement (v_L) and fluorescence measurement (v_F) of acto-RS.S1 dissociation by NTP.

	[NTP] (μM)*	[acto-RS.S1] (μM)*		v_H (s^{-1})*a*	v_L (s^{-1})*b*	v_F (s^{-1})*b*
ATP*cd*	1	actoS1(A1)	2	2.1	5.4	2.6
	1	actoS1(A2)	2	1.2		
	10	actoS1(A1)	2	15	27	9.7
	10	actoS1(A2)	2	1.9		
	25	actoS1(A1)	4	21	65	16
	25	actoS1(A2)	4	37		
aza-ATP*ce*	2	actoS1(A1)	4	0.18	1.4	1.3
CTP*ce*	2	actoS1(A1)	4	0.61	0.52	0.51

a, Rates obtained from quench-flow measurement.

b, Rates calculated using equation

$v = k/K_{0.5}[S]$, at low [S], or

$v = k[S]/(K_{0.5} + [S])$, at high [S].

[S]: the concentration of NTP or acto-S1, whichever is higher.

The maximum rate (k), apparent equilibrium constant ($K_{0.5}$) and apparent second order rate constant ($k/K_{0.5}$) for light scattering and fluorescence measurement were from Table III and IV, respectively.

c, Experimental conditions: 0.18 M KAc, 20 mM MOPS (pH 7.0), 20 mM phosphocreatine, 5 mM $MgCl_2$, 1 mM EGTA, at 10°C.

d, Data from Wang, X., personal communication.

e, Data from Belknap, B., personal communication.

*. All concentrations are final.

slower than the rate of light scattering (which measures ATP binding and acto-S1-ATP dissociation), hence both the fluorescence change and quench-flow experiment are thought to measure the ATP hydrolysis step, consistent with the observations of Sleep and Taylor (1976). Since the maximum rates of fluorescence change and quench-flow measurement are very close, the mechanism of slow fluorescence change preceding fast hydrolysis step can't be ruled out (M^*T <-> $M^{**}T$ <-> $M^{**}DP$, the first step is slow).

In the case of acto-RS.S1 dissociation by aza-ATP, the rates of light scattering and fluorescence are close to each other, and much faster than that measured in quench-flow experiment, so that both the light scattering and fluorescence measure aza-ATP binding and acto-S1 dissociation, while quench-flow experiment measures the aza-ATP hydrolysis step.

The rates of light scattering, fluorescence, and quench-flow measurement for CTP are quite similar. Since the second order rate constant of CTP binding to acto-RS.S1 is slow, an experiment at much higher concentrations of CTP and acto-S1 is needed to measure the maximum rate of CTP hydrolysis.

The maximum rates of the fluorescence change in the dissociation of acto-RS.S1 by ATP and CTP are slower than that of the light scattering. This means that the fluorescence changes measured in these cases occur after acto-S1 dissociation (MT^* <--> $M(T)^{**}$ in Model 8, $k_b = k_H + k_{-H}$).

It is difficult to determine the order of the dissociation and fluorescence change induced by aza-ATP, since both of the maximum rates are greater than 1000 s^{-1} and less reliable to interpret. Although the apparent second order rate constant of fluorescence change is slightly lower than that of light scattering, this may be caused by non-linear relationship between dissociation fraction and light scattering. At least, this fluorescence change reflects a process closely related to actomyosin dissociation by aza-ATP. Because of the similarity between apparent second order rate constants in fluorescence and light scattering measurement, aza-ATP fluorescence measurement was used to test actomyosin dissociation step when light scattering can't be directly monitored (Smith and White, 1985a).

No fluorescence change occurs with the dissociation of acto-RS.S1 by GTP. The predominant intermediate in NTP hydrolysis for GTP is thought to be (A)M.GTP, rather than (A)M.NDP.P for ATP and CTP, since GTP and ITP give no phosphate burst during the first turnover hydrolysis (Belknap et al., 1990). The unusual kinetic behavior of GTP indicates that the kinetic difference between GTP and ATP in muscle contraction mechanism is primarily due to the difference between the interaction of the amino acid residue(s) in myosin-S1 with the 6-NH_2 group in ATP, and that with 6-keto group in GTP (the structures of ATP and GTP are shown in Fig. 25). These observations suggest that the favored interaction of the amino acid residues in myosin-S1

Fig.25. Comparison of the structures of ATP and GTP.

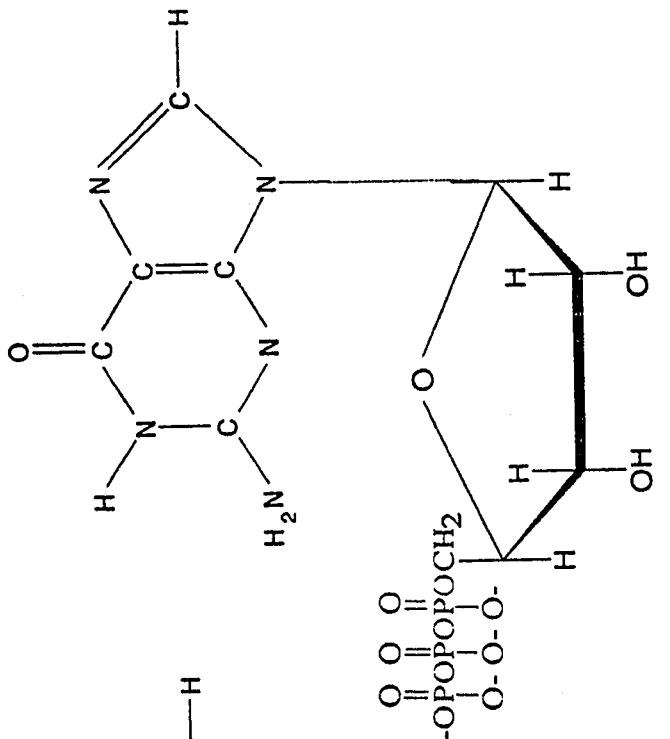

GTP

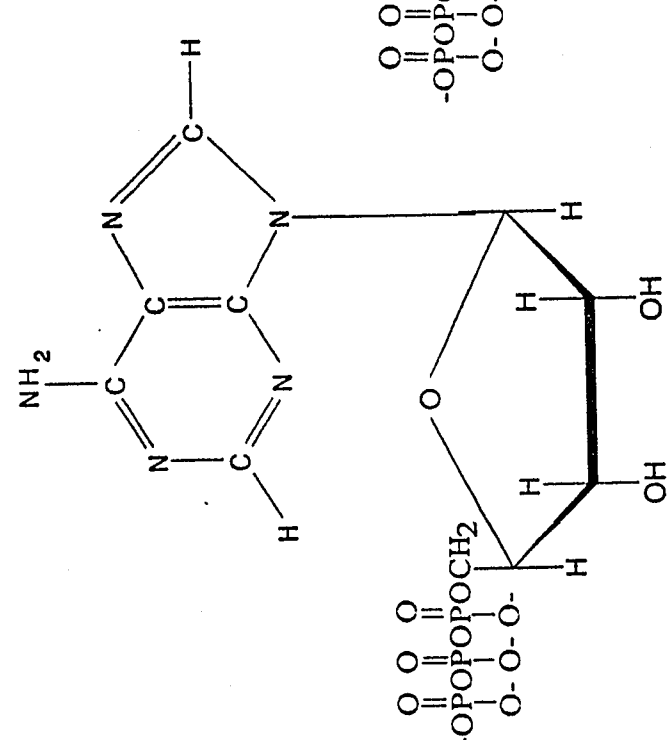

ATP

with 6-NH_2 group in ATP causes conformation change in myosin-S1 (which can be detected by fluorescence change). For ATP this interaction promotes hydrolysis and formation of the predominant intermediate, (A)M.ADP.P, the amount of which is proportional to the force generation in muscle fiber. The poor interaction of amino acid residue(s) in myosin-S1 with 6-keto group in GTP is less effective at promoting conformation change and therefore, the subsequent hydrolysis of GTP. As a result, the predominant intermediate remains in the state of (A)M.GTP. This offers a possible explanation for the absence of fluorescence change in the dissociation of acto-S1 by GTP, the absence of a phosphate burst in single turnover hydrolysis, and the poor force generation in muscle fiber. This hypothesis predicts the relationship between structure and function of actomyosin. The best technique to check this hypothesis is site-directed mutation on the amino acid residue(s) in myosin-S1 which interacts with 6-NH_2 of ATP.

The different solution conformations of CTP and GTP may also result in lower measured rate constant of binding of CTP and GTP to actomyosin (k_a/K_o) than ATP. Further investigation is needed for this hypothesis.

The fluorescence change induced by ATP and CTP in acto-S1 dissociation reflects the conformation change in myosin-S1 after the dissociation of acto-S1 (CCAD). CCAD and NTP hydrolysis may not be the same step, although they are closely related (Sleep and Taylor, 1976). The evidence to

support this statement is the observation of a biphasic fluorescence change in binding of unhydrolyzable ATP analog, AMP-PNP, to acto-S1 (Trybus and Taylor, 1982). The fast component is faster than dissociation, so that it reflects AMP-PNP binding, while the slow component of fluorescence change has essentially the same rate as light scattering. Since AMP-PNP dissociates acto-S1 much less rapidly than ATP, dissociation may become rate-limiting step in this reaction, and the slow component of the fluorescence change still measures CCAD, although AMP-PNP can't be hydrolyzed. The observation of fluorescence change by binding of AMP-PNP to myosin-S1 and acto-S1 also suggests that conformational changes may occur preceding the hydrolysis, because no fluorescence change would be expected by binding of unhydrolyzable AMP-PNP to myosin-S1 or acto-S1 if hydrolysis always precedes the fluorescence change. Hence, CCAD measured in diluted acto-S1 solution is preceded by acto-S1 dissociation, after which the interaction of the amino acid residue(s) in myosin-S1 with base moiety of NTP is allowed (Rayment et al., 1993a; Biosca et al., 1994). CCAD locates the functional amino acid residue(s) of myosin-S1 in a proper position for hydrolysis. Hydrolysis occurs at the end of CCAD, since the rate of hydrolysis is usually equal to or slower than that of CCAD (Sleep and Taylor, 1976). It is still possible that slow CCAD is followed by fast hydrolysis, if the rate of CCAD is equal to that of hydrolysis.

Mant-ATP binding induced fluorescence changes in myosin-S1 preceding acto-S1 dissociation were observed. The apparent second order rate constant of the fast phase in fluorescence measurement is faster than that measured in light scattering (Table III & IV). This fast fluorescence change is thought to measure the step AMT <--> AMT^* in Model 8, k_b(fast phase) = k_{TA} + k_{-TA}, while the slow phase fluorescence change measures step M^*T <--> $M^{**}(T)$, k_b(slow phase) = k_H + k_{-H} (in Model 8). The criterion for a sequential model is that, as the concentration of the variable increases, the amplitude coefficient decreases to negative (lag phase kinetics), then increases to positive (biphasic kinetics at higher concentrations), and finally reaches a constant (Smith and White, 1985a&b). The theoretical dependence of amplitude coefficient upon mant-ATP concentration is shown in Fig.26A, which is qualitatively the same as the experimental data (Fig. 10).

The fast phase of the fluorescence change observation in dissociation of acto-S1 by mant-GTP is much faster than the observation of dissociation measured in light scattering. Therefore, it is also thought to measure a fluorescence change of myosin-S1 preceding dissociation. However, a mechanism completely accounting for these results has not been formulated.

Fig.26. The theoretical dependence of amplitude coefficient (I_f/I_{tot}) upon the concentration of the variable in sequential and parallel model fitting using a computer program (Zhang et al., 1989).

A). The theoretical dependence of I_f/I_{tot} upon mant-ATP concentration in sequential model fitting (Model 8) for acto-RS.S1(A2) dissociation by mant-ATP. The model is simplified as follows:

$$AM + T \underset{k_{-AT}}{\overset{k_{AT}}{<---->}} AMT \overset{k_{TA}}{<---->} AM^{*}T \overset{k_{H}}{<---->} (A)M^{**}T$$

Here, the data at 20°C were used (Table IV). k_{AT} was the maximum collision rate constant (10^8 $M^{-1}s^{-1}$). k_{TA} was too fast to be measured, and estimated to be 10^4 s^{-1}. k_H was 100 s^{-1} (Table IV). k_{-AT} was 6.3×10^4 s^{-1}, estimated from apparent second order rate constant (fast phase), 1.6×10^7 $M^{-1}s^{-1}$ (Table IV). The rest of the rate constants were zero.

B). The theoretical dependence of I_f/I_{tot} upon actin concentration in parallel model fitting (Model 10) for actin binding to RS.S1-mant-NDP. The amplitude coefficient at 10°C was used (Table VI.B).

C). The theoretical dependence of I_f/I_{tot} upon actin concentration in sequential model fitting (Model 11) for actin binding to BV.S1-mant-ADP. The model is shown as follows:

$$A + M^{**}D \underset{k'_{-DA}}{\overset{k'_{DA}}{<---->}} AM^{**}D \overset{k_{DA}}{<---->} AM^{*}D \overset{k_{-AD}}{<---->} AM + D$$

Here, the data at 20°C were used (Table VI.B). k'_{DA} was 10^8 $M^{-1}s^{-1}$, which is the maximum collision second order rate constant. k_{DA} and k_{-AD} were 560 s^{-1} and 50 s^{-1}, respectively, from Table VI. k'_{-DA} was 1000 s^{-1}, determined from apparent second order rate constant (fast phase), 5.4×10^7 $M^{-1}s^{-1}$ (Table VI). The rest of the rate constants were zero.

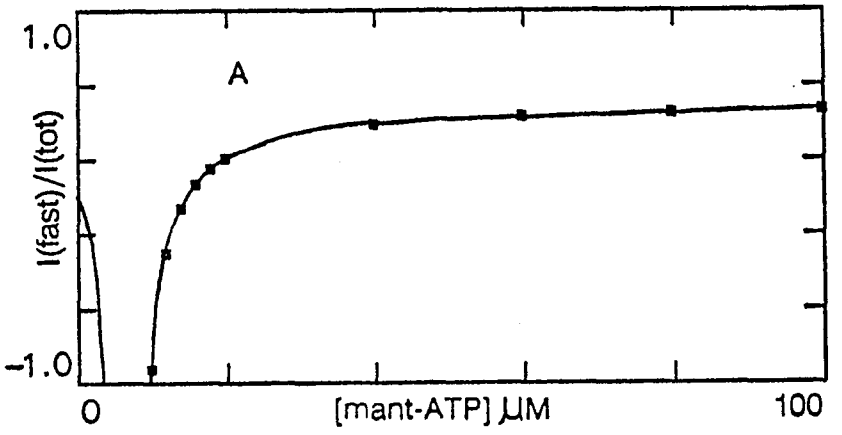

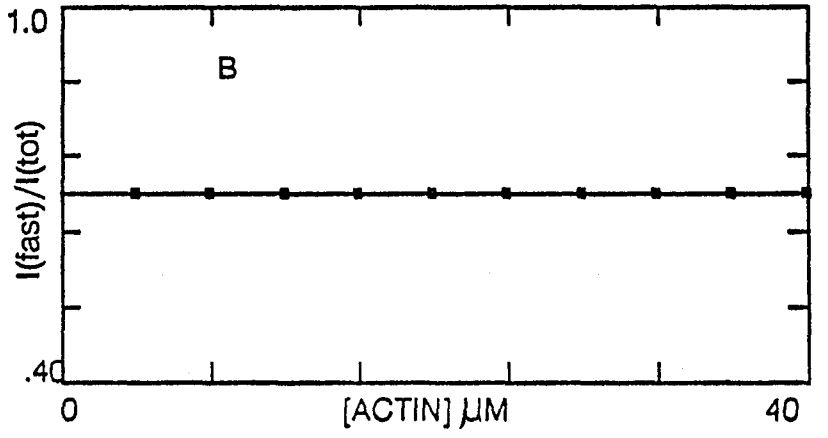

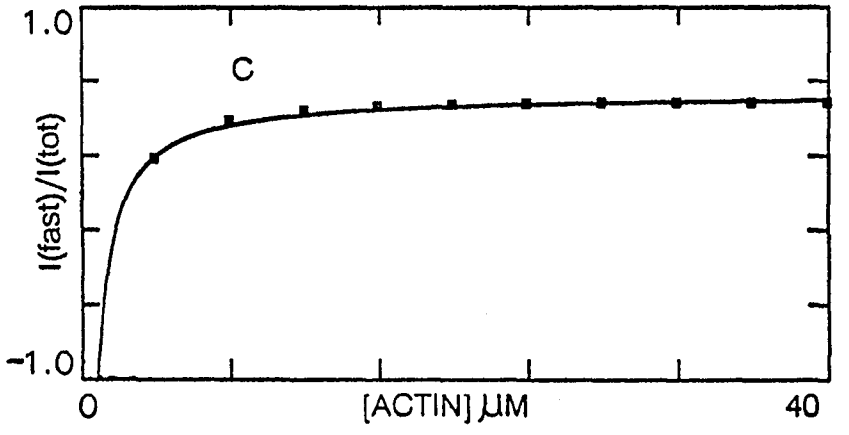

The Dissociation of NDP and NDP Analogs From Actomyosin

The dissociation of acto-S1-NDP by ATP was used to measure the rate constant of NDP dissociation, and its equilibrium constant to acto-S1 shown in following model (Model 9):

$$AMD \underset{K_i,\ k_{AD}}{\overset{k_{-AD}}{<---->}} AM + T <---> AMT ---> MT$$

Model 9

The dissociation rate constant (k_{-AD}) is equal to V_{max} measured by light scattering since dissociation of NDP is rate limiting step at saturated ATP concentration (White, 1977).

The kinetic data for the dissociation of actomyosin-NDP by ATP are shown in Table V. The K_i of ADP to acto-RS.HMM is essentially independent of ionic strength and temperature, which indicates that k_{AD} and k_{-AD} have similar small temperature and ionic strength coefficients.

The dissociation rate constants of NDP from acto-RS.HMM, acto-RS.S1(A1) and acto-RS.S1 (mixture of A1 and A2) are the same within experimental error. The k_{-AD} and K_i for acto-BV.S1 are 10 - 20 fold lower than that for acto-RS.S1.

The interaction of mant-NDP with actomyosin is characterized by a high k_{AD}, similar k_{-AD} and smaller K_i (compared to NDP). The apparent second order rate constants for binding of mant-NTP to acto-S1 are also higher than that of the corresponding NTP. The increased rate of binding is

presumably caused by the hydrophobic interaction between mant-group on mant-nucleotide and hydrophobic groups inside the myosin-S1.

The Binding of Actin To Myosin-mant-NDP

The binding of actin to myosin-S1-mant-NDP was used to investigate the step(s) preceding the NDP dissociation from actomyosin. The kinetic data are listed in Table VI. The large fluorescence decrease in actin binding to myosin-S1-mant-NDP indicates a substantial change in the environment of mant-NDP during this process.

The time courses of fluorescence changes observed upon actin binding to RS.S1(A1 or A2)-mant-NDP are better fit to double exponential equation (Eq. 2). Both the maximum rates of fast and slow components are slower than that of mant-NDP release, therefore, this fluorescence change reflects a conformation change in RS.S1 preceding the release of mant-NDP. The constant dependence of amplitude coefficient (I_f/I_{tot}) upon actin concentration suggests a parallel model (model 10)(Fig.26B), and is evidence against a sequential model (A+MD** <--> AMD** <--> AMD* <--> AMD <--> AM+D), which requires that the amplitude coefficient varies with actin concentration (Fig.26C). A possible explanation that the two components are due to 2′- and 3′- mant-ADP was tested using 2′-deoxy-3′-mant-ADP. The observations that the time courses of actin binding to RS.S1(A1)-mant-dADP are also fit better to double exponential equation is evidence

against the double exponential fluorescence decrease being caused by the mixture of 2′- and 3′-mant-NDP. A remaining explanation is that there are two conformations of myosin-S1 (Rosenfeld and Taylor, 1984; Lin and Cheung, 1991, 1992) with different affinity to actin. Therefore, the simplest model consistent with the data are the formation of initial complexes ($AM_1{}^*D$ and $AM_2{}^*D$), followed by conformation changes, and then, the release of mant-NDP (Model 10).

$$A + M_1{}^*D \text{ <--> } AM_1{}^*D \overset{k_{DA1}}{\text{<-->}} AM_1D \overset{k_{-AD}}{\text{<-->}} AM_1 + D$$

$$A + M_2{}^*D \text{ <--> } AM_2{}^*D \overset{k_{DA2}}{\text{<-->}} AM_2D \overset{k_{-AD}}{\text{<-->}} AM_2 + D$$

Model 10

M_1 and M_2 are two conformations of myosin-S1.

The fluorescence monitors step $AM_1{}^*D$ <--> AM_1D, and $AM_2{}^*D$ <--> AM_2D. k_{FL}(fast phase) and k_{FL}(slow phase) represent k_{DA1} and k_{DA2}, respectively (Model 10). The rate constants of these steps are much slower than the rate constant of mant-NDP dissociation ($k_{DA} < k_{-AD}$)(Table V & VI), suggesting that the conformation change preceding the mant-NDP dissociation is the slowest step in this reaction.

The binding of RS.HMM to actin is thought to via two-head binding, since the binding of actin to RS.S1(1 μM)-mant-ADP(2.5 μM), and to RS.HMM(1 μM S1 heads)-mant-ADP (2.5 μM) gives the same amplitude fluorescence change. This suggests

that mant-ADP on both heads of HMM are displaced during actin binding. This mechanism is different from the one-head-binding mechanism on kinesin dimer binding to microtubules (Hackney, 1994).

The time courses of actin binding to BV.S1-mant-NDP are also better fit to double exponential equation. The rate constants k_{FL}(fast phase) and k_{FL}(slow phase) represent k_{DA} and k_{-AD}, respectively (Model 11), since the rate of mant-ADP dissociation from acto-BV.S1 (77 s^{-1} and 49 s^{-1}, for light scattering and fluorescence measurement, respectively, at 20°C, Table V) is the same within error as the rate of slow phase of actin binding to BV.S1-mant-ADP (48 s^{-1} at 20°C, Table VI.B), while the fast fluorescence change represents the conformation change in BV.S1 preceding the release of mant-ADP. The dependence of amplitude coefficient upon actin concentration also provides the evidence for a sequential model (Model 11) rather than a parallel model (Model 10) (See Fig. 26 B&C for the theoretical dependence of amplitude coefficient upon actin concentration for parallel and sequential models). This result suggests that mant-ADP release is the slowest step. This is a significant difference between skeletal and cardiac muscle contraction mechanism at 20°C.

Theoretically, the amplitude coefficient associated with mant-ADP dissociation should be significantly increased when mant-ADP concentration is increased from 7.5 to 75 μM.

However, the time courses become noisy at high mant-ADP concentration and hence, the amplitude coefficient measurement is not reliable.

$$A + M^{**}D \leftrightarrow AM^{**}D \overset{k_{DA}}{\leftrightarrow} AM^{*}D \overset{k_{-AD}}{\leftrightarrow} AM + D$$

Model 11

k's are rate constants.
* and ** represent different fluorescence states.

Generally, a sequential model can't be distinguished from a more complicated branch model (Rosenfeld and Taylor, 1984; Smith and White, 1985b). However, the practical meaning for a branch model in this particular case has not been found.

For actin binding to BV.S1-mant-CDP or BV.S1-mant-GDP, the conformation change preceding the release of mant-NDP is the slowest step (see Table V & VI.B). The model is thought to be as follows (Model 12):

$$A + M^{*}D \leftrightarrow AM^{*}D \overset{k_{DA}}{\leftrightarrow} AMD \overset{k_{-AD}}{\leftrightarrow} AM + D$$

Model 12

Although the time courses are better fit to double exponential equation, the dependence of the rate of slow phase upon actin concentration is scattered and difficult to interpret. The rate constant of fast component, k_{FL}(fast phase), represents k_{DA}.

This reaction has also been investigated using pyrene-actin binding to myosin-S1-NDP. The maximum rates measured

with pyrene-actin are two to four times slower than that with mant-NDP, and independent of NDP structure (data from Zhang, X.). This seems reasonable since the conformation changes in actin and myosin during this process are two events, and only myosin has the specificity to NDP.

The binding of actin to myosin-S1-mant-NDP is a simplified experiment for the investigation of actin re-association with myosin-product. In real muscle contraction mechanism, actin binds to myosin-ADP-Phosphate, and phosphate release is the step proposed to be involved in force generation. However, since the equilibrium favors phosphate release in solution, the steps involving phosphate release are kinetically silent. In this research, the rates of actin binding to RS.S1-mant-ADP are the same in the absence or presence of 1 mM phosphate, probably because phosphate binds to myosin-S1-mant-ADP weakly. The presence of 0.2 mM aluminum fluoride doesn't affect the rate of RS.S1-mant-ADP dissociation by ATP (unpublished data of mine).

The Steps Which Limit Crossbridge Detachment In Muscle Fibers

Table XI summarized the maximum rates of some of the steps investigated in this work. These steps are in the non-dissociating part of the mechanism. The slowest of these steps is thought to limit the crossbridge detachment in muscle contraction. The maximum rates are essentially independent of the ionic strength, so that those measured in

Table XI. Determination of the steps which limit the crossbridge detachment from k_a[a], k_{FL}[b], k_{-AD}[c], and k_{min}[d].

	Temp. (°C)	k_a (s^{-1})	k_{FL} (s^{-1})	k_{-AD} (s^{-1})	k_{min} (s^{-1})
acto-RS.S1			A1;A2		
ATP	10	2154	--	1100	356[e]
CTP	10	717	--	1715	248[e]
aza-ATP	10	2210	--	1970	86[e]
mant-ATP	10	185	180; 73	913	ND
	20	340	728; 413	--	68[f]
	25	480	945;1378	--	160[f]
mant-CTP	10	48	147; 96	1310	ND
	20	96	457; 302	--	56[f]
	25	104	1059; 441	--	85[f]
acto-BV.S1					
ATP	20	589	--	75[g]	56[f]
CTP	20	220	--	397[g]	81[f]
mant-ATP	20	170	566	49-77	43[f]
mant-CTP	20	39	390	657	ND

a: The maximum rate of dissociation of acto-S1 by NTP or NTP analogs. Data from Table III.

b: The maximum rate of actin binding to myosin-S1-mant-NDP. Data from Table VI.

c: The maximum rate of dissociation of NDP (or NDP analogs) from acto-S1. Data from Table V.

d: The minimum rate which limits unloaded shortening velocity calculated from equation 6 ($k_{min} = V_m.SL/D$). V_m, the maximum rate of unloaded shortening velocity, determined from fiber shortening experiment. SL, the length of half sarcomere, 1100 nm. $V_m.SL$ can be directly obtained from in-vitro motility assay. Step size D was chosen as 5 nm (White et al., 1993; Table VII).

e: V_m data from fiber shortening experiment (Pate et al., 1993).

f: $V_m.SL$ data from in-vitro motility assay (Table VII).

g: data from Robinson, A., personal communication.

ND, not determined.

These maximum rates were measured in different ionic strength conditions. See individual table legends for experimental conditions.

different ionic strengths can be compared. The maximum rates of the steps listed in Table XI are a) the dissociation of acto-S1 by NTP or NTP analogs (k_a); b) the dissociation of NDP and NDP analogs from actomyosin (k_{-AD}); c) the fluorescence change preceding the dissociation of NDP or NDP analogs (k_{FL}); d) the rate of the predicted slowest step which limits crossbridge detachment in muscle contraction (K_{min}) calculated using equation 6.

The maximum rates of acto-RS.S1 dissociation by ATP, CTP and aza-ATP (k_a), and those of the dissociation of ADP, CDP, and aza-ADP from acto-RS.S1 are 3 - 25 times faster than corresponding k_{min}, so that these two steps can't be the rate limiting step, when ATP, CTP and aza-ATP are used as substrates.

The values of k_a, k_{FL}, and k_{-AD} for acto-RS.S1 using mant-ATP as substrate are 3 - 10 times faster than k_{min}, so that it is difficult to determine the rate limiting step of crossbridge detachment in this situation. A fiber shortening experiment using mant-ATP as substrate is suggested here to accurately measure V_m and k_{min} for rate limiting step determination.

The maximum rate of dissociation of acto-RS.S1 by mant-CTP is close to k_{min}, and is at least one of the steps which limits crossbridge detachment. While k_{FL} and k_{-AD} are 5 - 22 times faster than k_{min} and can't be rate limiting step.

The k_a for dissociation of acto-BV.S1 by ATP and mant-ATP are 4 - 10 times faster than k_{min}, the maximum rate of

conformation change preceding the release of mant-ADP from acto-BV.S1 is about 12 times faster than k_{min}, so that these steps can't be rate limiting. The k_{-AD} for ADP and mant-ADP dissociation from acto-BV.S1 are close to k_{min}, and are thought to be the step which limits crossbridge detachment in muscle fiber, consistent with the observation of Siemankowski et al. (1985).

The rate limiting steps in acto-BV.S1 using CTP and mant-CTP as substrates are not determined because of the incomplete data.

The fact that crossbridge detachment is limited at different steps for skeletal and cardiac muscle provides the evidence for the difference in the structures and kinetic mechanisms of these two muscles.

REFERENCES

Bagshaw, C.R., J.F. Eccleston, F. Eckstein, R.S. Goody, H. Gutfreund, and D.R. Trentham. The Magnesium Ion-dependent adenosine Triphosphate of Myosin. Two-step Processes of Adenosine Triphosphate association and Adenosine Diphosphate Dissociation. Biochem. J. **141** (1974): 351-364.

Bagshaw, C.R. and D.R. Trentham. The Reversibility of Adenosine Triphosphate Cleavage by Myosin. Biochem. J. **133** (1973): 323-328.

Barany, M. ATPase Activity of Myosin Correlated with Speed of Muscle Contraction. J. Gen. Physiol. suppl. **50** (1967): 197-218.

Belknap, B., J. McDowell, and H. White. Novel Steady-state and Pre-steady-state Kinetics of GTP and ITP Hydrolysis by Cardiac Myosin-S1 and Actomyosin-s1. Biophys. J. **57** (1990): 549a.

Belknap, B., X.Q. Wang, and H.D. White. The Bond Splitting Step Is Rate Limiting for Skeletal Actomyosin-S1 ATP Hydrolysis. Biophys. J. **61** (1992): 440a.

Biosca, J.A., C. Lionne, F. Travers, and T. Barman. A Kinetic Reevaluation Supports The Structural Two Steps Model For ATP Binding To Actomyosin. Biophys. J. **66** (1994): 78a.

Brenner, B. and E. Eisenberg. Rate of Force Generation In Muscle - Correlation With Actomyosin ATPase Activity In Solution. Proc. Natl. Acad. Sci. USA **83** (1986): 3542-3546.

Burton, K. Myosin Step Size: Estimates From Motility Assays and Shortening Muscle. J. Mus. Res. Cell Motil. **13** (1992): 590-607.

Burton, K. and J. Sleep. Effect of Different Metal-Nucleotide Complexes On Actomyosin Kinetics In Fibers and In Solution. Biophys. J. **51** (1987): 6a.

Coates, J.H., A.H. Criddle, and M.A. Geeves. Pressure-relaxation Studies of Pyrene-labelled Actin and Myosin Subfragment 1 From Rabbit Skeletal Muscle. Evidence For Two States of Acto-subfragment 1. Biochem. J. **232** (1985): 351-356.

Criddle, A.H., M.A. Geeves, and T. Jeffries. The Use of Actin Labelled With N-(1-pyrenyl)iodoacetamide To Study The Interaction of Actin With Myosin Subfragments and Troponin/Tropomyosin. Biochem. J. **232** (1985): 343-349.

Eccleston, J.F. and D.R. Trentham. Magnesium Ion Dependent Rabbit Skeletal Muscle Myosin Guanosine and Thioguanosine Triphosphatase Mechanism and a Novel Guanosine Diphosphatase Reaction. Biochemistry **18** (1979): 2896-2904.

Ferenczi, M. A., Y.E. Goldman, and R.M. Simmons. The Dependence of Force and Shortening Velocity on Substrate Concentration in Skinned Muscle Fibers from Rana Temporaria. J. Physiol. (London) **350** (1984): 519-543.

Ford, L.E., A.F. Huxley, and R.M. Simmons. Tension Responses To Sudden Length Change In Stimulated Frog Muscle Fibers Near Slack Length. J. Physiol. (London) **269** (1977): 441-515.

Geeves, M.A. and H. Gutfreund. The Use of Pressure Perturbations To Investigate the Interaction of Rabbit Muscle Myosin Subfragment 1 With Actin In The Presence of MgADP. FEBS Lett. **140** (1982): 11-15.

Goldman, Y. E. Kinetics Of The Actomyosin ATPase In Muscle-Fibers. Ann. Rev. of Physiol. **49** (1987): 637-654.

Goldman, Y. E., M. G. Hibberd, J. A. Mccray, and D. R. Trentham. Relaxation of Muscle-fibers By Photolysis of Caged ATP. Nature **300** (1982): 701-705.

Grammer, J.C. and R. G. Yount. Photochemical Evidence That Ser-243 of Myosin's Heavy Chain Is Near The Phosphate Binding Site of ATP. Biophys. J. **59** (1991): 226a.

Hackney, D.D. Evidence For Alternating Head Catalysis by Kinesin During Microtubule-stimulated ATP Hydrolysis. Proc. Natl. Acad. Sci. USA **91** (1994): 6865-6869.

Hanson, J. and H.E. Huxley. The Structural Basis of Contraction In Striated Muscle. Symp. Soc. Exp. Biol. **9** (1955): 228-258.

Harada, Y., K. Sakurada, T. Aoki, D.D. Thomas, and T. Yanagida. Mechanochemical Coupling In Actomyosin Energy Transduction Studied By In Vitro Movement Assay. J. Mol. Biol. **216** (1990): 49-68.

Hibberd, M.G., J.A. Dantzig, and D.R. Trentham. Phosphate Release and Force Generation In Skeletal Muscle Fibers. Science **228** (1985): 1317-1319.

Hiratsuka, T. New Ribose-modified Fluorescent Analogs of Adenine and Guanine Nucleotides Available as Substrates For Various Enzymes. Biochim. et Biophys. Acta **742** (1983): 496-508.

Hiratsuka, T. and K. Uchida. Preparation and Properties of 2'(or 3')-O-(2,4,6-trinitrophenyl) Adenosine 5'-triphosphate, An Analog of Adenosine Triphosphate. Biochim. et Biophys. Acta **320** (1973): 635-647.

Huxley, A.F. Muscle Structure and Theories of Contraction. Prog. Biophys. Biophys. Chem. **7** (1957): 255-318.

Huxley, A.F. and R.M. Simmons. Proposed Mechanism of Force Generation in Striated Muscle. Nature **233** (1971): 533-538.

Huxley, H.E. Structural Arrangements and the Contraction Mechanism In Striated Muscle. Proc. R. Soc. B. **160** (1964): 442-448.

Huxley, H.E. The Mechanism of Muscle Contraction. Science **164** (1969): 1356-1366.

Huxley, H. E. and M. Kress. Crossbridge Behaviour During Muscle Contraction. J. Mus. Res. Cell Motil. **6** (1985): 153-161.

Johnson, K. A. and E. W. Taylor. Intermediate States of Subfragment 1 and Actosubfragment 1 ATPase: Reevaluation of The Mechanism. Biochemistry **17** (1978): 3432-3442.

Kabsch, W., H. G. Mannherz, D. Suck, E. F. Pai, and K. C. Holmes. Atomic-structure of The Actin - DNase-I complex. Nature **347** (1990): 37-44.

Kawai, M. and H. R. Halvorson. Role of MgATP and MgADP In The Crossbridge Kinetics In Chemically Skinned Rabbit Psoas Fibers: Study of a Fast Exponential Process. Biophys. J. **55** (1989): 595-603.

Kawai, M. and H. R. Halvorson. Two Step Mechanism of Phosphate Release and the Mechanism of Force Generation in Chemically Skinned Fibers of Rabbit Psoas Muscle. Biophys. J. **59** (1991): 329-342.

Kron, S.J. and J.A. Spudich. Fluorescent Actin Filaments Move On Myosin Fixed To A Glass Surface. Proc. Natl. Acad. Sci. USA **83** (1986): 6272-6276.

Kron, S. J., Y. Y. Toyoshima, T. Q. P. Uyeda, and J. A. Spudich. Assays for Actin Sliding Movement Over Myosin-Coated Surfaces. Meths. Enz. **196** (1991): 399-416.

Lin, S.H. and H.C. Cheung. Two-State Equalibria of Myosin Subfragment 1 and Its Complexes with ADP and Actin. Biochemistry **30** (1991): 4317-4322.

Lin, S.H. and H.C. Cheung. The Kinetics of A Two-state Transition of Myosin Subfragment 1 - A Temperature-jump Relaxation Study. FEBS Lett. **304** (1992): 184-186.

Lymn, R.W. and E.W. Taylor. Mechanism of Adenosine Triphosphate Hydrolysis by Actomyosin. Biochemistry **10** (1971): 4617-4624.

Maita, T., E. Yajima, S. Nagata, T. Miyanishi, S. Nakayamea, and G. Matsuda. The Primary Structure of Skeletal-muscle Myosin Heavy-chain .4. Sequence of the Rod, and the Complete 1,938-residue Sequence of the Heavy-chain. J. Biochem. (Tokyo) **110** (1991): 75-87.

Margossian, S.S. Reversible Dissociation of Dog Cardiac Myosin Regulatory Light Chain 2 and Its Influence on ATP Hydrolysis. J. Biol. Chem. **260** (1985): 13747-13754.

McNally, E. M., R. Kraft, M. Bravozehnder, D. A. Taylor, and L. A. Leinwand. Full-length Rat Alpha and Beta Cardiac Myosin Heavy-chain Sequences - Comparisons Suggest a Molecular-basis for Functional Differences. J. Mol. Biol. **210** (1989): 665-671.

Millar, N.C. and E. Homsher. The Effect of Phosphate and Calcium on Force Generation in Glycerinated Rabbit Skeletal Muscle Fibers: A Steady-State and Transient Kinetic Study. J. Biol. Chem. **265** (1990): 20234-20240.

Mornet, D., R. Bertrand, P. Pantel, E. Audemard, and R. Kassab. Proteolytic Approach to Structure and Function of Actin Recognition Site in Myosin Heads. Biochemistry **20** (1981): 2110-2120.

Mornet, D., P. Pantel, E. Audemard, and R. Kassab. The Limited Tryptic Cleavage of Chymotryptic S-1: An Approach To The Characterization of the Actin Site In Myosin Heads. Biochem. Biophys. Res. Comm. **89** (1979): 925-932.

Neal, S.E., J.F. Eccleston, and M.R. Webb. Hydrolysis of GTP by p21NRAS, the NRAS protooncogene Product, Is Accompanied by A Conformational Change In the Wild-type Protein: Use of A Single Fluorescent Probe at the Catalytic Site. Proc. Natl. Acad. Sci. USA. **87** (1990): 3562-3565.

Nyitray, L., E.B. Goodwin, and A.G. Szent-Gyorgyi. Complete Primary Structure of A Scallop Striated Muscle Myosin Heavy Chain: Sequence Comparison with Other Heavy Chains Reveals Regions that Might Be Critical For Regulation. J. Biol. Chem. **266** (1991): 18469-18476.

Pate, E., K. Franks, H.D. White, and R. Cooke. The Use of Differing Nucleotides to Investigate Crossbridge Kinetics. J. Biol. Chem. **268** (1993): 10046-10053.

Rayment, I., H.M. Holden, M. Whittaker, C.B. Yohn, M. Lorenz, K.C. Holmes, and R.A. Milligan. Structure of the Actin-Myosin Complex and Its Implications for Muscle Contraction. Science **261** (1993a): 58-65.

Rayment, I., W.R. Rypniewski, K. Schmidt-Base, R. Smith, D.R. Tomchick, M.M. Benning, D.A. Winkelmann, G. Wesenberg, and H.M. Holden. Three Dimensional Structure of Myosin Subfragment-1: A Molecular Motor. Science **261** (1993b): 50-58.

Rosenfeld, S. S. and E. W. Taylor. Reactions of 1-N^6-Ethenoadenosine Nucleotides with Myosin Subfragment-1 and Acto-subfragment-1 of Skeletal and Smooth-muscle. J. Biol. Chem. **259** (1984): 11920-11929.

Siemankowski, R. F. and H. D. White. Kinetics of the Interaction Between Actin, ATP, and Cardiac Myosin-S1. J. Biol. Chem. **259** (1984): 5045-5053.

Siemankowski, R. F., M. O. Wiseman, and H. D. White. ADP Dissociation From Actomyosin Subfragment-1 Is Sufficiently Slow to Limit the Unloaded Shortening Velocity In Vertebrate Muscle. Proc. Natl. Acad. Sci. USA **82** (1985): 658-662.

Sleep, J.A. and R.L. Hutton. Actin Mediated Release of ATP From A Myosin-ATP Complex. Biochemistry **17** (1978): 5423-5430.

Sleep, J.A. and R.L. Hutton. Exchange Between Inorganic Phosphate and Adenosine 5′-Triphosphate in the Medium by Actomyosin Subfragment 1. Biochemistry **19** (1980): 1276-1283

Sleep, J.A. and E.W. Taylor. Intermediate States of Actomyosin Adenosine triphosphatase. Biochemistry **15** (1976): 5813-5817.

Smith, S. J. and H. D. White. Kinetic Mechanism of 1-N-6-Etheno-2-aza-ATP and 1-N-6-Etheno-2-aza-ADP Binding to Bovine Ventricular Actomyosin-S1 and Myofibrils. J. Biol. Chem **260** (1985a): 15156-15162.

Smith, S. J. and H. D. White. Kinetic Mechanism of 1-N-6-Etheno-2-aza-ATP Hydrolysis by Bovine Ventricular Myosin Subfragment-1 and Actomyosin Subfragment-1 - The Nucleotide Binding Steps. J. Biol. Chem. **260** (1985b): 15146-15155.

Stryer, L. *Biochemistry* (3rd ed.). **Chap. 36** (1988): 921-948.

Sutoh, K. An Actin-binding Site on the 20K Fragment of Myosin Subfragment 1. Biochemistry **21** (1982): 4800-4804.

Szilagyi, L., M. Balint, F.A. Streter, and J. Gergely. Photoaffinity Labelling with An ATP Analog of The N-terminal Peptide of Myosin. Biochem. Biophys. Res. Comm. **87** (1979): 936-945.

Thirlwell, H., F. Bancel, and M.A. Ferenczi. Relaxation of Rigor Tension By Photolysis Of Caged-ATP In Permeabilized Muscle Fibers Of The Rabbit. Biophys. J. **64** (1993): 251a.

Tonomura, Y. *Muscle Proteins, Muscle Contraction, and Cation Transport*. University Park Press, Baltimore (1973): pp. 259-271.

Toyoshima, Y.Y., S.J. Kron, and J.A. Spudich. The Myosin Step Size: Measurement of the Unit Displacement per ATP Hydrolyzed In An In Vitro Assay. Proc. Natl. Acad. Sci. USA **87** (1990): 7130-7134.

Trentham, D.R., R.G. Bardsley, J.F. Eccleston, and A.G. Weeds. Elementary Processes of the Magnesium Ion-dependent Adenosine Triphosphatase Activity of Heavy Meromyosin. A Transient Kinetic Approach to the Study of Kinases and Adenosine Triphosphatases and A Colorimetric Inorganic Phosphate Assay In Situ. Biochem. J. **126** (1972): 635-644.

Trybus, K. M. and E. W. Taylor. Transient Kinetics of Adenosine 5′-Diphosphate and Adenosine 5′-(Beta, Gamma-Imidotriphosphate) Binding to Subfragment-1 and Actosubfragment-1. Biochemistry **21** (1982): 1284-1294.

Uyeda, T.Q.P., S.J. Kron, and J.A. Spudich. Myosin Step Size Estimation From Slow Sliding Movement of Actin Over Low Densities of Heavy Meromyosin. J. Mol. Biol. **214** (1990): 699-710.

Walker, M., H.D. White, Belknap. B., and J. Trinick. Electron Cryomicroscopy of Acto-Myosin-S1 during Steady-State ATP Hydrolysis. Biophys. J. **66** (1994): 1563-1572.

Weber, A. Parallel Response of Myofibrillar Contraction and Relaxation to Four Different Nucleoside Triphophates. J. Gen. Physiol. **53** (1969): 781-791.

Weeds, A.G. and R.S. Taylor. Separation of Subfragment 1 Isoenzymes from Rabbit Skeletal Muscle Myosin. Nature **257** (1975): 54-56.

White, H. D. Measurement of the Rate and Equilibrium Constant of ADP Binding to Rabbit Skeletal Actomyosin-HMM. Biophys. J. **17** (1977): 40a.

White, H. D. Special Instrumentation and Techniques for Kinetic Studies of Contractile-systems. Meths. Enz. **85** (1982): 698-708.

White, H.D. Kinetics of Tryptophan Fluorescence Enhancement in Myofibrils during ATP Hydrolysis. J. Biol. Chem. **260** (1985): 982-986.

White, H.D., B. Belknap, and W. Jiang. Kinetics of Binding and Hydrolysis of a Series of Nucleoside Triphosphates by Actomyosin-S1: Relationship between Solution Rate Constants and Properties of Muscle Fibers. J. Biol. Chem. **268** (1993): 10039-10045.

White, H. D. and I. Rayment. Kinetic Characterization of Methylated Myosin Subfragment-1. Biochemistry **32** (1993): 9859-9865.

White, H.D. and E.W. Taylor. Energetics and Mechanism of Actomyosin Adenosine Triphosphatase. Biochemistry **15** (1976): 5818-5826.

Woodward, S.K.A., J.F. Eccleston, and M.A. Geeves. Kinetics of the Interaction of 2'(3')-O-(N-methylanthraniloyl)-ATP with Myosin Subfragment 1 and Actomyosin Subfragment 1: Characterization of Two Acto.S1.ADP Complexes. Biochemistry **30** (1991): 422-430.

Yanagida, T., T. Arata, and F. Oosawa. Sliding Distance of Actin Filament Induced by A Myosin Crossbridge during One ATP Hydrolysis Cycle. Nature **316** (1985): 366-369.

Yount, R.G., C.R. Cremo, J.C. Grammer, and B.A. Kerwin. Photochemical Mapping of the Active Site of Myosin. Phil. Trans. R. Soc. Lon. Biol. **336** (1992): 55-61.

Zhang, X. Z., A. Strand, and H. D. White. A General Pre-steady-state Solution to Complex Kinetic Mechanisms. Anal. Biochem. **176** (1989): 427-431.